Fatigue behaviour of UHPFRC and R-UHPFRC - RC composite members

THÈSE N^{O} 6068 (2014)

PRÉSENTÉE LE 20 MARS 2014

À LA FACULTÉ DE L'ENVIRONNEMENT NATUREL, ARCHITECTURAL ET CONSTRUIT
LABORATOIRE DE MAINTENANCE, CONSTRUCTION ET SÉCURITÉ DES OUVRAGES
PROGRAMME DOCTORAL EN STRUCTURES

ÉCOLE POLYTECHNIQUE FÉDÉRALE DE LAUSANNE

POUR L'OBTENTION DU GRADE DE DOCTEUR ÈS SCIENCES

PAR

Tohru MAKITA

acceptée sur proposition du jury:

Prof. A. Schleiss, président du jury
Prof. E. Brühwiler, directeur de thèse
Prof. D. A. Hordijk, rapporteur
Prof. T. Keller, rapporteur
Prof. T. Vogel, rapporteur

ÉCOLE POLYTECHNIQUE
FÉDÉRALE DE LAUSANNE

Suisse
2014

Table of Contents

Foreword

The present thesis by Tohru Makita is part of a more than 13 year-long research activity of the MCS group to develop Ultra High-Performance Fibre-Reinforced Composites (UHPFRC) for the improvement of existing reinforced concrete structures by adding a layer of UHPFRC on top of an existing reinforced concrete element. Previous doctoral theses at MCS allowed to develop the novel building material UHPFRC, to identify the importance of adding steel rebars to obtain R-UHPFRC and to investigate the structural behaviour of R-UHPFRC – RC composite members under bending and shear.

In his doctoral thesis, Tohru Makita investigates the fatigue behaviour of R-UHPFRC – RC structural members. He explores the advantages of this novel structural system for effective strengthening of existing RC structures by means of an extensive experimental campaign and thorough analytical modelling. The thesis topic is particularly relevant for bridge deck slabs where increasing road and rail traffic loading are more and more subjected to fatigue. In view of the significant socio-economic impact of intervention on existing transportation infrastructure, cost-effective strengthening methods are urgently needed. This thesis contributes to this ambitious goal.

With his doctoral thesis, Tohru Makita provides the proof of his capabilities to conduct a significant scientific study and to solve complex scientific questions by applying a sound engineering approach. The present thesis is of very good overall quality and delivers results and findings that are already useful and applied in practical applications for the strengthening of reinforced concrete bridge deck slabs using UHPFRC.

In the name of the whole team of MCS, I thank him for his constant and thorough investment to the thesis topic as well as for his professional skills and personal qualities.

Lausanne, January 2014 Professor Eugen Brühwiler

Summary

Ultra-High Performance Fibre Reinforced Composites (UHPFRC) is a cementitious material, generally made of cement, quartz sand, silica fume and fibres. It has excellent properties: a relatively high compressive strength (≥ 150 MPa) and tensile strength (≥ 7 MPa), a strain-hardening behaviour under tensile stress (given a certain volume of fibres) and a very low permeability because of an optimised dense matrix. These properties make UHPFRC suitable for "hardening" those parts of structural members that are subjected to mechanically and environmentally severe actions. For instance, overlaying UHPFRC or UHPFRC combined with steel rebars (R-UHPFRC) on the top surface of reinforced concrete (RC) bridge deck slabs is an efficient intervention for increasing the ultimate resistance and improving the durability of the elements. This method is particularly efficient in the parts where UHPFRC essentially carries tensile stress caused by wheel loading. In this case, repeated tensile stress cycles are imposed on the UHPFRC (R-UHPFRC) layer and sufficient fatigue resistance of UHPFRC (R-UHPFRC) as well as composite UHPFRC (R-UHPFRC) – RC member needs to be verified in the design process.

The objective of this thesis is to study the fatigue behaviour of UHPFRC, R-UHPFRC and composite R-UHPFRC – RC members (RU-RC members) with a comprehensive experimental program. Constant amplitude uniaxial tensile fatigue tests were conducted on UHPFRC and R-UHPFRC plates, while bending fatigue tests were conducted on RU-RC beams with an experimental set-up representing a strip of an RC bridge deck cantilever slab strengthened with R-UHPFRC.

UHPFRC showed a fatigue endurance limit with respect to 10 million cycles above which fatigue stress induces significant damage leading to rather short fatigue lives. The fatigue endurance limit of UHPFRC at 10 million cycles was determined to be 70 % of the elastic limit strength. Relatively large variations were observed in local deformations of UHPFRC due to variations in the material properties, in particular the elastic limit strength and the strain-hardening behaviour. These variations in local deformations confer significant stress and deformation redistribution capacity on the bulk UHPFRC material thus enhancing the fatigue behaviour. The fatigue fracture surface of UHPFRC showed features of fatigue fracture surfaces of steel. The fatigue crack propagation was identified by a smooth surface while the final fracture led to rather rough surface.

The fatigue endurance limit of R-UHPFRC at 10 million cycles was determined to be 54 % of the ultimate strength. Considering that at this force level, UHPFRC is in the strain-hardening domain, the steel rebars improve the fatigue stress bearing capacity of UHPFRC by distributing the applied fatigue stress. The respective contribution of UHPFRC and steel rebars to the fatigue resistance of R-UHPFRC depends on the maximum fatigue force level. Stress distribution and transfer between UHPFRC and steel rebars enhances the fatigue stress bearing capacity of both material components.

Although some scatter was observed in the test results, the fatigue endurance limit of

RU-RC beam at 10 million cycles was determined to be about 50 % of the ultimate strength. Deformation growth of the R-UHPFRC layer was attributed to the decrease of deformation modulus (the ratio of stress to strain) of UHPFRC due to fatigue, effectuating a stress transfer from the UHPFRC to the steel rebars. Fatigue failure process of the RU-RC beams was determined by fatigue fracture of the steel rebars in the R-UHPFRC layer. The fatigue stress range in the steel rebars in the R-UHPFRC layer is thus the most relevant parameter for the fatigue resistance of the RU-RC beams. Fatigue design rules for RU-RC members under bending fatigue were proposed concerning the fatigue safety verification in terms of macro-level (moment resistance of RU-RC member) and meso-level (stress range in the steel rebars in the R-UHPFRC layer).

Tensile fatigue behaviour of UHPFRC was analysed based on elementary damage mechanics theory. If significant damage is caused in the UHPFRC in the early stage, then damage develops with constant rate during most of the fatigue life until the material fractures due to tensile fatigue. In this case, a bi-linear damage evolution model was deduced and a method to determine the remaining fatigue life was proposed.

Decrease of deformation modulus of UHPFRC in R-UHPFRC due to fatigue was investigated and similar behaviour was observed in fatigue decreasing curves of deformation modulus of UHPFRC among all R-UHPFRC specimens. An empirical relationship between modulus of deformation of UHPFRC in R-UHPFRC and the number of fatigue cycles was proposed to characterise the tensile fatigue behaviour of R-UHPFRC. By applying the proposed relationship to the RU-RC beam, the deformation range of the R-UHPFRC layer was calculated based on Euler-Bernoulli beam theory. It is understood from fatigue force distribution among components of the RU-RC beam that the R-UHPFRC layer reduces fatigue stress in the top steel rebars of the RC part. Thus, RC member is effectively strengthened for fatigue by applying R-UHPFRC.

***Keywords**: Ultra-High Performance Fibre Reinforced Concrete (UHPFRC), reinforced UHPFRC, composite member, fatigue behaviour, fatigue endurance limit, strengthening of bridge deck slab*

Résumé

Les Béton Fibrés Ultra-Performant (BFUP) sont des matériaux cimentaires, généralement composés de ciment, de sable de quartz, de fumée de silice et de fibres. Les BFUP ont d'excellentes propriétés: de hautes résistances à la compression (≥ 150 MPa) et à la traction (≥ 7 MPa), un comportement écrouissant en traction (obtenu grâce à un certain volume de fibres) et une très faible perméabilité grâce à une matrice dense et optimisée. Ces propriétés font du BFUP un matériau adapté pour le "durcissement" des zones parties d'éléments structuraux soumis à des actions mécaniques et environnementales sévères. Par exemple, il est possible d'ajouter une couche de BFUP ou de BFUP combiné avec barres d'armature (BFUP armé) sur la face supérieure des dalles de pont en béton armé. Ceci est une intervention efficace pour augmenter la résistance ultime et améliorer la durabilité de la structure en particulier dans les régions où la couche de BFUP est solicitée en traction. Dans ce cas, des cycles répétés de traction sont imposé à la couche de BFUP (ou BFUP armé) et la résistance à la fatigue du BFUP (ou BFUP armé) aussi bien que de l'élément composé BFUP (ou BFUP armé) – béton armé doit être vérifiée lors du dimensionnement.

L'objectif de cette thèse est d'étudier, à l'aide d'un programme expérimental complet, le comportement en fatigue du BFUP, du BFUP armé et des éléments composé BFUP armé – béton armé. Des essais de fatigue en traction uniaxiale d'amplitude constante ont été réalisés sur des plaques de BFUP et de BFUP armé. Des essais de fatigue ont aussi été effectués sur des poutres composées BFUP armé – béton armé avec un montage expérimental représentant une bande de dalle en porte-à-faux.

Le BFUP a montré une limite d'endurance à la fatigue pour 10 millions de cycles au-dessus de laquelle les cycles de contraintes induisent un endommagement significatifs conduisant à des durées de vies en fatigues assez courtes. La limite d'endurance à la fatigue des BFUP à 10 millions de cycles a été déterminée à 70 % de la résistance élastique. Une variation relativement grande des déformations locales sur le volume du BFUP a été observée. Ceci est dû à la variabilité des propriétés du matériau, en particulier la résistance élastique et le comportement écrouissant. Ces variations dans les déformations locales confirment la capacité significative de distribution des contraintes et des déformations sur tout le volume du BFUP améliorant donc le comportement en fatigue. La surface de rupture de fatigue du BFUP a montré les mêmes caractéristiques que les surfaces de rupture de fatigue de l'acier. La propagation de la fissure de fatigue est identifiable par une surface de rupture lisse, alors que la rupture finale conduit à une surface plutôt rugueuse.

La limite d'endurance à la fatigue du BFUP armé à 10 millions de cycles a été déterminée à 54 % de la résistance maximale. Considérant que, à ce niveau de force, le comportement du BFUP est dans le domaine écrouissant, les barres d'armature améliorent la résistance à la fatigue du BFUP en distribuant la contrainte appliquée. La contribution respective du BFUP et des barres d'armature pour la résistance à la fatigue du BFUP armé dépend du niveau maximal

de force d'un cycle de fatigue. La distribution et transfert des contraintes entre le BFUP et les barres d'armature augmentent la résistance à la fatigue des deux composants matériaux.

Bien qu'une certaine dispersion a été observée dans les résultats des tests, la limite d'endurance à la fatigue des poutres composées BFUP armé – béton armé à 10 millions de cycles a été déterminée à environ 50 % de la résistance ultime. L'augmentation des déformations dans la couche de BFUP armé a été attribué à la diminution du module de déformation (le rapport de la contrainte à la déformation) des BFUP en raison de l'endommagement causé par les cycles de fatigue ce qui entraîne un transfert des contraintes du BFUP aux barres d'armature. La rupture par fatigue des poutres composées BFUP armé – béton armé est déterminée par la rupture par fatigue des barres d'armature de la couche de BFUP armé. Le niveau de contraintes de fatigue dans barres d'armature de la couche de BFUP armé est donc le paramètre le plus important de la résistance à la fatigue des poutres composées BFUP armé – béton armé. Des règles de dimensionnement pour la fatigue des éléments composés BFUP armé – béton armé soumis à des efforts de flexion cycliques ont été proposées. Le dimensionnement pour la fatigue doit se faire au macro-niveau (moment résistant de l'élément composé BFUP armé – béton armé) et au méso-niveau (intervalle de contrainte dans les barres d'armature de la couche de BFUP armé).

Le comportement en fatigue en traction du BFUP a été analysé sur la base de la théorie de la mécanique de l'endommagement. Si le BFUP est endommagé de manière significative lors des premiers cycles de chargement en traction, alors l'endommagement se développe ensuite à un taux constant pour une grande partie de la durée de la vie en fatigue, jusqu'à la rupture finale. Dans ce cas, un modèle bilinéaire de l'évolution de l'endommagement a été déduit et une méthode pour déterminer la durée de vie en fatigue restante a été proposée.

La diminution du module de déformation du BFUP par fatigue dans une section de BFUP armé a été déterminée et un comportement semblable a été observé pour les résultats sur tous les spécimens de BFUP armé. Une relation empirique entre le module de déformation du BFUP dans une section en BFUP armé et le nombre de cycles appliqués a été proposée. En appliquant cette relation empirique à la poutre composée BFUP armé – béton armé, la gamme de déformations de la couche de BFUP armé a pu être calculé avec la théorie d'Euler-Bernoulli. Par la répartition de la force de fatigue entre les différents éléments d'une poutre composée BFUP armé – béton armé, le BFUP armé réduit les contraintes de fatigue dans les barres d'armature placées dans le haut de la section de béton armé. Ainsi, en appliquant une couche de BFUP armé, l'élément de béton armé est efficacement renforcé pour la fatigue.

***Mots-clés**: Béton Fibrés Ultra-Performant (BFUP), BFUP armé, élément composé, comportement en fatigue, limite d'endurance à la fatigue, renforcement de dalles de pont*

Zusammenfassung

Ultra-Hochleistungs-FaserBeton (UHFB) ist ein zementöser Verbundwerkstoff zusammengesetzt aus Zement, Quarzsand, Silikatstaub und Fasern. UHFB weist ausgezeichnete Eigenschaften auf: eine relativ hohe Druckfestigkeit (grösser als 150 MPa) und Zugfestigkeit (grösser als 7 MPa), eine ausgeprägte Verfestigung unter Zugbeanspruchung (bei einem gewissen Fasergehalt) sowie eine sehr hohe Dichtigkeit wegen seiner optimierten, kompakten Matrix. Aufgrund dieser Eigenschaften eignet sich UHFB dazu, jene Bereiche eines Tragwerks "zu härten", die sehr starken mechanischen Beanspruchungen und Umwelteinflüssen unterworfen sind. Beispielsweise kann UHFB oder UHFB bewehrt mit Bewehrungsstäben (Stahl-UHFB) als Verstärkungsschicht in Verbund auf Bauteilen aus Stahlbeton aufgebracht werden, um so den Tragwiderstand und die Dauerhaftigkeit von Bauteilen zu verbessern. Diese Methode ist besonders für Bauteile interessant, wo die UHFB-Schicht vorwiegend durch Zugspannungen infolge Radlasten beansprucht wird. In diesem Fall wirken wiederholte Zugspannungszyklen auf den UHFB ein, womit bei der Bemessung ein genügender Ermüdungswiderstand von UHFB (resp. Stahl-UHFB) und von UHFB – Stahlbeton Verbundbauteilen nachzuweisen ist.

Das Ziel dieser Dissertation besteht darin, das Ermüdungsverhalten von UHFB, Stahl-UHFB und Stahl-UHFB – Stahlbeton Verbundbauteilen (RU-RC Balken) mit einem umfassenden Versuchsprogramm zu untersuchen. Dazu wurden Ermüdungsversuche mit konstanten Spannungsamplituden an Zugprobekörpern aus UHFB und Stahl-UHFB durchgeführt, während die Ermüdungsversuche an den RU – RC Biegebalken einen Plattenstreifen aus einer Brückenfahrbahnkragplatte darstellen, der mit einer Stahl-UHFB Schicht verstärkt ist.

Die Versuchsergebnisse deuten auf eine Ermüdungsdauerfestigkeit bei 10 Millionen Spannungswechseln hin, welche maximal pro Ermüdungsversuch gefahren wurden. Eine Ermüdungsbeanspruchung oberhalb dieser Dauerfestigkeit führte zu einer bedeutenden Ermüdungsschädigung mit einer entsprechend eher kurzen Ermüdungslebensdauer. Die Dauerfestigkeit von UHFB lag bei etwa 70% der elastischen Festigkeit des UHFB. Es konnten vergleichsweise grosse Abweichungen der lokalen Verformungen des UHFB gemessen werden, was auf Variationen der Materialeigenschaften zurückzuführen war, insbesondere bei der elastischen Zugfestigkeit und der Entfestigungsverformung. Diese lokal unterschiedlichen Materialeigenschaften verleihen dem UHFB ein bedeutendes Spannungs- und Verformungsumlagerungsvermögen und verbessern dadurch insgesamt das Ermüdungsverhalten. Die Ermüdungsbruchfläche von UHFB zeigte Merkmale von Ermüdungsbruchflächen von Stahl, indem das Ermüdungsrisswachstum zu einer eher glatten Oberfläche führte, während die Restbruchfläche uneben und rau war.

Die Ermüdungsdauerfestigkeit von Stahl-UHFB bei 10 Millionen Spannungswechseln lag bei etwa 54% des Tragwiderstands des Probekörpers. Bei dieser Ermüdungsbeanspruchung war der UHFB im verfestigenden Bereich beansprucht. Das Ermüdungsverhalten zeichnete sich dadurch aus, dass der jeweilige Beitrag von UHFB und Bewehrung am Ermüdungswiderstand

von Stahl-UHFB vor allem von der maximalen Ermüdungsspannung abhängt. Es findet eine Umlagerung der Spannungen vom UHFB zur Bewehrung statt, was schliesslich das Ermüdungstragfähigkeitsvermögen beider Werkstoffe verbessert.

Die Ermüdungsdauerfestigkeit der RU-RC Biegebalken bei 10 Millionen Spannungswechseln lag bei etwa 50% des Tragwiderstands. Die Zunahme der Verformungen in der Stahl-UHFB Schicht war durch die Abnahme des Verformungsmoduls (als Verhältnis von Spannung zu Verformung) des UHFB infolge Ermüdung erklärbar, was zu einer Spannungsumlagerung vom UHFB zu den Bewehrungsstäben führte. Das Ermüdungsversagen der RU-RC Biegebalken wurde durch den Ermüdungsbruch der Bewehrungsstäbe in der Stahl-UHFB Schicht bestimmt. Dies bedeutet, dass die Ermüdungsspannungsamplitude in den Bewehrungsstäben der Stahl-UHFB Schicht die massgebende Einflussgrösse der Ermüdungsfestigkeit der RU-RC Balken war. Aus diesen Erkenntnissen wurden Regeln für den Ermüdungsnachweis von RU-RC Biegebauteilen auf Makro-Stufe (Biegetragwiderstand des RU-RC Bauteils) und Meso-Stufe (Spannungsamplitude in der Bewehrung der Stahl-UHFB Schicht) hergeleitet.

Zudem wurde das Ermüdungsverhalten von UHFB unter Zugspannungen mit Hilfe von Ansätzen aus der Schädigungsmechanik analysiert. Daraus konnte die Erkenntnis gewonnen werden, dass bei Ermüdungsversagen von UHFB die Schädigung im UHFB während beinahe der gesamten Ermüdungslebensdauer mit einer konstanten Geschwindigkeit fortschreitet, wobei eine bedeutende Schädigung im UHFB bereits im Frühstadium der Ermüdungslebensdauer auftritt. Daraus konnten ein bilineares Schadensfortschrittsmodell hergeleitet und eine Methode zur Ermittlung der Restlebensdauer hergeleitet werden.

Schliesslich wurde die Abnahme des Verformungsmoduls des UHFB im Stahl-UHFB infolge Ermüdung untersucht. Es wurde ein ähnliches Ermüdungsverhalten festgestellt, indem das Verformungsmodul aller Stahl-UHFB Probekörper abnahm. Daraus ergab sich eine empirische Beziehung zwischen dem Verformungsmodul von UHFB im Stahl-UHFB und der Anzahl Ermüdungsspannungswechsel, mit der das Ermüdungsverhalten von Stahl-UHFB unter Zugbeanspruchung beschrieben wird. Durch die Anwendung dieser Beziehung konnten mit Hilfe der Euler-Bernoulli Biegetheorie die Verformungsamplituden der geprüften RU-RC Biegebalken berechnet werden. Es konnte so die Erkenntnis gewonnen werden, dass die Ermüdungsbeanspruchung vor allem von der Stahl-UHFB Schicht aufgenommen wird. Dadurch wird die Spannungsamplitude in der Bewehrung des Stahlbetonbauteils deutlich reduziert, womit der Stahlbeton in Bezug auf die Ermüdung durch das Aufbringen einer Stahl-UHFB Schicht wirksam verstärkt wird.

***Stichworte**: Ultra-Hochleistungs-Faserbeton (UHFB), Stahl-UHFB, Verbundbauteil, Ermüdungsverhalten, Ermüdungsdauerfestigkeit, Verstärkung von Brückenfahrbahnplatten.*

Acknowledgements

Foremost, I would like to express my sincere gratitude to my thesis director Prof. Eugen Brühwiler for the opportunity to conduct research at his laboratory MCS, for the continuous support of my doctoral study and research, for his patience, motivation, enthusiasm, and immense knowledge. His guidance helped me in all the time of research and writing of this thesis. I could not have imagined having a better director and mentor for my doctoral study.

I would like to thank Dr. Emmanuel Denarié for his willingness to discuss problems and for his inspiring thoughts and ideas.

My sincere thanks go to the members of the jury for their time, effort and valuable input: Prof. Dirk Hordijk, Prof. Thomas Keller, Prof. Thomas Vogel and the president of the jury Prof. Anton Schleiss.

I would like to extend my gratitude to Prof. Minoru Kunieda, Dr. Hidetoshi Miyauchi and Mr. Yasushi Kamihigashi for their help and support; to Central Nippon Expressway Company Limited (NEXCO-Central) for allowing me to pursue a doctoral degree at EPFL and for their financial support.

The experimental program of this thesis could not have been conducted without the help of the engineers and technical staff at IIC. I would like to thank them: Sylvain Demierre, Gilles Guignet, Léa Frédérique Dubugnon, Patrice Gallay, Roland Gysler and Gérald Rouge.

I would like to thank my present and former colleagues at MCS for discussions and help: Christine Benoit-Roulin, Florence Grandjean, Hamid Sadouki, Alix Grandjean, Cornelius Oesterlee, Agnieszka Ewa Switek, Talayeh Noshiravani, Alexis Kalogeropoulos, Mohammadhadi Kazemi Kamyeb, Mark Anthony Treacy, Marina Rocha, Maléna Bastien Masse, Vasileios Grigoriou and Christophe Thierry Loraux.

Finally, I would like to thank my family for their support.

List of Figures

Chapter 1

Chapter 2

Chapter 3

Chapter 4

Chapter 5

List of Tables

Chapter 1

Introduction

This page is intentionally left blank.

Introduction

1.1 Context and motivation

In more economically developed countries, most of the infrastructures in service today were constructed during the middle to end of 20th century. Since design codes used for those infrastructures didn't consider the performance necessary for today's infrastructures in terms of ultimate, serviceability and fatigue limit states, these infrastructures need to be updated to satisfy current requirements through interventions.

As for road bridges, in order to keep up with the increase of traffic load, bridge deck slabs are often required to increase their load bearing capacity. Since road operators have to manage a large number of bridges with limited budget, more efficient and effective methods are called for to strengthen bridge deck slabs. In this context, a novel concept was proposed to overlay Ultra-High Performance Fibre Reinforced Composites (UHPFRC) or UHPFRC combined with steel rebars (R-UHPFRC) on top of bridge deck slabs for strengthening in 1999 [1.1]. Due to the properties of UHPFRC such as high compressive and tensile strength (≥ 150 and 7 MPa, respectively), tensile strain-hardening behaviour and high packing density, application of UHPFRC to the specific zone of structural members subjected to severe mechanical and environmental actions is an effective method.

For bridge deck slabs, fatigue loading is one of the most detrimental actions because of rather high live-to-dead-load ratio and hence large stress range is caused in components of bridge deck slabs. Comprehension and consideration of the fatigue behaviour of bridge deck slabs is essential in the design and examination processes of bridges. In view of this, when UHPFRC or R-UHPFRC are applied as strengthening elements to existing (and potentially also to new) bridge deck slabs, it is necessary to understand the fatigue behaviour of composite UHPFRC (R-UHPFRC) – bridge deck slab members. In addition, the fatigue behaviour of UHPFRC and R-UHPFRC as a strengthening element also needs to be understood for more focused application of those elements to fatigue vulnerable members like bridge deck slabs.

Since 1999, Laboratory of Maintenance and Safety of Structures (MCS) at École Polytechnique Fédérale de Lausanne (EPFL) has been conducting extensive research of UHPFRC as a cast-in-place strengthening material for existing structures. To date, eight doctoral theses have been published to investigate UHPFRC in terms of materials and structural engineering (Figure 1.1) ([1.2, 1.3, 1.4, 1.5, 1.6, 1.7, 1.8, 1.9]). In the domain of structural engineering, static behaviour of UHPFRC, R-UHPFRC and composite R-UHPFRC – reinforced concrete (RC) members (RU-RC members) have been studied in detail. As for fatigue behaviour, however, a limited investigation had been conducted solely on RU-RC members. At other institutes, although some researchers have published reports on the fatigue behaviour of UHPFRC ([1.10, 1.11, 1.12, 1.13, 1.14]) and R-UHPFRC ([1.15]), no reports on the fatigue behaviour of RU-RC members are found. Comprehensive studies have not been conducted about the fatigue behaviour of UHPFRC as a strengthening material and structural members strengthened with the UHPFRC.

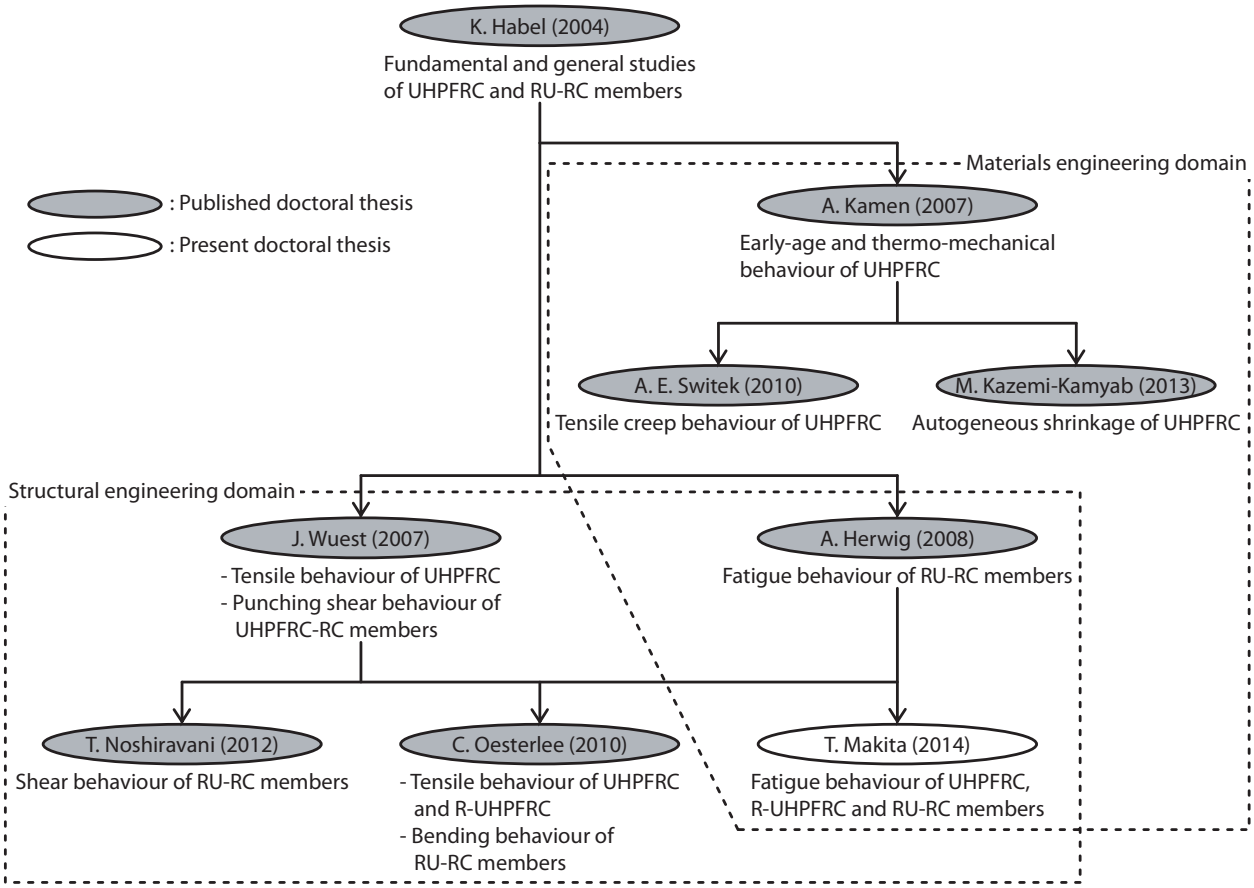

Figure 1.1 Research of UHPFRC by MCS at EPFL

1.2 Objective

When UHPFRC or R-UHPFRC is overlaid on top of RC bridge deck slab as the strengthening element, tensile fatigue stress is imposed on those overlays at the cantilever part by fatigue loading. Considering high tensile strength and tensile strain-hardening behaviour of UHPFRC, application of UHPFRC or R-UHPFRC to structural member solicitated by tensile stress is an effective intervention.

The general objectives of this thesis are as follows:

1) To understand the tensile fatigue behaviour of UHPFRC and R-UHPFRC

2) To understand the bending fatigue behaviour of RU-RC members

3) To develop empirical models for the tensile fatigue behaviour of UHPFRC and R-UHPFRC

4) To develop a model for the bending fatigue behaviour of RU-RC members

1.3 Methodology

In order to investigate the fatigue behaviour of UHPFRC, R-UHPFRC and RU-RC members, an experimental method was used. Uniaxial tensile fatigue tests were conducted on UHPFRC and R-UHPFRC plates, while bending fatigue tests were conducted on RU-RC beams.

Uniaxial tensile test was employed as the fatigue testing method of UHPFRC and R-UHPFRC instead of bending test because in bending fatigue test, stress redistribution occurs in bent section and the weakest link might not be located in the maximum bending moment zone or section [1.16], and thus one may question whether bending fatigue test provides objective results.

An experimental set-up representing a strip of RC bridge deck cantilever strengthened with R-UHPFRC was used in the bending fatigue tests of RU-RC beams. RU-RC beams were placed with R-UHPFRC layer of the top and fatigue force was applied to the RU-RC beams at the cantilever edge to cause negative bending moment.

The fatigue test results were analysed by drawing *S*-*N* diagram where the ratio of applied maximum fatigue stress/force to static strength was used as fatigue solicitation indicator *S*.

Fatigue behaviour of the specimens was analysed macroscopically using measurements obtained from the specimens. Fracture mechanism of UHPFRC and R-UHPFRC under tensile fatigue was understood by examination of the fracture surfaces based on fractography.

1.4 Scope

This thesis deals with the condition where tensile fatigue stress is imposed on UHPFRC. The behaviour of UHPFRC under compressive fatigue stress and tension-compression fatigue stress is outside the scope of this thesis.

The mix of UHPFRC used for the specimens in the experimental campaign was developed by MCS at EPFL. The material properties of UHPFRC and its time-dependent behaviour are not a subject of this thesis.

Thin plates of UHPFRC and R-UHPFRC and thin slab strips of RU-RC members were used as the specimens in the experimental campaign. Steel rebar ratio was not varied for the R-UHPFRC and RU-RC specimens. All the fatigue tests were conducted as force-controlled constant amplitude fatigue tests.

1.5 Overview

This thesis consists of five published and submitted papers with introduction and conclusion chapters (Figure 1.2):

Chapter 2 Tensile fatigue behaviour of Ultra-High Performance Fibre Reinforced Concrete (UHPFRC)
(published online in *Materials and Structures* on 23 April, 2013)

Chapter 3 Tensile fatigue behaviour of Ultra-High Performance Fibre Reinforced Concrete combined with steel rebars (R-UHPFRC)
(published in *International Journal of Fatigue*, Vol. 59, pp. 145-152)

Chapter 4 Fatigue behaviour of bridge deck slab elements strengthened with reinforced UHPFRC
(presented at *IABMAS 2012* and published in the proceedings edited by Biondini F., Frangopol D. M., Stresa, Italy, pp. 1974-1980)

Chapter 5 Damage models for UHPFRC and R-UHPFRC tensile fatigue behaviour
(submitted to *Engineering Structures* [version after revisions])

Chapter 6 Modelling of fatigue behaviour of bridge deck slab elements strengthened with reinforced UHPFRC
(submitted to *IABMAS 2014*)

Fatigue tests of UHPFRC, R-UHPFRC and RU-RC beams are summarised in Chapters 2, 3 and 4, respectively. Fatigue endurance limit at 10 million cycles was determined and characteristic fatigue behaviour was investigated. Fatigue fracture surfaces of UHPFRC and R-UHPFRC were examined to understand the fracture process in Chapters 2 and 3. Rules were deduced for the design of RU-RC members under bending fatigue and the corresponding fatigue safety verification in Chapter 4.

Damage models for tensile fatigue behaviour of UHPFRC and R-UHPFRC are developed in Chapter 5. The tensile fatigue behaviour of UHPFRC was analysed based on elementary damage mechanics theory and characteristics of damage evolution in UHPFRC were understood. A bi-linear damage evolution model of UHPFRC was proposed, with which the remaining fatigue life is determined. Fatigue damaging relationship was deduced to characterise the tensile fatigue behaviour of R-UHPFRC.

Finally, Chapter 6 presents a model to describe the fatigue behaviour of RU-RC beams. By considering fatigue damaging of R-UHPFRC adopting the relationship deduced in Chapter 5, the model was developed which determines stress and deformation evolution in components of the RU-RC beam. Experimental results were used to validate the model. In addition, function of R-UHPFRC in fatigue strengthening of RC member was discussed.

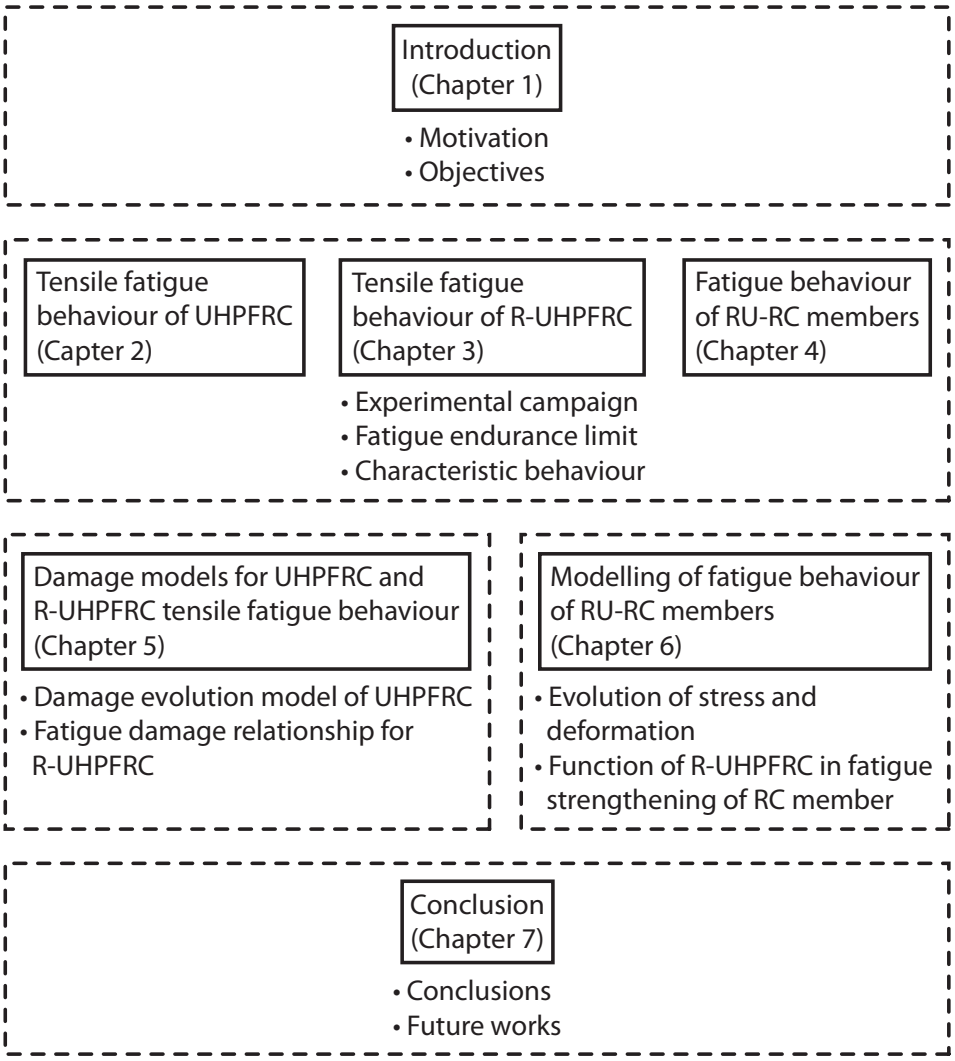

Figure 1.2 Structure of thesis

This page is intentionally left blank.

Chapter 2

Tensile fatigue behaviour of Ultra-High Performance Fibre Reinforced Concrete (UHPFRC)

Published online in *Materials and Structures* on 23 April, 2013

This page is intentionally left blank.

Tensile fatigue behaviour of Ultra-High Performance Fibre Reinforced Concrete (UHPFRC)

Abstract

The tensile fatigue behaviour of Ultra-High Performance Fibre Reinforced Concrete (UHPFRC) under constant amplitude fatigue cycles is presented. Three series of uniaxial tensile fatigue tests up to a maximum of 10 million cycles were conducted with the objective to determine the endurance limit of UHPFRC that was supposed to exist for this material. The fatigue tests reveal that an endurance limit exists in all three domains of UHPFRC tensile behaviour at *S*-ratios ranging from 0.70 to 0.45 with *S* being the ratio of the maximum fatigue stress to the elastic limit strength of UHPFRC. Rather large variation in local specimen deformations indicates significant stress and deformation redistribution capacity of the UHPFRC bulk material enhancing the fatigue behaviour. The fatigue fracture surface of UHPFRC shows features of the fatigue fracture surfaces of steel, i.e. fatigue crack propagation is identified by a smooth surface while final fracture leads to rather rough surface. Various fatigue damaging mechanisms due to fretting and grinding as well as tribocorrosion are identified.

Keywords: UHPFRC, tensile fatigue, endurance limit, fatigue deformation growth, fractography, determination of elastic limit strength

2.1 Introduction

Due to ever increasing traffic demands, deck slabs of bridges are subjected to significant fatigue loading. A novel method of rehabilitation and strengthening of bridge deck slabs in reinforced concrete (RC) is the casting of a 30 to 50 mm layer of Ultra-High Performance Fibre Reinforced Concrete (UHPFRC) with or without steel rebars on top of the existing slab. This method has proven to be technically more efficient and more economic than conventional methods consisting of adding an additional RC layer on the deck slab [2.1, 2.2, 2.3, 2.4]. In order to validate this concept, the fatigue behaviour of UHPFRC needs to be known and the fatigue strength determined.

UHPFRC is a cementitious fibre reinforced composite material showing eminent mechanical properties such as relatively high strength, i.e., tensile strength higher than 10 MPa with significant deformation capacity, compressive strength higher than 180 MPa and low-permeability providing very high resistance against penetration of water and other substances, thus enhancing durability.

A typical stress-strain response of UHPFRC from a quasi-static tensile test shows the following three domains (Figure 2.1):

- The elastic domain is governed by the behaviour of the matrix until it reaches its tensile strength, called the elastic limit strength. Microcracks start to form at the stress level in

the vicinity of the elastic limit.

- These microcracks are bridged and controlled by fibres. After entering the strain-hardening domain more microcracks develop in the whole specimen volume. A considerable reduction in modulus of deformation, i.e. the ratio of stress to strain, is observed. The strain-hardening extends until the ultimate resistance or tensile strength is reached in the weakest section of the specimen.
- In the strain-softening domain beyond ultimate strength, a discrete macrocrack forms in this weakest section and becomes eventually visible. Consequently, deformation localizes in the macrocrack zone while the zones outside are unloading. Finally the specimen fractures into two parts at the end of softening.

In this paper, a microcrack is defined as a crack not visible to the naked eye and its width is smaller than 0.05 mm. A macrocrack is defined as a crack visible to the naked eye and its width is larger than 0.05 mm; it occurs only in the post-peak softening domain.

The objective of this paper is to describe the tensile fatigue behaviour of UHPFRC. Despite a more demanding test set-up, uniaxial tensile fatigue tests (rather than bending tests) were conducted on monolithic UHPFRC plates thus providing more objective results. The experimental campaign is described and the test results are analysed and interpreted.

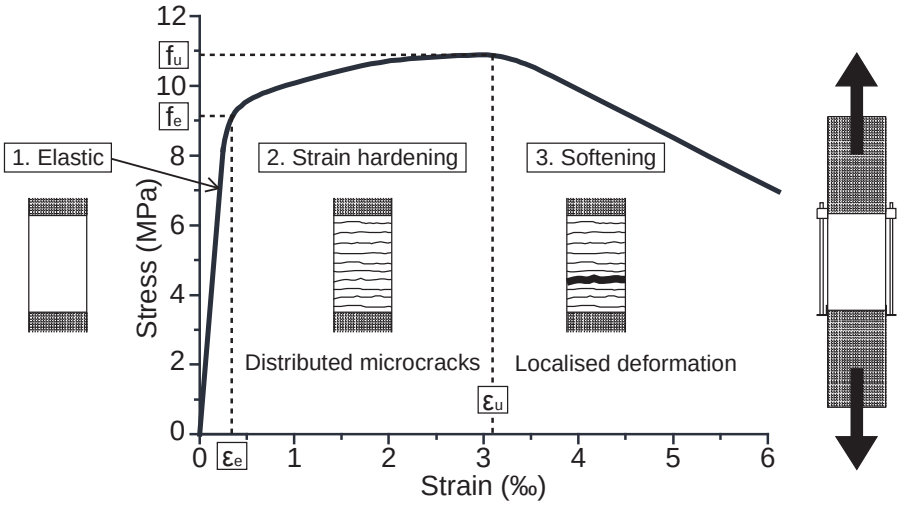

Figure 2.1 Schematic representation of tensile response of UHPFRC

2.2 Literature review

Four-point bending fatigue tests were carried out on specimens made of CERACEM®, a commercial UHPFRC [2.5]. A linear relation was found between the number of cycles and the deflection growth rate in the stage where deflection constantly increased. An endurance limit at 10 million cycles could however not be determined due to the large scatter of test results which was attributed to strength variations within the specimens.

Behloul et al. [2.6] performed three-point bending fatigue tests on Ductal® using steel

fibres. Specimens were first subjected to quasi-static flexural force preceding bending fatigue tests until the strain in the extreme tension fibre at the mid-span of specimens reached 0.30 ‰. Only one combination of fatigue minimum and maximum force, i.e. 10 % and 90 % of the bending elastic limit strength was applied under force control. Fatigue testing was stopped after about 1 million cycles where only little damage was observed on all specimens. After fatigue testing, the specimens were subjected to quasi-static flexural force again and there was no influence of preceding bending fatigue loading on the ultimate resistance of the specimens. An endurance limit at 1million cycles was estimated to be at about 54 % of the elastic limit strength.

Farhat et al. [2.7] conducted force-controlled three-point bending fatigue tests on High Performance Fibre Reinforced Cementitious Composites (HPFRCCs) named CARDIFRC® using specimens of two sizes. Scatter was observed in the results from larger specimens. Consistent results were obtained from the smaller specimens. The endurance limit at 1 million cycles was evaluated to be at 85 % of the flexural strength of the specimens. No visible cracks were observed on the fatigue tested smaller specimens that sustained 1million cycles. The fracture surfaces of larger specimens revealed areas devoid of fibres in the fracture surface, especially in the tensile zone or had many but poorly orientated fibres. Moreover, image analysis showed that the fracture surface had less homogenous and less dense fibre distribution when compared to other sections of the specimen.

Parrant et al. [2.8] carried out four-point bending fatigue tests on UHPFRC of the $CEMTEC_{multiscale}$® type including three different types of fibres. The endurance limit was evaluated as 65 % of bending tensile stress for 2 million cycles.

Fitik et al. [2.9, 2.10] performed uniaxial stress reversal and tensile fatigue tests on Ultra High Performance Concrete (UHPC) using four different mixes. The scatter in test results was attributed to local defects initiating and accelerating failure progression. Deformation growth during the fatigue tests was demonstrated to be divided into three stages similar to concrete, namely rapid deformation growth due to initial crack formation in the first stage, stable deformation growth with constant crack propagation rate in the second stage and rapid deformation growth to failure caused by instable crack growth.

This literature review reveals that comprehensive uniaxial tensile fatigue testing of UHPFRC has not been performed so far and knowledge of tensile fatigue behaviour of UHPFRC is rather scarce. In previous studies, bending fatigue tests were often conducted because of experimental simplicity and the number of cycles was often limited to 1 million. One may question whether bending fatigue tests provide objective results as stress redistribution occurs in bent sections [2.11].

2.3 Experimental campaigns

2.3.1 Specimens, test set-up and instrumentation

The in-house developed UHPFRC mix called HIFCOM 13 was used for the experiments. This mix is characterised by 3.0 vol.-% content of 13 mm long steel fibres with a diameter of 0.16 mm and by the use of CEM III/B type cement which contains a high percentage of blast furnace slag (66 % to 80 %) (Table 2.1).

The chosen specimen is 750 mm long with a cross section of 150 mm × 40 mm (Figure 2.2). Specimens were cast in wooden forms and demoulded 7 days after casting, and then kept in the testing hall at constant climate condition. In order to cause fracture within the 250 mm-long central zone of the specimen, aluminium plates (250 mm long, 150 mm wide and 2 mm thick) were glued using epoxy resin to both surfaces of the specimen end parts as strengthening elements.

Two 250 mm-long Linear Variable Differential Transducers (LVDTs) and five displacement transducers with a 50mm measurement length were used to measure the specimen deformation (Figure 2.2). LVDTs were set up on both of specimen sides such as to capture global specimen deformation. In this paper the average of deformation as measured by the two LVDTs are always referred to as global deformation. The five displacement transducers were set up on the specimen surface to measure local specimen deformation in five consecutive zones. Force was measured by the load cell installed in the actuator of the 1,000 kN servo-hydraulic testing machine.

Deformation and force data were recorded with a frequency of 200 Hz. The initial and final phases of the test were recorded permanently, while between these phases data was recorded for 1 second every 600 cycles.

All specimens were cast on the same day. They had an age of more than 56 days when tested.

Table 2.1 Composition of UHPFRC (HIFCOM 13)

Component	Type	Mass [kg/m^3]	Remarks
Cement	CEM III/B	1277.4	
Silica fume	Elkem Microsilica 971 U	95.8	7.5 % of cement mass
Sand	Quartz sand MN 30	664.6	d_{max}<0.5 mm
Steel fibres	Bekaert OL 13/0.16 mm	235.5	3.0 vol.-%, brass coating
Superplasticiser	Sikament P5	42.3	3.3 % of cement mass
Water		198.0	W/C=0.155

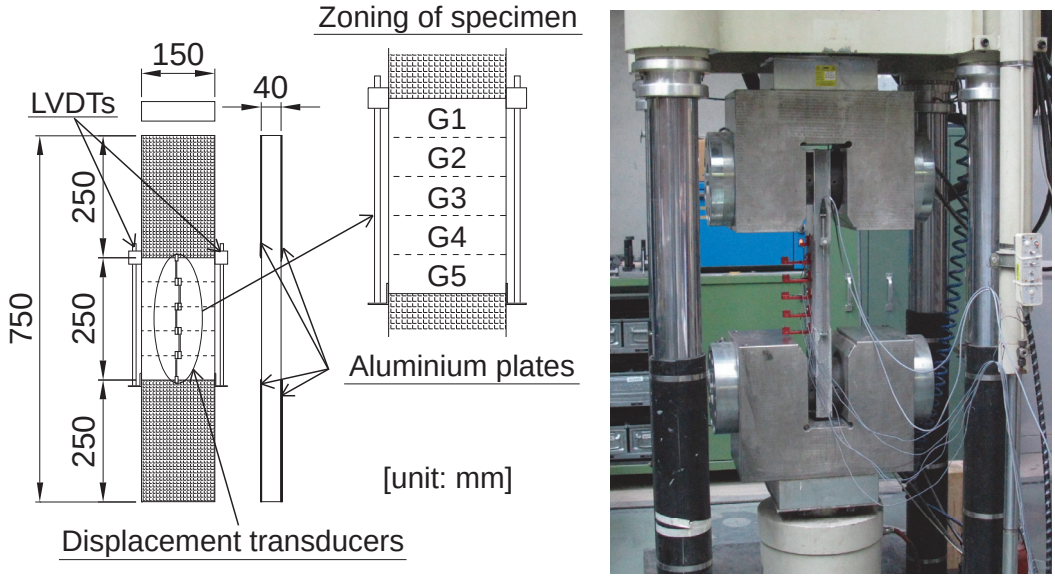

Figure 2.2 Specimen geometry, measuring devices and testing set-up

2.3.2 Determination of elastic limit strength

Three quasi-static tensile tests were conducted per test parameter to determine the quasi-static specimen behaviour as well as the elastic limit and ultimate strengths. Ultimate strength is defined as the maximum force UHPFRC was resisting during the test divided by the nominal cross section area. The elastic limit strength cannot always be identified clearly by a distinct point on the stress-strain curve. Adopting methods to determine modulus of elasticity of concrete and yield strength of steels, a method to determine the elastic limit strength of UHPFRC was developed as shown in Figure 2.3:

- Firstly, point P1 is chosen at 3 MPa assuming that this lower stress level is at about 30 % of the expected elastic limit strength (of about 10 MPa) such as to eliminate initial nonlinear stress carrying effects often observed for cementitious materials; point P2 at 6 MPa is chosen as an upper stress level of about 60 % of the expected elastic limit strength.
- A line L1 passing through P1 and P2 is drawn to find P3 as the intersection with the strain axis.
- Line L1 is then translated by 0.1 ‰ to obtain the parallel line L2 which intersects with the recorded stress-strain curve to finally define the elastic limit strength (point P5) and the corresponding elastic limit strain.
- Moreover, the modulus of elasticity of UHPFRC E_U is determined as the slope of line L.

Using this method, average elastic limit strength and strain of the investigated UHPFRC was determined to be 8.2 MPa and 0.32 ‰ respectively.

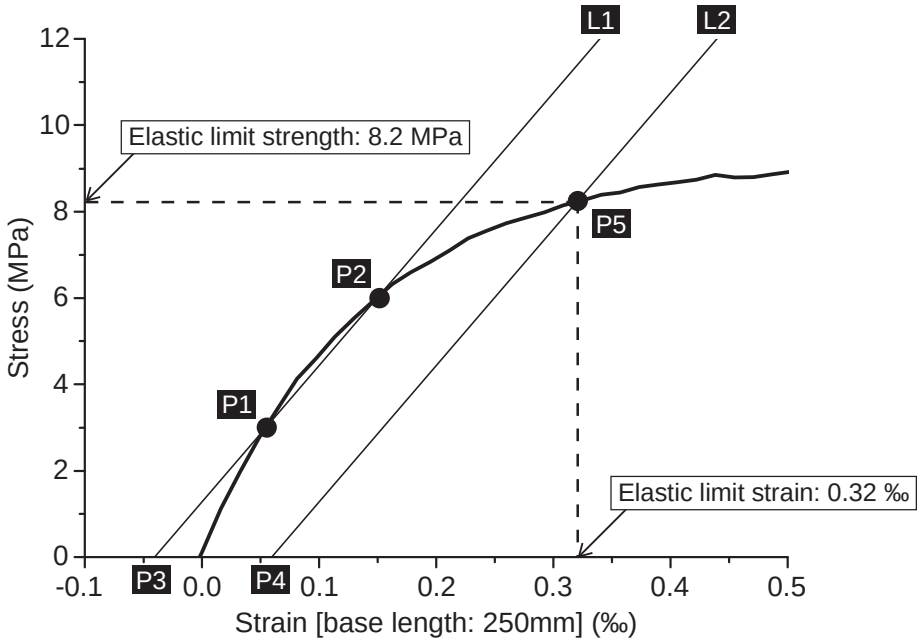

Figure 2.3 Determination of elastic limit strength of UHPFRC

2.3.3 Testing program

2.3.3.1 Objectives

Three series of constant amplitude tensile fatigue tests were conducted at various imposed fatigue stress levels as characterized by varying maximum stress and pre-applied deformation. Each fatigue test series is characterised referring to the quasi-static stress-strain curve following (Figure 2.4):

- S1 series: maximum stress high in the elastic domain
- S2 series: initial application of deformation entering into the strain-hardening domain followed by fatigue testing
- S3 series: initial application of deformation entering into the softening domain followed by fatigue testing

The objective of the S1 series was the determination of the endurance limit within the elastic domain. The comprehension of tensile fatigue behaviour beyond the elastic limit after losing the initial modulus of deformation of the specimen was the objective for the S2 and S3 series.

In this paper, the endurance limit is defined as a stress level below which no fatigue failure occurs up to 10 million cycles. With respect to bridge deck slabs, 10 million extreme stress cycles are considered to be realistic for heavily trafficked bridges. Also, limited available time for the experimental campaign imposed a maximum number of 10 million cycles which is usually considered as a lower bound of the very high cycle fatigue domain [2.12].

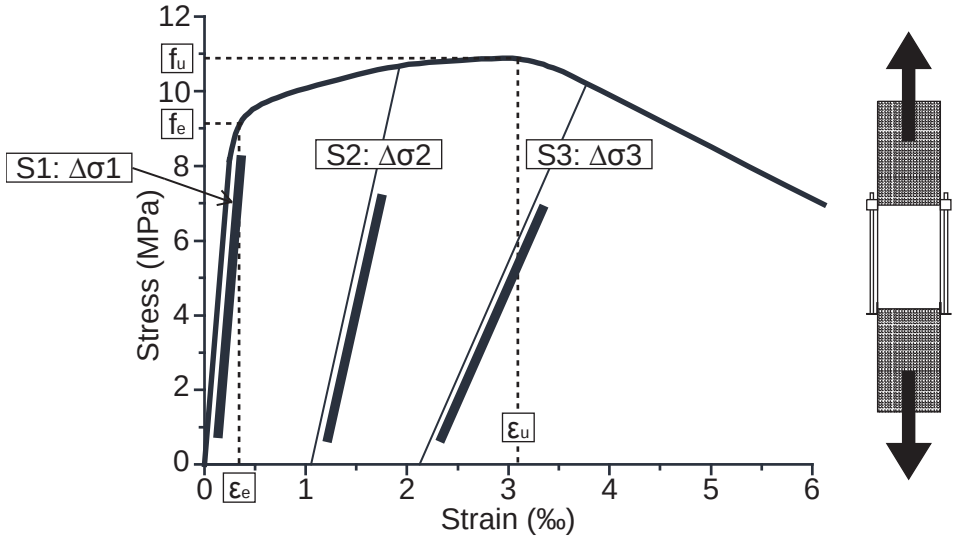

Figure 2.4 Schematic representation of tensile response of UHPFRC and definition of tensile fatigue test series

2.3.3.2 S1 series: tensile fatigue behaviour within the elastic domain

In preliminary fatigue tests, a specimen sustained 10 million cycles at a maximum stress of 7.2 MPa (and minimum stress of 0.82 MPa), then a second time 10 million cycles after increasing to 8.5 MPa maximum tensile stress and failed (fractured) finally after 7.45 million cycles at a maximum tensile fatigue stress of 10 MPa.

From this preliminary test result the endurance limit of the investigated UHPFRC was supposed to exist between 8.5 MPa and 10 MPa which is in the domain of the elastic limit strength. To verify this supposition, S1 series were conducted to have maximum stress at high stress levels within the elastic domain.

Maximum stress was determined by the following procedure: first, the specimen was subjected to quasi-static tensile stress until one LVDT reached a target deformation (corresponding to strains of either 0.20 ‰, 0.25 ‰ or 0.30 ‰) and unloaded. The stress that caused the target deformation was then applied as maximum stress level for the fatigue test. Because of the variation of elastic limit strength (which is most likely due to local variations of fibre distribution and orientation [2.13]), deformation (instead of stress) provides more reliable information about the tensile behaviour of UHPFRC.

Three target strain values were chosen assuming that if the strain caused by the initial cycle is smaller than 0.25 ‰, UHPFRC under the corresponding tensile fatigue stress can sustain 10 million cycles. This threshold strain value of 0.25 ‰ was justified from results of the preliminary tensile fatigue test. The idea of a threshold strain value for the endurance limit was also taken from findings of Parrant et al. [2.8].

The minimum fatigue stress was always set equal to 10 % of the average elastic limit strength as determined from three quasi-static tensile tests. In the real structural member, complete unloading is unlikely to occur. Therefore, small stress was given as a minimum fatigue stress. 10 % of the average elastic limit strength was arbitrarily chosen.

2.3.3.3 S2 and S3 series: fatigue behaviour after preloading into the strain-hardening and softening domains

When a UHPFRC layer is cast on an existing concrete element, tensile eigenstresses develop in the UHPFRC due to restrained shrinkage. The combination of these eigenstresses and stresses due to external action effects, i.e. due to permanent and traffic loads in the case of bridge deck slab, may result in tensile stress in the UHPFRC entering into the strain-hardening domain. Subsequently, initial deformation modulus is significantly reduced preventing further stress increase in the UHPFRC layer [2.14]. S2 and S3 series were designed to reproduce such situations. For this, deformation corresponding to strains of between 0.5 ‰ and 4 ‰ in S2 series and to strains of between 3 ‰ and 6 ‰ for S3 series was imposed prior to starting the fatigue test.

Maximum fatigue stress was applied using again the method for S1 series considering the stress-strain curve obtained from the initially imposed quasi-static tensile deformation. The stress causing a specific global deformation was imposed as maximum fatigue stress, i.e. the stress corresponding to strains of either 0.10 ‰, 0.15 ‰ or 0.20 ‰. The minimum fatigue stress was always 10 % of maximum stress in both S2 and S3 series.

2.3.3.4 Testing procedure

All quasi-static tensile tests were conducted in a displacement-controlled mode with a displacement rate of 0.02 mm/min.

The fatigue stress application procedure was as follows. Firstly, stress was increased to the specified maximum stress under displacement control mode with a rate of 0.02 mm/min, then sinusoidal wave cyclic stress was imposed under force control mode with a frequency of 10 Hz. 10 seconds were needed for the transition period from quasi-static to the constant amplitude cyclic stress regime.

When a specimen sustained 10 million cycles, this result was regarded as ‘run-out’, and the test subsequently was continued at an increased maximum tensile fatigue stress.

2.4 Results and discussion of experimental tests

2.4.1 Fatigue strength and endurance limit

2.4.1.1 Overview of results

Table 2.2 summarises the results of tensile fatigue tests on UHPFRC specimens. Specimens were regarded as failed when the average of two global deformation readings reached 2.5 mm, corresponding to 10 ‰ of strain.

Due to logistic reasons, S1-1_i and S2-4_i test had to be stopped at 5 million cycles, and S2-4_ii test at 2 million cycles. S1-3_i test was continued until 20 million cycles in order to observe how the behaviour of UHPFRC changes when it is subjected to the fatigue cycles twice as high as the specified one, i.e. 10 million cycles. As a result, no obvious change was observed in the fatigue behaviour of UHPFRC.

Table 2.2 Results of tensile fatigue tests of UHPFRC

Preliminary test

Test No.		σ_{max} [MPa]	σ_{min} [MPa]	N [×10^6]	Remarks
1	i	7.2	0.82	10.00	run-out
	ii	8.5	0.82	10.00	run-out
	iii	10.0	0.82	7.45	

S1 series

Test No.		σ_{max} [MPa]	σ_{min} [MPa]	N [×10^6]	Remarks
1	i	5.0	0.82	5.00	run-out
	ii	6.6	0.82	0.35	
2		6.1	0.00	0.29	
3	i	7.8	0.82	20.00	run-out
	ii	8.7	0.82	0.43	
4		8.1	0.82	0.28	
5	i	8.2	0.82	10.00	run-out
	ii	10.8	0.82	0.06	
6		8.2	0.82	0.29	
7		8.5	0.82	0.15	
8		9.4	0.82	0.16	

Table 2.2 (continued) Results of tensile fatigue tests of UHPFRC

S2 series

Test No.		σ_{max} [MPa]	$f_{e,i}$ [MPa]	$\sigma_{max}/f_{e,i}$	ε_{pre} [‰]	N [×10^6]	Remarks
1		7.4	10.9	0.68	0.48	7.78	
2	i	6.3	10.1	0.62	0.50	10.07	run-out
	ii	7.8		0.77		10.06	run-out
	iii	8.8		0.87		7.09	
3	i	5.9	10.5	0.56	1.13	10.00	run-out
	ii	8.4		0.80		3.11	
4	i	6.9	10.7	0.64	1.99	5.00	run-out
	ii	9.0		0.84		2.00	run-out
	iii	10.4		0.97		0.06	
5	i	7.6	12.5	0.61	2.01	10.00	run-out
	ii	11.7		0.94		0.11	
6		5.2	9.0	0.58	2.09	7.87	
7	i	6.7	10.3	0.65	3.00	10.08	run-out
	ii	8.7		0.84		0.08	
8	i	6.0	10.3	0.58	4.00	11.36	run-out
	ii	7.9		0.77		1.60	

S3 series

Test No.		σ_{max} [MPa]	$f_{e,i}$ [MPa]	$\sigma_{max}/f_{e,i}$	ε_{pre} [‰]	N [×10^6]	Remarks
1	i	6.0	10.0	0.60	3.02	10.00	run-out
	ii	7.2		0.72		10.02	run-out
	iii	8.3		0.83		3.01	
2		5.3	11.5	0.46	4.00	9.20	
3	i	4.9	10.7	0.46	5.01	10.00	run-out
	ii	6.7		0.63		2.61	
4	i	4.5	8.4	0.54	5.03	10.00	run-out
	ii	6.6		0.79		0.01	
5		4.4	8.8	0.50	6.11	0.03	

$\sigma_{max(min)}$: imposed maximum (minimum) fatigue stress

N: sustained number of fatigue cycles

$f_{e,i}$: elastic limit strength of each UHPFRC specimen

ε_{pre}: pre-applied strain

An *S*-*N* diagram (Wöhler diagram) is adequate to represent results from fatigue tests and to determine the fatigue resistance. For cementitious materials, the ratio of maximum applied fatigue stress to tensile strength is often used as fatigue stress indicator *S*, in order to eliminate variations in material composition, specimen size and testing setup. A log scale is commonly used for the number of stress cycles *N*.

Figure 2.5 shows the *S*-*N* diagrams as obtained in the present study for UHPFRC, where *S* is determined as the ratio of maximum fatigue stress to the elastic limit strength f_e.

- In the case of the S1 series, the elastic limit strength obviously could not be determined for each specimen, and the average value of elastic limit strength as obtained from three quasi-static tensile tests was used to calculate *S*.
- As the specimens of S2 and S3 series were subjected to preloading beyond the elastic limit strength before fatigue testing, the value of elastic limit strength $f_{e,i}$ could be determined for each specimen.

2.4.1.2 Test series S1

Rather large scatter is observed on the *S*-*N* diagram (Figure 2.5a) which may be due to elastic limit strength value used to calculate the fatigue stress indicator *S*. Obviously, this elastic limit strength value is either too high or too low for single specimens in comparison with their own specific elastic limit strength. Consequently, *S* values of some tests are quite higher or lower than 1 despite the fact that the applied maximum fatigue stress was always smaller than the elastic limit strength.

Nevertheless, the results may be used to estimate the endurance limit of the S1 series. From the overall test results including all run-outs, the endurance limit may be estimated to be around *S* = 0.70 (as indicated by the horizontal dashed lines in Figure 2.5a). At maximum fatigue stress levels above the endurance limit, the results indicate rather short fatigue lives confirming the hypothesis that UHPFRC under fatigue tensile stress above a certain limit, i.e. the endurance limit, shows only small fatigue resistance.

2.4.1.3 Test series S2

The results shown in Figure 2.5b indicate a fatigue strength that may be expressed by a linear relation between $\sigma_{max}/f_{e,i}$ and Log *N*. A linear regression line was determined (without considering run-outs) with a correlation coefficient of -0.69, indicating reasonably good dependency between the two variables:

$$\frac{\sigma_{max}}{f_{e,i}} = -0.105 \cdot \mathrm{Log}N + 1.436 \qquad \textbf{Eq. 2.1}$$

The test results including the run-outs again allow estimating the endurance limit to be at an *S*-level of about 0.55 to 0.65 (as indicated by the horizontal dashed lines in Figure 2.5b).

2.4.1.4 Test series S3

Only few results are available (Figure 2.5c) and a relation describing the fatigue strength cannot be determined. The endurance limit may be estimated to be at about S = 0.45 (as indicated by a dashed horizontal line in Figure 2.5c).

Moreover, the magnitude of pre-applied deformation seems to have a major influence on the fatigue behaviour. Specimen S3-5 (not shown on Figure 2.5c) was subjected during preloading to a relatively high deformation into softening domain of 6 ‰ which was significantly higher than for the other specimens. Due to this preloading, a significant damage was probably induced in the specimen and subsequently, only relatively short fatigue life resulted. This indicates low fatigue strength for high deformation into the softening domain. This may be explained by significant fibre pull-out due to such large deformations.

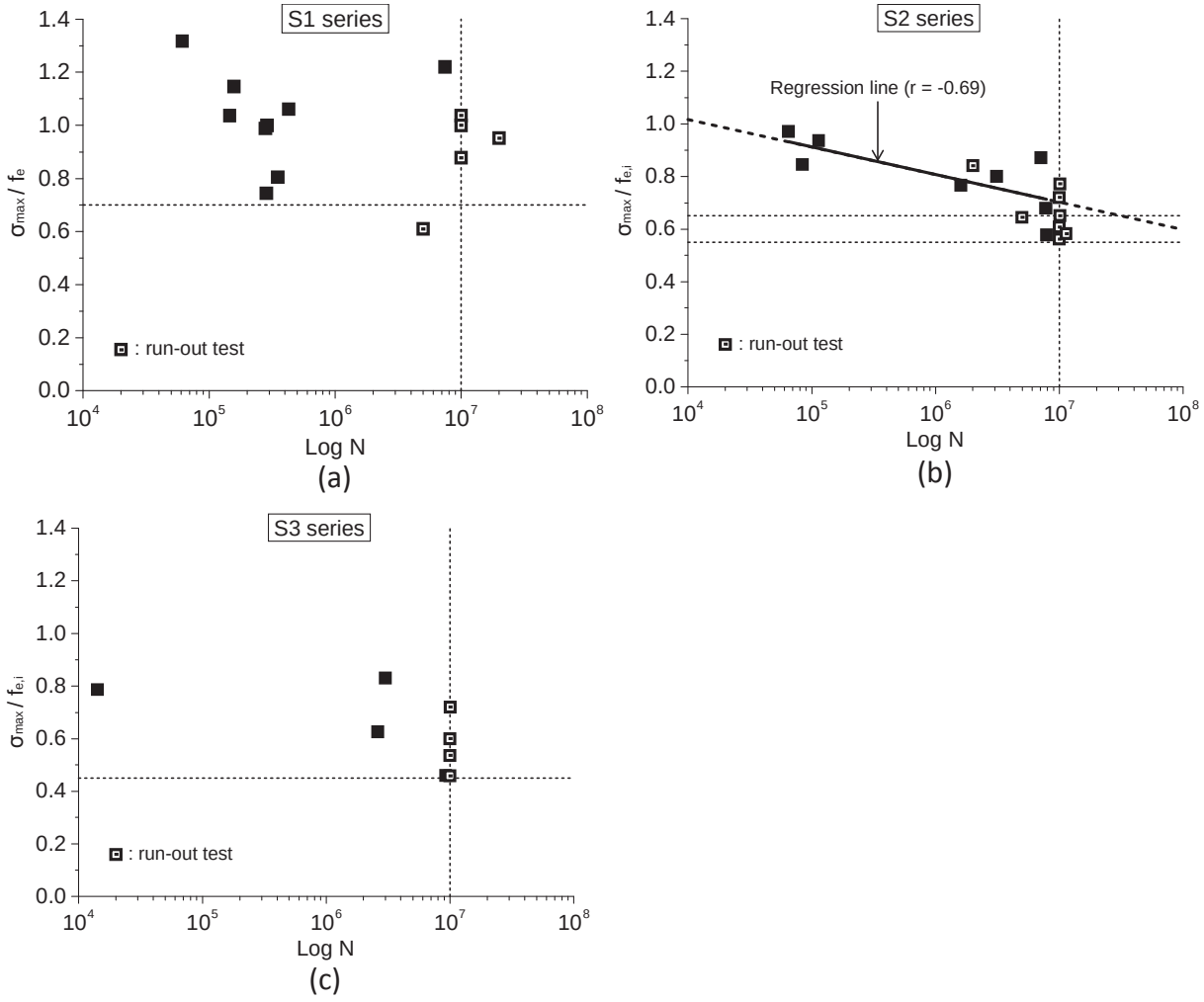

Figure 2.5 *S-N* diagrams of (a) S1 series, (b) S2 series and (c) S3 series

2.4.2 Deformation behaviour

In the present study, uniaxial tensile force was applied to specimens in both quasi-static and fatigue tests. Given the constant specimen cross section, nominal tensile stress in UHPFRC

is equal in any cross section. Yet, local deformation as measured with the five displacement transducers varied significantly over the specimen length as discussed in the following based on experimental observations.

Figure 2.6a shows stress-local deformation curves as obtained from quasi-static tensile preloading of S3-1 fatigue test, and Figure 2.6b is a magnified view of the stress-local deformation relationship. Loading was stopped when the global strain reached 3 ‰ (Figure 2.6c).

In the initial phase, deformation of all zones G1 to G5 increased similarly until stress reached about 4.5 MPa from where on significantly larger deformation readings were recorded in the G4 zone which entered first into the hardening domain. At 5 MPa, deformation readings increased significantly also in G5, followed by G1 and G3 zones at about 8 MPa and finally G2 zone at about 13 MPa. The very different response of each G-zone indicates variations in elastic limit strength, hardening behaviour and deformation modulus along the specimen when stressed in the strain-hardening domain as illustrated in Figure 2.7.

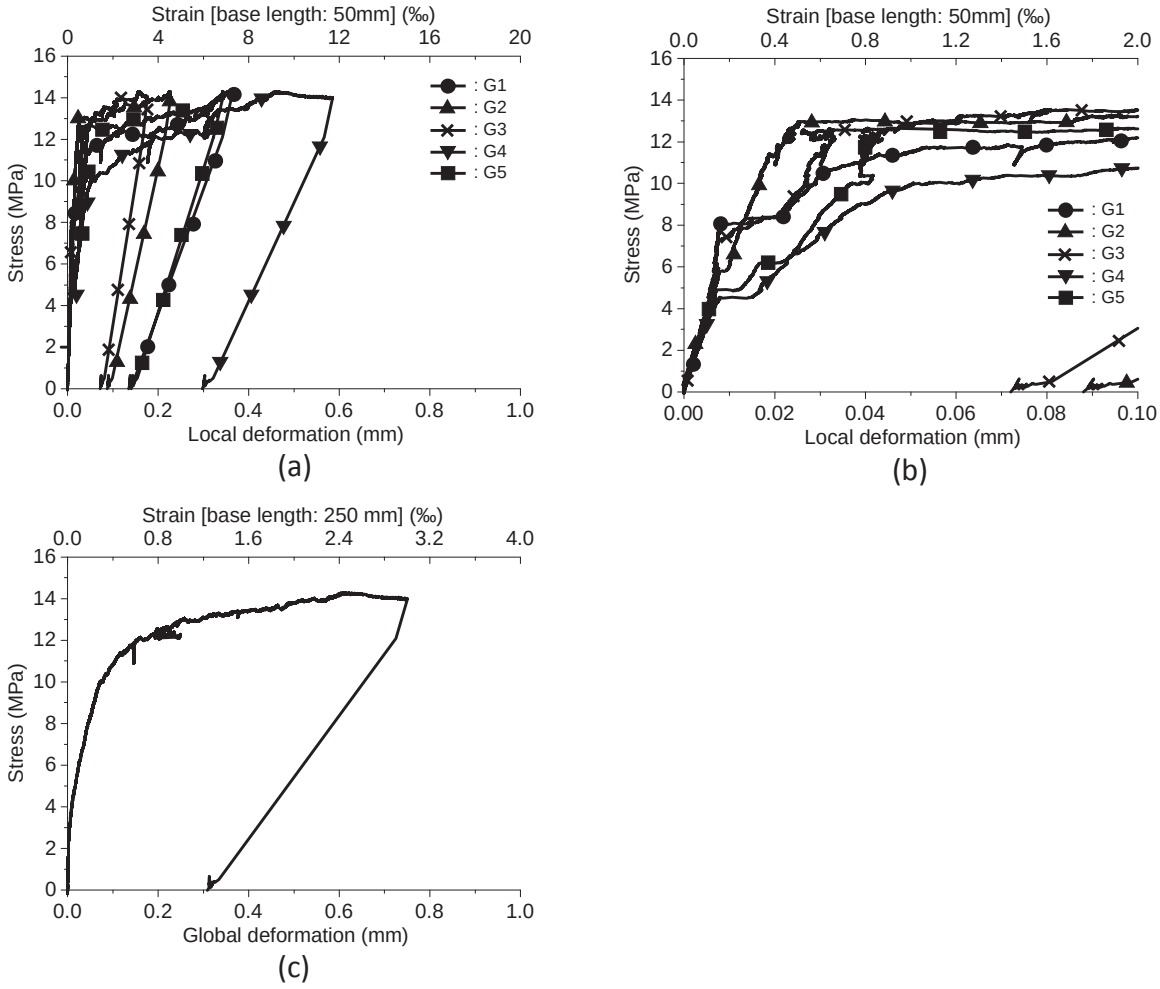

Figure 2.6 Stress-deformation curves obtained from quasi-static tensile preloading preceding the S3-1 test (a) local deformation, (b) zoom of stress-local deformation curve [0 to 0.1 mm], (c) global deformation

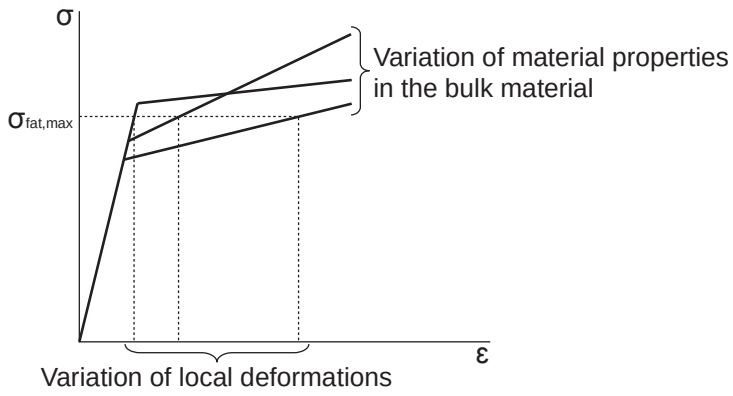

Figure 2.7 Variation of local deformation of UHPFRC under constant tensile fatigue stress

2.4.3 Deformation growth due to fatigue

2.4.3.1 Introduction

Tensile fatigue testing was conducted while imposing constant maximum and minimum stresses and the growth of specimen deformation as a function of stress cycles was recorded. There are thus some similarities with tensile creep testing. Fatigue deformation growth may thus include some creep deformation.

In the following, recorded deformation growth of UHPFRC specimens from the S1 series only is examined. In fact, in the S2 and S3 series, specimens showed no significant deformation growth as these specimens had already some initial deformation due to the preloading prior to the fatigue test. The deformation growth during the fatigue test was then relatively small and constant. Only in the final phase before failure, deformations increased substantially.

2.4.3.2 Deformation growth from S1 series

Fatigue deformation as recorded from the S1 series may be subdivided into four distinct types of behaviour:

1) Redistribution of localised deformation

Specimen S1-3 showed after about 9.1 million fatigue cycles a sudden increase in deformation in the G1 zone leading to a macrocrack with an opening reaching about 0.1 mm (Figure 2.8b). The specimen continued then to carry fatigue stress cycles up to 20 million cycles. This observation again confirms the capacity of UHPFRC to redistribute localised deformation. It is interesting to note that this localised deformation could not be captured by the global deformation readings (Figure 2.8a) because this localisation occurred outside the measuring domain of the LVDTs for global deformation.

After 20 million stress cycles, maximum stress was increased from 7.8 MPa to 8.7 MPa (S1-3_ii test), and similar deformation localisation occurred in two different zones (G2 and G3 zones), while the specimen continued to carry fatigue stress (Figure 2.9). Finally, the specimen

failed in G2 zone at 428,072 cycles while the two other zones with deformation localisation showed decreasing deformation values towards the end of the test.

Similar deformation growth curves were recorded from other specimens. It seems that even after localisation of deformation resulting in macrocrack openings of 0.1 mm, UHPFRC has the capacity to carry on tensile fatigue cycles by redistribution of localised deformation. The mechanism of this redistribution is supposed to be based on arresting further macrocrack growth when it enters into a zone with denser and better orientated fibres.

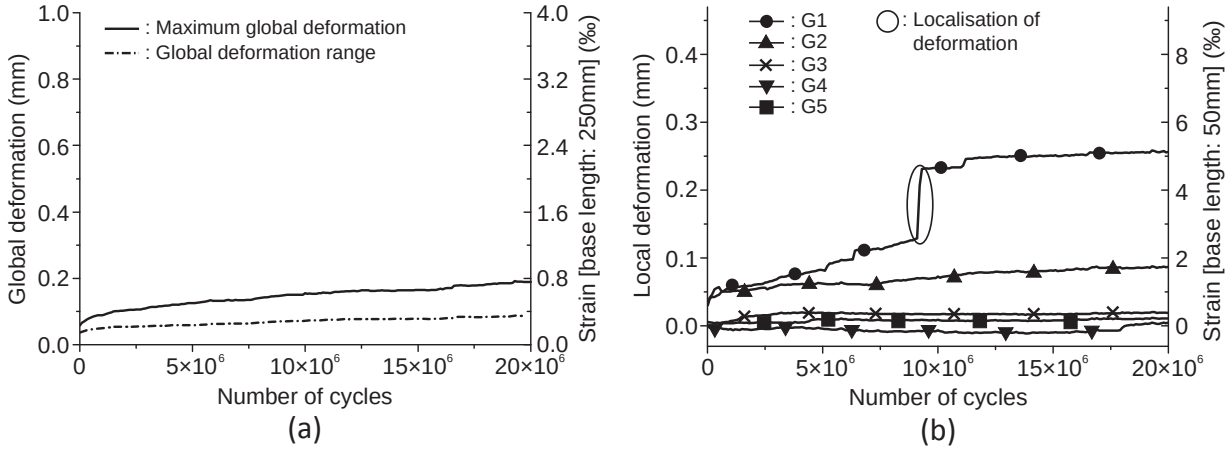

Figure 2.8 Deformation growth curve of the S1-3_i test (a) global deformation and global deformation range, (b) local deformation

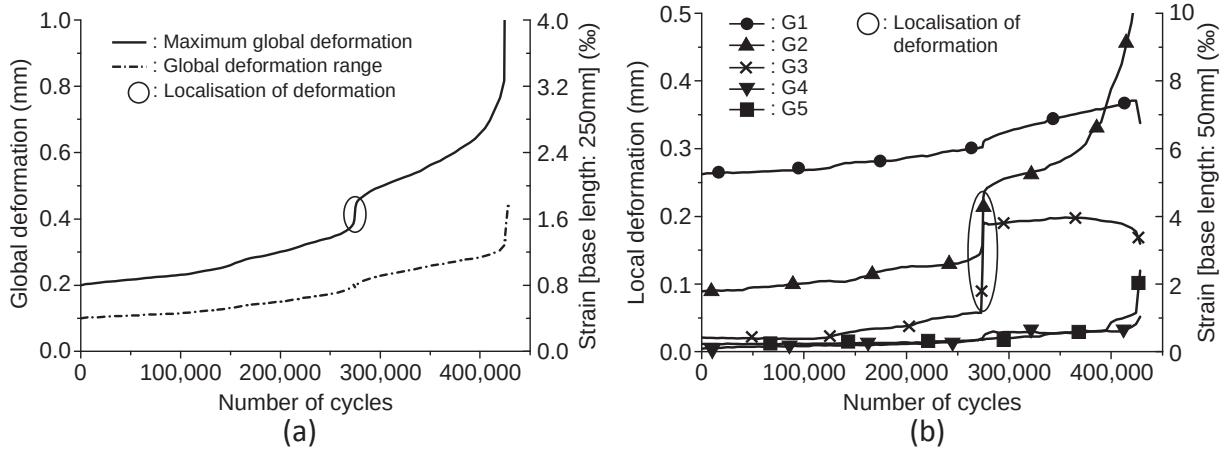

Figure 2.9 Deformation growth curve of the S1-3_ii test (a) global deformation and global deformation range, (b) local deformation

2) Variations in local deformation

Variations in local deformation measured with the five displacement transducers were also observed in tensile fatigue tests.

Figure 2.10b shows the growth of local deformations during the S1-5_ii test as a function of fatigue cycles. Deformation of the G4 zone increased very rapidly during the first 9,000 cycles,

and after 9,000 cycles its growth rate became suddenly relatively low. This may be attributed to the capacity of the UHPFRC to redistribute deformation under a given imposed stress while probably developing some change in microcrack pattern. Deformation development of the G3 and G5 zones was similar during the first 9,000 cycles; then, the deformation growth rate of the G3 zone became higher, while the deformation growth rate of the G5 zone reduced significantly to almost zero. The deformation growth rate of the G1 and G2 zones was quite constant during the fatigue test, implying that these zones were not influenced by deformation redistribution that occurred at 9,000 cycles. It can also be noted that deformation and deformation growth rate of the G1 and G3 zone were similar after 32,000 cycles until failure, and deformation of the G2 zone was gradually approaching deformation of the G5 zone.

Fatigue fracture occurred in the G4 zone. Consequently, deformation growth curve of the G4 zone was similar to the global deformation growth curve (Figure 2.10a). Although deformation behaviour of each G-zone influenced global specimen behaviour, the G4 zone predominantly influenced the global deformation behaviour of this specimen. From this it may be stated that the G1 to G3 and G5 zones were intact and still had fatigue stress carrying capacity after the fatigue fracture of the specimen.

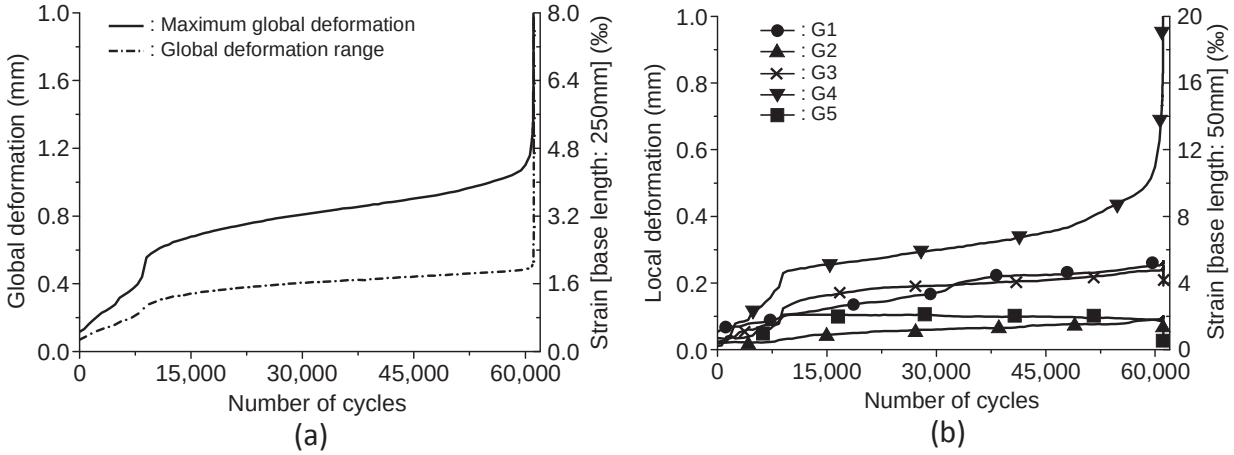

Figure 2.10 Deformation growth curve of the S1-5_ii test (a) global deformation and global deformation range, (b) local deformation

3) Change in deformation range

The deformation range, i.e. difference between maximum and minimum deformation, became larger with increasing number of fatigue cycles. The increase in rate of the deformation range was slightly smaller than that of maximum deformation, but the trends of both rates were similar. As stress cycles increased, maximum deformation also increased while minimum deformation remained almost constant, as shown in Figure 2.8a, 2.9a, and 2.10a where the dashed line represents the global deformation range.

4) Deformation growth and evolution of deformation modulus

Figure 2.11 shows the maximum global deformation plotted against the modulus of deformation *E* calculated as follows:

$$E = \frac{\sigma_{max} - \sigma_{min}}{\varepsilon_{max,i} - \varepsilon_{min,i}} \qquad \textbf{Eq. 2.2}$$

where σ_{max} and σ_{min} are the applied maximum and minimum fatigue stress (being constant); $\varepsilon_{max,i}$ and $\varepsilon_{min,i}$ are maximum and minimum global strain at cycle *i*. These curves were constructed for all specimens of the S1 series.

All curves show a similar trend despite the differences in applied stress level. A strong decrease of deformation modulus of UHPFRC is observed when the material enters into the domain corresponding to the strain-hardening domain observed in the quasi-static tensile test ("the equivalent strain-hardening domain" hereafter). Deformation modulus of UHPFRC decreases from about 38.9 GPa to 9.7 GPa when the material global strain grows from 0.32 ‰ to 1.66 ‰ corresponding respectively to the elastic limit and ultimate strength of UHPFRC determined from three quasi-static tensile tests. Thus, the stress carrying capacity of UHPFRC under tensile fatigue significantly decreases when the material deformation is within the equivalent strain-hardening domain. Habel [2.15] reported similar findings from cyclic tensile tests on a different UHPFRC mix (CEMTEC$_{multiscale}$®).

Decrease in the deformation modulus within the equivalent strain-hardening domain may be caused by progressive matrix cracking and fibre pull-out. In the softening domain, the decrease of deformation modulus became lower because of deformation localisation occurring in the macrocrack; further matrix cracking stopped and fibre pull-out occurred only in the localised macrocrack.

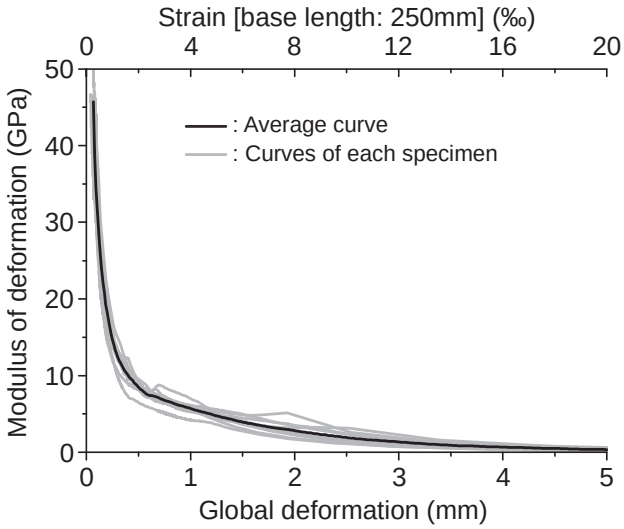

Figure 2.11 Relation between maximum global deformation and modulus of deformation

2.4.4 Uniaxial tensile tests

All the quasi-static and fatigue tests in this paper were conducted in the mode of uniaxial tension. Due to the possibility of asymmetric crack formation causing the specimens to bend, it was considered that uniaxial tensile force wasn't properly imposed on the specimens.

In order to investigate if the tests were done in uniaxial tension, the possibility of asymmetric crack formation was monitored by setting up displacement transducers on both surfaces of several specimens (five displacement transducers on each surface) during the S2 and S3 series. Deflection of the specimens wasn't explicit in measurements of the displacement transducers. Therefore, applied tensile force was regarded as uniaxial.

2.4.5 Fracture surface

2.4.5.1 Introduction

Fracture surfaces may provide important information to understand failure of materials. Fractography, aiming to analyse the characteristics of a fracture surface to indicate fracture mechanisms [2.16], has been used for failure analysis of metals for several decades. Since UHPFRC shows features of mechanical behaviour of metals, UHPFRC fatigue fracture surfaces were analysed by fractography to understand the fracture mechanisms of UHPFRC under tensile fatigue. Visual observation of fracture surfaces revealed three specific features as discussed in the following.

2.4.5.2 Matrix spalling and pulverisation

Figure 2.12 shows the fracture surface of a specimen that sustained more than 10 million fatigue cycles. Spalling of small matrix particles and pulverised matrix can be identified. It is speculated that pulverized matrix also contains unhydrated cement and silica fume. Spalling might have occurred when fibres were partially or fully pulled out of the matrix in a direction other than the fibre axis [2.17], as shown on Figure 2.13a. This mechanism is called snubbing [2.18], and bent fibres also observed on fracture surfaces are just a consequence of snubbing (Figure 2.13b).

Pulverisation of the matrix may be due to abrasion of spalling particles while the irregular faces of the rough fracture surface were subjected to fretting and grinding under fatigue cycles. As the fracture surfaces must be in contact for fretting, this mechanism can be referred to as roughness-induced closure which is one of the fatigue crack closure mechanisms in metals [2.19].

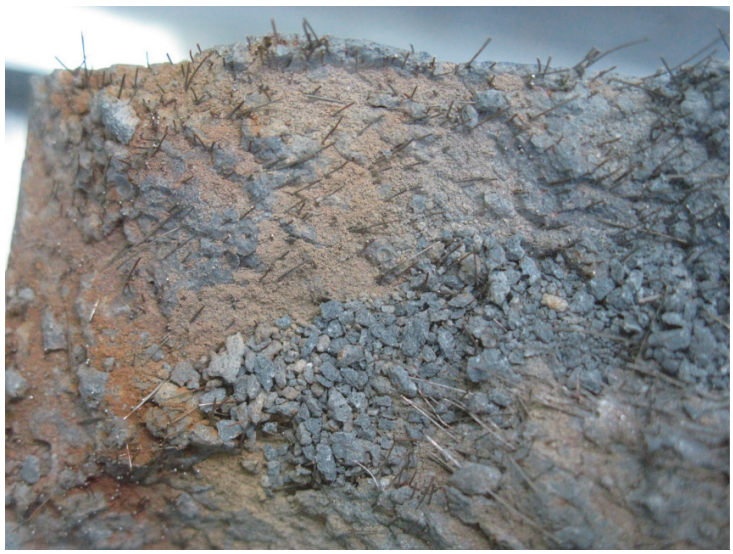

Figure 2.12 Fracture surface showing matrix spalling and pulverization

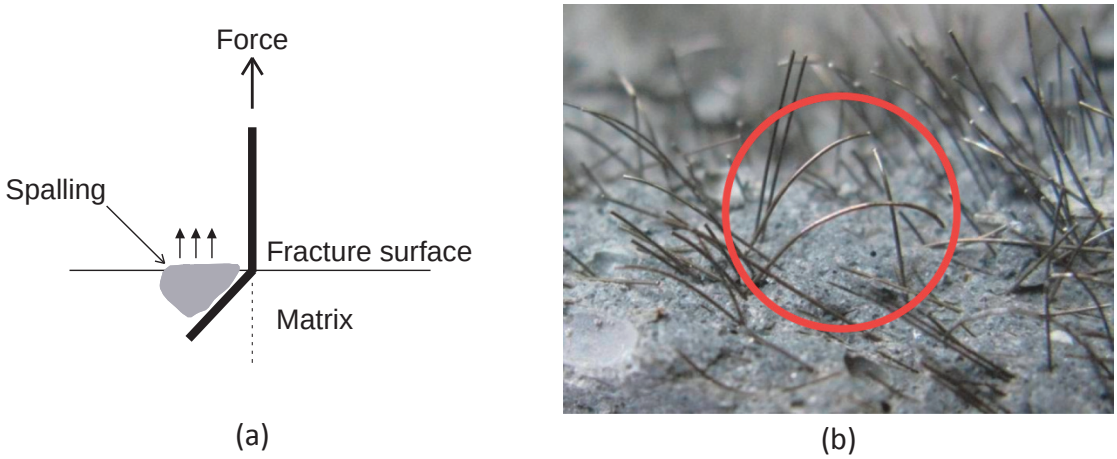

Figure 2.13 (a) Snubbing of fibre (after [2.18]) and (b) bent fibres due to snubbing

2.4.5.3 Smooth fracture surface area

Figure 2.14 shows a distinct area where the surface is smooth and shows only few fibres when compared to the rest of the fatigue fracture surface. This smooth area coincides with the location of fatigue fracture initiation. Similar smooth area is also observed on fatigue fracture surface of steel (Figure 2.15).

Two processes may explain the formation of a smooth fatigue fracture surface area:

- Due to the UHPFRC fabrication process, there is some variation in fibre distribution in the material volume, and consequently, local zones with smaller fibre content may exist [2.13]. Such zones have a lower stress carrying capacity and precocious microcracking is rather likely to occur leading to a significant fretting and grinding of the microcrack surfaces polishing them.
- A second process may be due to tribocorrosion fracture of fibres: fibres transfer tensile stress across micro- and macrocracks through the interface with the matrix (fibre bridging) (Figure 2.16). Under fatigue cycles, fibre pull-out and slip-back movement occur after

debonding of the fibres from the matrix (Figure 2.17), wearing away both the fibres and the matrix [2.21]. In the present study, the fibres are originally coated with a thin brass layer which is first removed by abrasion with the matrix. The bare steel surface of the fibres bridging the micro- and macrocrack is now exposed to the atmosphere. However, average relative humidity is about 40 % in the testing hall and corrosion of the bare steel is unlikely to occur because the corrosion rate of iron increases significantly at 60 % relative humidity [2.22]. More humidity or lower corrosion potential would thus be necessary for corrosion of the bare steel. As all water is consumed in the process of cement hydration in UHPFRC, supply of more humidity seems to be improbable. Lowering of corrosion potential can also be caused by wear of fibres with matrix, which is known as tribocorrosion phenomena which leads to corrosion of bare steel even in atmospheres with low humidity [2.23]. Corroding fibres bridging the fracture surface gradually lose their volume and are eventually fractured rather than pulled out of the matrix (Figure 2.18).

It may be stated that fatigue fracture mechanism of UHPFRC and steel seems to be similar. A macrocrack is initiated from the weakest location in the element and propagates under fatigue stress cycles. Gradually, the element loses its stress carrying capacity (resulting in a decrease in modulus of deformation). Finally, when the applied maximum fatigue stress reaches the ultimate resistance of the uncracked remaining cross section, the specimen fails. Fatigue crack propagation is identified by the smooth surface while final fracture leads to rather rough surface of UHPFRC.

Although fatigue fracture mechanisms of UHPFRC and steel show some similarities, fatigue crack propagation behaviour of UHPFRC and steel is dissimilar because of the difference in material structure. At meso-level, fatigue crack propagation in UHPFRC occurs when fibres are pulled out or fractured, and its behaviour might depend on fibre distribution. On the contrary, material structure of steel in meso-level is homogeneous and fatigue crack propagation occurs due to microplastic deformation [2.24].

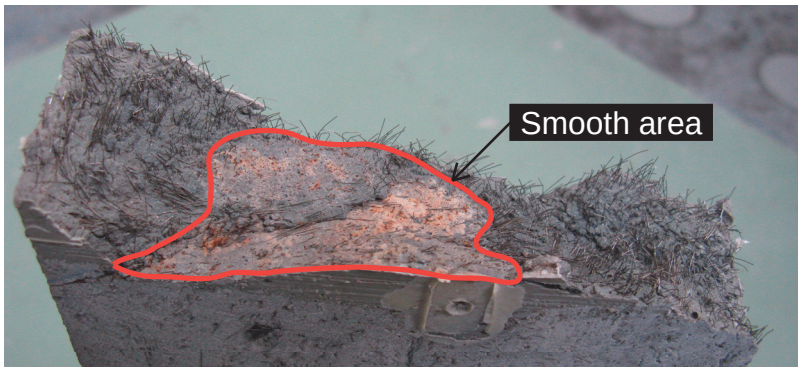

Figure 2.14 Smooth area of fatigue fracture surface of UHPFRC

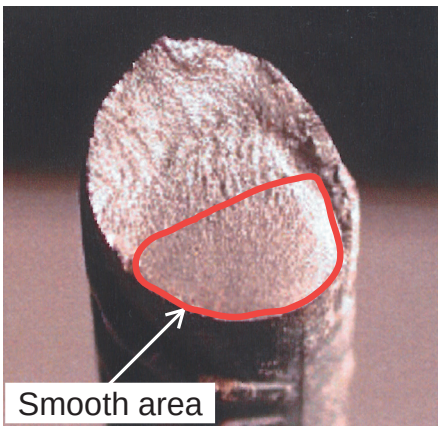

Figure 2.15 Fatigue fracture surface of a steel rebar [2.20]

Figure 2.16 Fibre bridging at cracked section

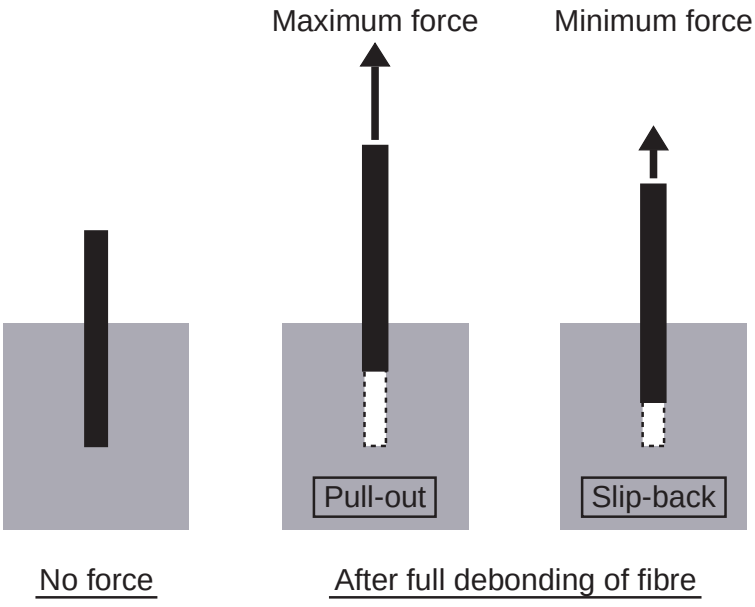

Figure 2.17 Fibre pull-out and slip-back movement

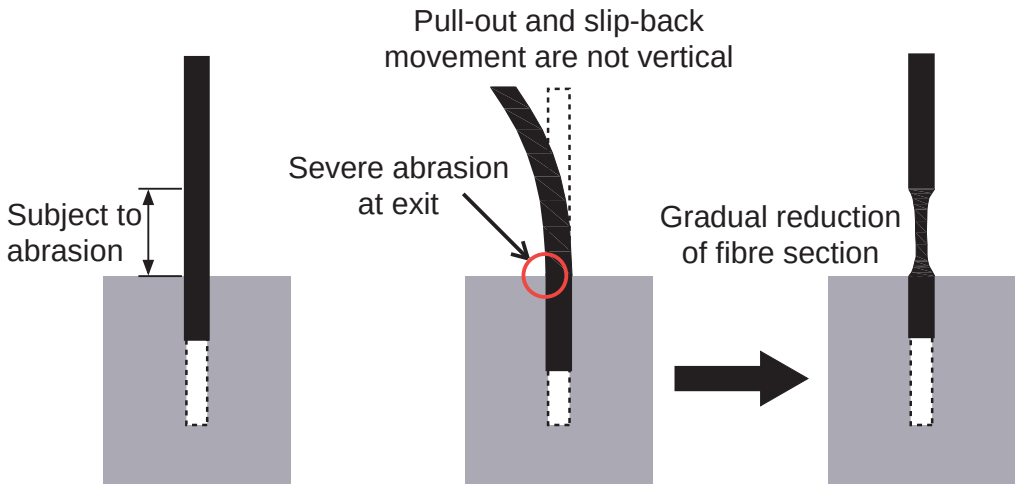

Figure 2.18 Abrasion of fibre with matrix

2.4.5.4 Rust-coloured powdery products

It was systematically observed that rust-coloured powdery products covered a part of the fracture surface, nearly matching the smooth surface area. Rust colour in small area around fibres was thicker than in other areas, implying that rust-coloured powdery products were provided by corrosion products from the fibres. Also, the rust-coloured powdery products were supposed to be mixes of pulverised matrix and corrosion products. In order to confirm this supposition, Energy Dispersive X-ray Spectroscopy (EDS) was used to analyse these powdery products, and the fracture surface of S3-2 test specimen covered with the rust-coloured powdery products was examined using a Scanning Electron Microscope (SEM).

Figure 2.19 shows the material composition of powdery products taken form the fracture surface analysed by EDS. Major components of normally coloured products were silicon and calcium, which are main matrix components while rust-coloured products had significant amounts of iron and oxygen, i.e. iron oxide, confirming the existence of corrosion products. Moreover, SEM analysis of fracture surface revealed the existence of significant amounts of corrosion products in rust-coloured area.

Figure 2.20 shows SEM images of both normally coloured and rust-coloured areas of fatigue fracture surface of the S3-2 test specimen. In the normally coloured area, components of matrix such as hydration products, sand and slag grains were identified. In the rust-coloured area, whitish parts indicate corrosion products and a hole seems to be created by fibre pull-out.

Figure 2.21a shows a steel fibre in the rust-coloured area. Rough fibre surface is clearly recognised. This is in contrast with the surface of a steel fibre (of same type) in its original condition (Figure 2.21b) with a flat and smooth surface. Figure 2.21a also suggests that the fibre surface (from the rust-coloured area) was roughened by abrasion and fretting with the surrounding matrix.

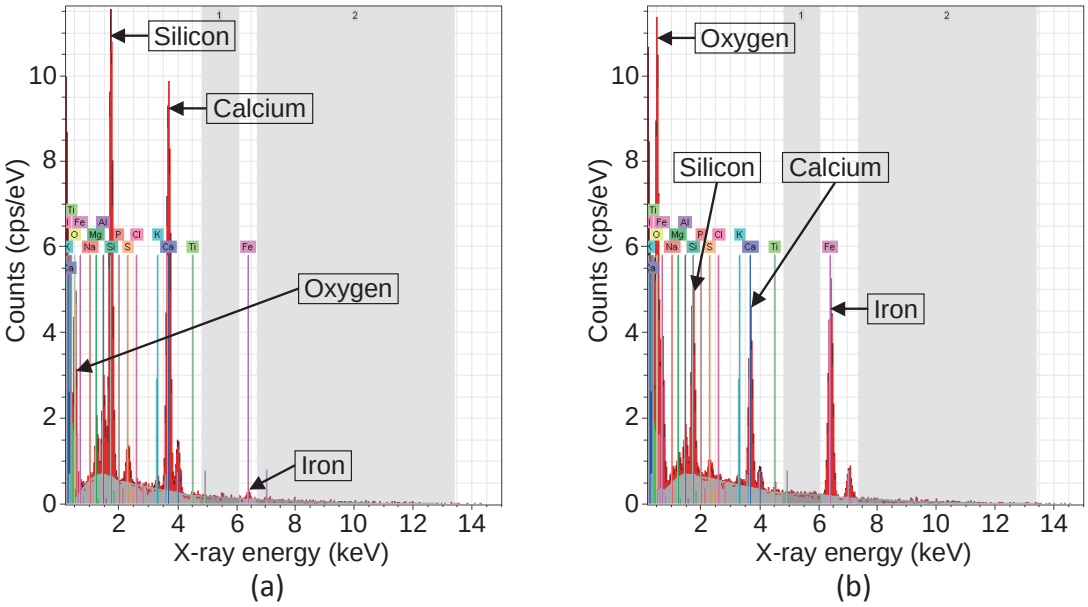

Figure 2.19 Material composition of products from the fracture surface of the S3-2 test specimen (a) normally coloured area, (b) rust-coloured area

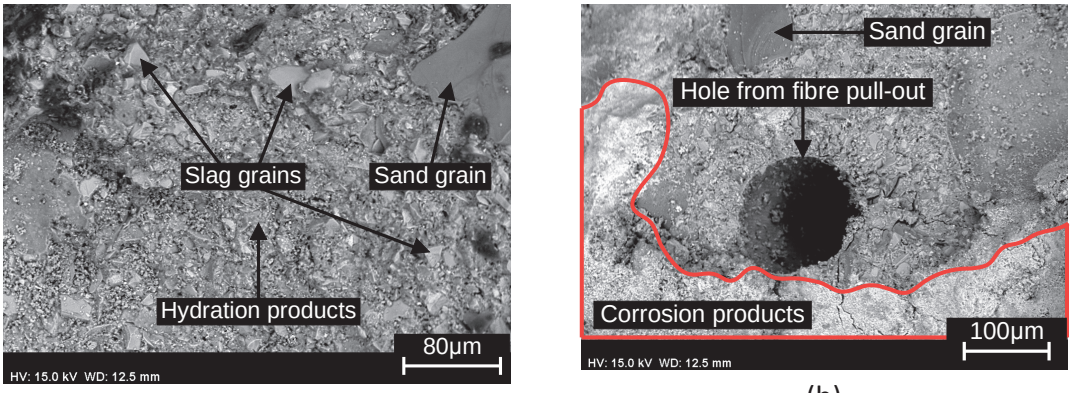

Figure 2.20 SEM images of fatigue fracture surface (S3-2 test specimen) (a) normally-coloured and (b) rust-coloured areas

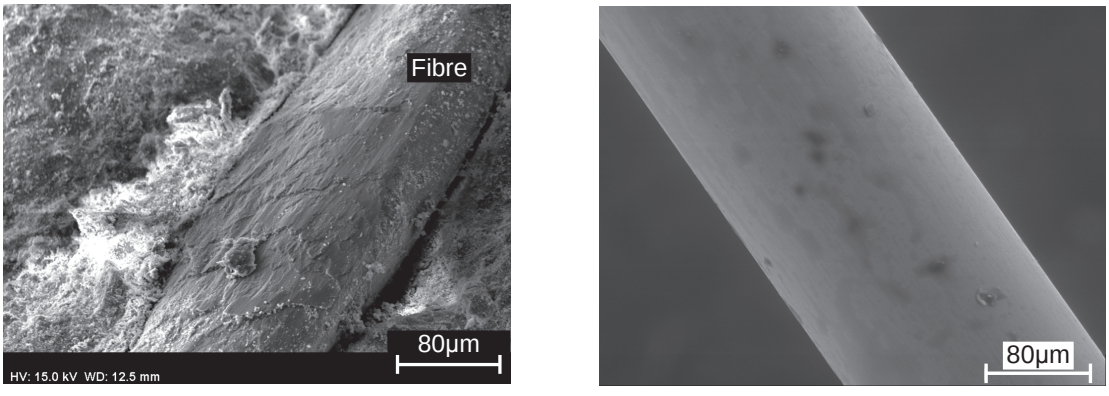

Figure 2.21 SEM images of steel fibres: (a) steel fibre from the rust-coloured area of fracture surface, (b) steel fibre in its original condition

2.5 Conclusion

The following conclusions can be drawn regarding the tensile fatigue behaviour of Ultra-High Performance Fibre Reinforced Concrete (UHPFRC) as obtained from uniaxial constant amplitude tensile fatigue tests:

1) The elastic limit strength seems to be a significant property to describe the fatigue strength of UHPFRC. A method is proposed to determine the elastic limit strength.

2) UHPFRC shows a fatigue endurance limit with respect to 10 million cycles above which fatigue stress induces significant damage leading to rather short fatigue lives. An endurance limit was obtained in all three domains of UHPFRC tensile behaviour and at a stress levels of (1) S = 0.7 in the elastic domain, (2) S = 0.6 in the strain hardening domain and (3) S = 0.45 in the strain softening domain, for S being the ratio between the maximum fatigue stress and the elastic limit strength of UHPFRC.

3) UHPFRC specimens subjected to a given tensile stress show rather large differences in local deformations. This is due to variations in material properties, in particular elastic limit strength and strain hardening behaviour. These variations in local deformation confer significant stress and deformation redistribution capacity to the UHPFRC bulk material enhancing thus the fatigue behaviour.

4) The fatigue fracture surface of UHPFRC shows features of fatigue fracture surfaces of steel. Fatigue crack propagation is identified by a smooth surface while final fracture leads to rather rough surface.

5) UHPFRC fatigue fracture surface shows clear signs of matrix spalling and pulverisation which is the result of snubbing, fibre pull-out – slip-back movements as well as abrasion of fibres with the matrix, due to fretting and grinding under fatigue cycles. Smooth areas also show rust-coloured powdery products which are due to tribocorrosion as depicted by spectroscopy and SEM analyses.

Appendix: Additional tensile fatigue tests of UHPFRC

The fatigue endurance limit determined for the S1 series was supposed to be of slightly poor reliability because rather large scatter was observed on the *S*-*N* diagram. In order to verify the fatigue endurance limit determined for S1 series (*S* = 0.70), additional tensile fatigue tests were performed. This fatigue test series is named S1.5 series and characterised referring to the quasi-static stress-strain curve following (Figure 2.22):

- S1.5 series: initial application of deformation corresponding to 0.5 ‰ strain followed by fatigue testing

0.5 ‰ strain is just beyond the elastic limit strain of UHPFRC and this level of pre-applied strain is considered not to impair fatigue stress carrying capacity of UHPFRC seriously based on S2 series test results. Since the elastic limit strength of each specimen is determined, in *S*-*N* diagram of S1.5 series, fatigue stress indicator *S* is obtained to be the ratio of maximum fatigue stress σ_{max} to the elastic limit strength of each specimen $f_{e,i}$ where variations in material composition, specimen size and testing setup for each specimen are rigorously eliminated. Thus, less scatter is expected to be observed on the *S*-*N* diagram.

Maximum fatigue stress determined in the same way as S2 and S3 series, and the stress corresponding to strains of either 0.20 ‰, 0.225 ‰ or 0.25 ‰ was applied as the maximum fatigue stress. Minimum fatigue stress was always set equal to 10 % of maximum fatigue stress. The same testing procedure was taken as S1 to S3 series.

Figure 2.23 shows the *S*-*N* diagram as obtained from S1.5 series test results (Table 2.3) including S2-1 and S2-2 test results whose pre-applied strains were 0.48 ‰ and 0.50 ‰, respectively. The results indicate a fatigue strength that may be expressed by a linear relationship between $\sigma_{max}/f_{e,i}$ and Log *N*. A linear regression line was determined (without considering run-outs) with a correlation coefficient of -0.79, indicating good dependency between the two variables:

$$\frac{\sigma_{max}}{f_{e,i}} = -0.085 \cdot \mathrm{Log}N + 1.364 \qquad \textbf{Eq. 2.3}$$

The test results including the run-outs allow estimating the fatigue endurance limit to be at an *S*-level of about 0.70 (as indicated by the horizontal dashed lines in Figure 2.23). Considering that S1.5 series test specimens were statically deformed beyond the elastic limit strain preceding the fatigue tests, the fatigue endurance limit of S1 series being *S* = 0.70 is plausible because deformation was not imposed on S1 series test specimens beyond the elastic limit strain preceding the fatigue tests and thus the specimens of S1 series were not damaged before fatigue testing.

Table 2.3 Results of S1.5 series tensile fatigue tests of UHPFRC

Test No.		σ_{max} [MPa]	$f_{e,i}$ [MPa]	$\sigma_{max}/f_{e,i}$	N [×10^6]	Remarks
1		5.7	6.8	0.84	0.39	·
3		6.4	6.4	1.00	0.02	
4		7.2	10.0	0.72	10.00	run-out
6		7.8	8.8	0.89	1.95	
7		8.3	9.9	0.84	0.83	
8	i	8.9	11.3	0.79	11.14	run-out
	ii	11.0		0.97	0.07	

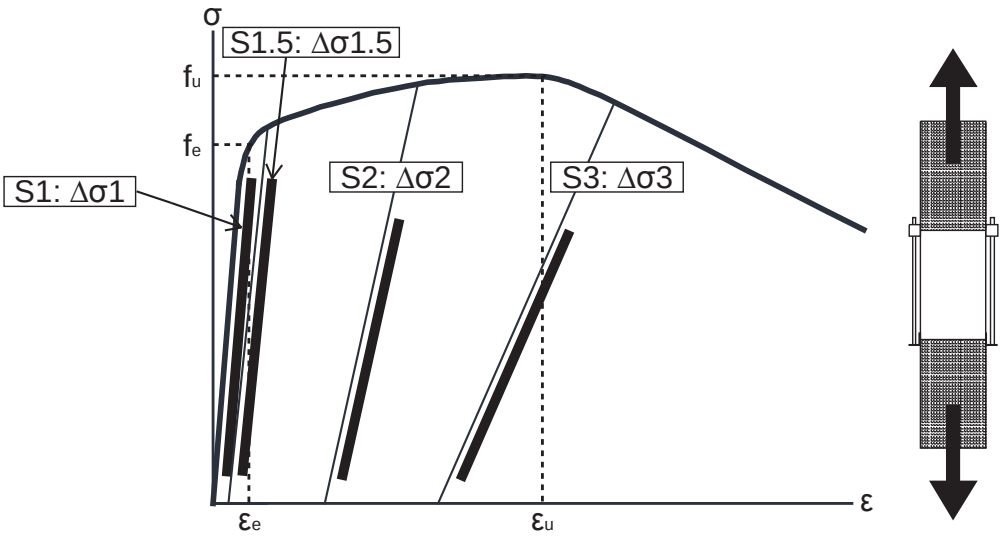

Figure 2.22 Schematic representation of tensile response of UHPFRC and definition of tensile fatigue test series

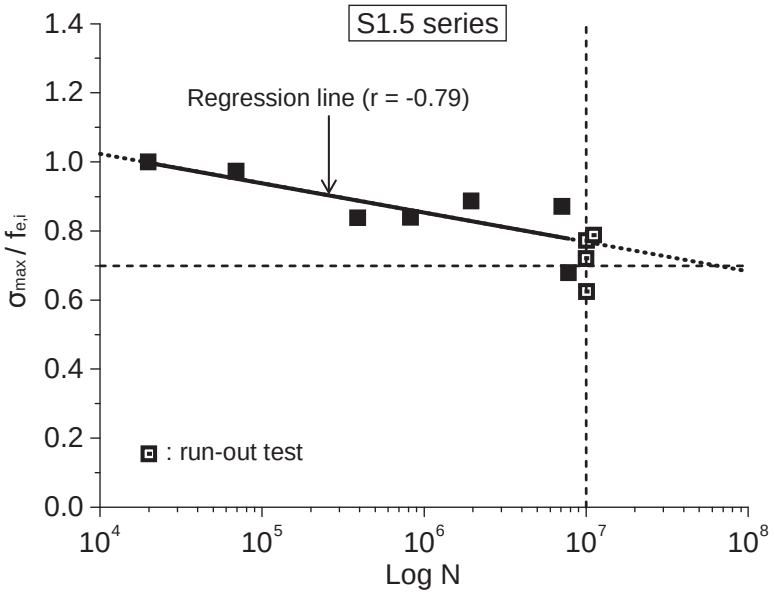

Figure 2.23 *S-N* diagram of S1.5 series

Chapter 3

Tensile fatigue behaviour of Ultra-High Performance Fibre Reinforced Concrete combined with steel rebars (R-UHPFRC)

Published in *International Journal of Fatigue*, Vol. 59, pp. 145-152

This page is intentionally left blank.

Tensile fatigue behaviour of Ultra-High Performance Fibre Reinforced Concrete combined with steel rebars (R-UHPFRC)

Abstract

Ultra-High Performance Fibre Reinforced Concrete (UHPFRC) combined with steel rebars, subsequently called R-UHPFRC, is a promising building material implying a novel technology for the improvement of concrete structures. Steel rebars enhance effectively the resistance of UHPFRC while reducing variability in the tensile behaviour of monolithic UHPFRC due to variation in fibre distribution and orientation. When a thin layer of R-UHPFRC is overlaid on top of a concrete bridge deck slab, it is subjected to repeating wheel loads and fatigue limit state needs to be considered. This paper presents the results of tensile fatigue tests on R-UHPFRC elements for the determination of its fatigue behaviour. Experimental results show a fatigue endurance limit at 10 million cycles at a solicitation level of S = 0.54 for S being the ratio between the maximum fatigue force and the ultimate strength. Over the fatigue life of the specimens, stress was transferred from UHPFRC to steel rebars. Fatigue resistance of R-UHPFRC shows that it has a significant potential for fatigue strengthening of reinforced concrete structural elements like bridge deck slabs.

Keywords: Ultra-High Performance Fibre Reinforced Concrete with steel rebars, tensile fatigue, fatigue endurance limit, stress transfer, fatigue deformation behaviour

3.1 Introduction

Ultra-High Performance Fibre Reinforced Concrete (UHPFRC) is a cementitious composite material, generally consisting of cement, quartz sand, silica fume and fibres. It has eminent properties: relatively high compressive strength (≥ 180 MPa) and tensile strength (≥ 10 MPa), strain-hardening behaviour under tensile stress (given a certain volume of fibres) and very low permeability because of an optimised dense matrix. These properties make UHPFRC suitable for “hardening” those parts of structural members that are subjected to mechanically and environmentally severe actions. Since the tensile behaviour of UHPFRC depends on fibre orientation and distribution [3.1], it is proposed that steel rebars are arranged in UHPFRC, subsequently called R-UHPFRC, to provide a significant increase in resistance and improvement of structural behaviour for UHPFRC. Also, variation in tensile behaviour of UHPFRC due to fibre orientation and distribution is reduced when steel rebars are added.

In recent years, the necessity to improve the load bearing capacity of bridges is growing due to the increase of traffic loads for more efficient transport of industrial products. Strengthening of concrete bridge deck slabs is often conducted by adding a layer of reinforced concrete (RC) on top of the slab. However, thickness of the RC layer sometimes becomes so large for fulfilling structural safety requirements that it is necessary to increase the load

bearing capacities of other structural members to support the increased self-weight due to the massive additional RC layer. Application of relatively thin R-UHPFRC overlays instead of RC layer leads to no or only minor increase of self-weight since usually cover concrete of the existing elements needs to be removed. Besides, dense matrix of UHPFRC provides waterproofing properties which in addition allows efficient use of the UHPFRC technology [3.2].

Although the static behaviour of R-UHPFRC has been investigated by some researchers ([3.3, 3.4, 3.5, 3.6]), few research results have been reported so far in the literature on the fatigue behaviour of R-UHPFRC. Four-point bending fatigue tests were conducted on beams made of Compact Reinforced Composite (CRC), an UHPFRC combined with high percentage of steel rebars (5 to 20 %) [3.7]. After determining ultimate static strength of the beam to be 39.77 kN, three levels of maximum fatigue force, i.e. 42 %, 70 % and 86 % of static yield strength (= 38 kN), were determined while minimum fatigue force was always 0 kN. Each combination of the fatigue force had one specimen. Specimens subjected to 70 % and 86 % of static yield strength failed at 403,790 and 52,430 cycles respectively, whereas the specimen subjected to 42 % of static yield strength sustained 5,305,150 cycles and was regarded as reaching run-out. It is concluded that very few cracks were observed on the specimens until failure or end of the test and the matrix didn't lose the ability to transfer fatigue force because applied maximum fatigue force remained constant in displacement controlled mode.

This literature review reveals that uniaxial tensile fatigue testing of R-UHPFRC has not been performed so far and knowledge of tensile fatigue behaviour of R-UHPFRC is scarce. There are several papers about the fatigue behaviour of UHPFRC ([3.8, 3.9, 3.10, 3.11, 3.12]) and steel rebar respectively ([3.13, 3.14, 3.15]). To some extent the fatigue behaviour of R-UHPFRC might be understood as a simple superposition of the fatigue behaviour of UHPFRC and steel rebar. However, since both UHPFRC and steel rebars carry tensile stress and stress distribution is supposed to occur between the two materials, it is necessary to investigate the fatigue behaviour of R-UHPFRC structural members.

The objectives of the present paper are to describe the tensile fatigue behaviour of R-UHPFRC and to investigate the effective function of steel rebars. Uniaxial tensile fatigue tests were chosen approximately reproducing the situation of an R-UHPFRC overlay on top of bridge deck slabs, including tensile fatigue stresses in the cantilever parts (Figure 3.1). Experimental tests are detailed and results are analysed.

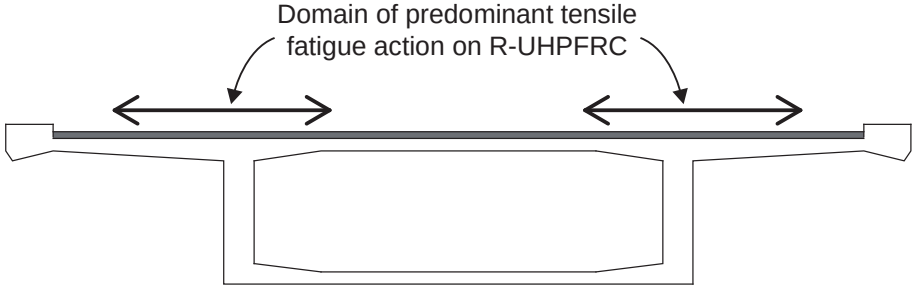

Figure 3.1 Bridge deck slab strengthened with R-UHPFRC layer

3.2 Experimental campaign

3.2.1 Specimens, instrumentation and test set-up

The mix of UHPFRC is characterised by 3.0 vol.-% content of 13 mm long steel fibres with a diameter of 0.16 mm and by the use of CEM III/B type cement which contains a high percentage of blast furnace slag (66 % to 80 %) (Table 3.1). Three prisms with a section of 40 mm × 40 mm and a length of 160 mm were cast with the same UHPFRC as used for the fabrication of R-UHPFRC specimens, and tested 56 days after casting. Average compressive strength and modulus of elasticity were 217 MPa and 47 GPa respectively. Steel rebars arranged in the UHPFRC were of B500B grade with a nominal yielding strength of 500 MPa.

The specimen is 750 mm-long and 40 mm-thick with varying width ('dog-bone shaped' specimen) to force fracture to occur within the 250 mm-long tapered central part of the specimen. The width of the central and end parts of the specimen were 110mm and 150 mm respectively, and there were 45 mm-long transitional zones between the central and end part (Figure 3.2).

The fabrication procedure of the specimen was as follows. First, three steel rebars of 8 mm diameter with a spacing of 40 mm were arranged in the wooden forms. Rectangle shaped specimens with 150 mm-width were cast and demoulded 7 days after casting, and then kept in the testing hall at constant climatic condition for more than 312 days. Aluminium plates (250 mm long, 150 mm wide and 2 mm thick) were then glued using epoxy resin to both surfaces of the specimen end parts as strengthening elements. By using a water jet cutter, the rectangle shaped specimens were cut into the dog-bone shape.

Two 250 mm-long Linear Variable Differential Transducers (LVDTs) and five displacement transducers with a 50 mm measurement length were used to measure the specimen deformation (Figure 3.2). LVDTs were glued to both specimen sides such as to capture global specimen deformation. In the present paper the average of deformation as measured by the two LVDTs are always referred to as global deformation. The five displacement transducers were set up on the specimen surface to measure local specimen deformation in five consecutive zones. Force was measured by the load cell installed in the actuator of the 1,000 kN servo-hydraulic testing machine.

Table 3.1 Composition of UHPFRC mix

Component	Type	Mass [kg/m^3]	Remarks
Cement	CEM III/B	1277.4	
Silica fume	Elkem Microsilica 971 U	95.8	7.5 % of cement mass
Sand	Quartz sand MN 30	664.6	d_{max} < 0.5 mm
Steel fibres	Bekaert OL 13/0.16 mm	235.5	3.0 vol.-%, brass coating
Superplasticiser	Sikament P5	42.3	3.3 % of cement mass
Water		198.0	W/C = 0.155

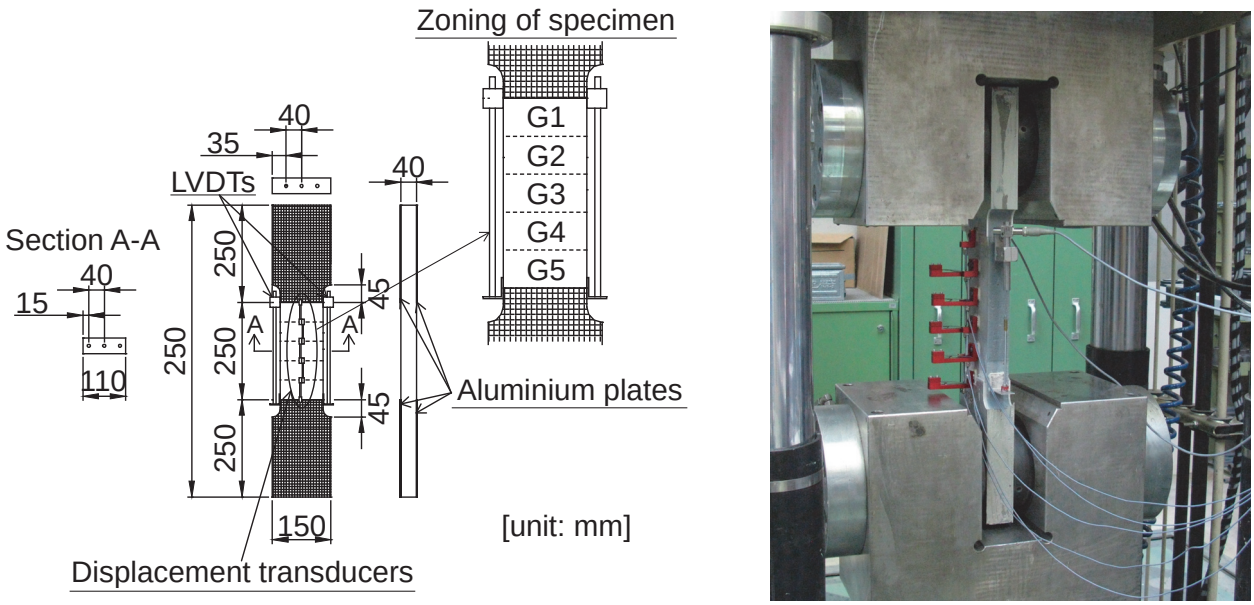

Figure 3.2 Specimen geometry, measuring devices and test set-up

3.2.2 Testing program

A single quasi-static tensile test was first performed to understand the behaviour of the R-UHPFRC under quasi-static tensile force using the same specimen as for the fatigue test.

Then, a fatigue test program was established with the objective to explore the fatigue endurance limit of R-UHPFRC. Fatigue force was determined with reference to stress range of steel rebars because the fatigue behaviour of R-UHPFRC was assumed to depend on the fatigue behaviour of steel rebars.

It was found in [3.16] that although the constant amplitude fatigue endurance limit of straight steel rebars at 2 million cycles was 170 MPa according to design codes, RC slab-like beams sustained more than 10 million fatigue cycles with stress range of about 230 MPa in steel rebars. In view of these findings, maximum fatigue force was chosen to cause stress range between 170 MPa and 230 MPa in steel rebars, while minimum fatigue force was always 10 % of maximum fatigue force.

Testing procedure was as follows: first, the specimen was subjected to quasi-static tensile force until the average reading of the two LVDTs reached the target deformation (corresponding to strains between 1.0 ‰ and 1.5 ‰) and then unloaded. The force corresponding to the target deformation was adopted as maximum force level for the fatigue test. Because of the variation of elastic limit strength of UHPFRC (which is likely due to local variations of fibre distribution and orientation [3.1]), deformation (instead of force) provides more reliable information on the tensile behaviour of R-UHPFRC. Consequently, fatigue tests were conducted under force control at constant amplitude in a servo-hydraulic machine at a frequency of 10 Hz.

Deformation and force data were recorded with a frequency of 200 Hz. The initial and final phases of the test were permanently recorded, while between these phases data was recorded

for 1 second every 600 cycles.

When a specimen sustained 10 million cycles, this result was regarded as 'run-out', and the test subsequently was continued at an increased maximum tensile fatigue force.

In the present paper, the fatigue endurance limit is defined as the force level below which no fatigue failure occurs up to 10 million cycles. With respect to bridge deck slabs, 10 million extreme force cycles are considered to be realistic to occur during the service life for heavily trafficked bridges. Also, limited available time for the experimental campaign imposed a maximum number of 10 million cycles which is usually considered as a lower bound of the very high cycle fatigue domain [3.17].

3.3 Results of experimental tests

3.3.1 Quasi-static tensile behaviour of R-UHPFRC

The tensile behaviour of R-UHPFRC is explained by analysing the force-global deformation curve obtained from a single quasi-static tensile test (Figure 3.3). Letters in brackets (A) to (G) in the curve show characteristic points, by referring to which the tensile behaviour of R-UHPFRC is described:

- The elastic domain (point (A) to (B)) is governed by the behaviour of UHPFRC until reaching the force corresponding to the elastic limit strength of UHPFRC F_e (called 'elastic limit strength of R-UHPFRC' hereafter). Invisible microcracking in UHPFRC matrix starts at this force level.
- These microcracks are bridged and controlled by fibres. After UHPFRC enters into the strain-hardening domain beyond point (B), more microcracks develop in the UHPFRC volume. Although UHPFRC reduces its modulus of deformation (the ratio of stress to strain) considerably, there is no significant decrease of R-UHPFRC stiffness due to the steel rebars which are still in the elastic domain. High bond strength between UHPFRC and steel rebars enables the perfect composite behaviour of R-UHPFRC [3.6].
- Steel rebars start to yield at point (C). The domain between point (C) and (D) is the transition from elastic to plastic behaviour of steel rebars. When steel rebars become fully plastic at point (D), a discrete macrocrack forms in the weakest section of UHPFRC and R-UHPFRC enters into the softening domain. This macrocrack then becomes visible.
- Steel rebars fracture one by one. Three steel rebars are arranged in the specimens, and the first, second and third fracture of steel rebars occurs at point (E), (F) and (G) respectively. Beyond (G), force is carried by UHPFRC and finally the specimen fractures completely in two parts at the end of UHPFRC softening.

The tensile behaviour of R-UHPFRC may be described by the linear superposition of the tensile behaviour of UHPFRC and steel rebars [3.6]. From this it follows that the ultimate strength of R-UHPFRC F_u attained at point (D) (120.0 kN) is decomposed into two units of force

carried by UHPFRC and steel rebars respectively, and considering nominal yield stress in steel rebars at point (D) being f_{sy} = 500 MPa (B500B grade steel), the ultimate strength of UHPFRC σ_{Uu} as obtained from this test is calculated as:

$$\sigma_{Uu} = \frac{F_u - A_s \cdot f_{sy}}{A_U} = \frac{120 \cdot 1000 - \pi \cdot 4^2 \cdot 3 \cdot 500}{110 \cdot 40 - \pi \cdot 4^2 \cdot 3} \approx 10.5\,\text{MPa} \qquad \textbf{Eq. 3.1}$$

where A_s is the sectional area of three steel rebars; A_U the sectional area of UHPFRC.

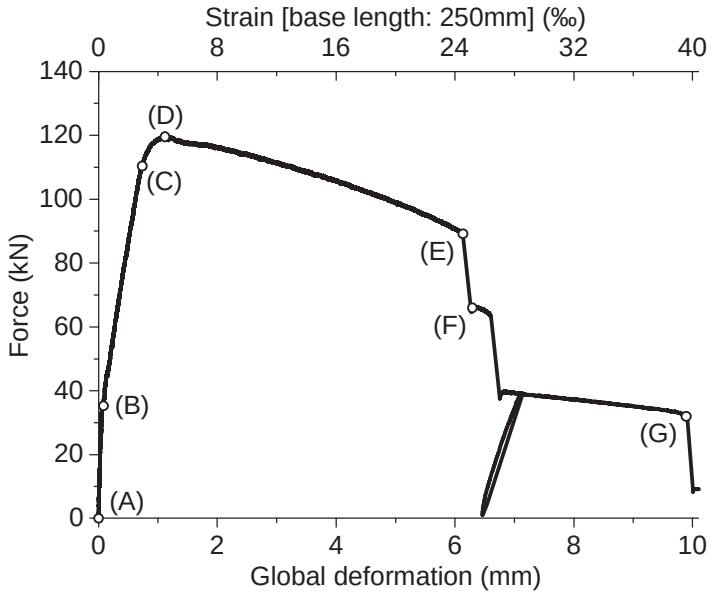

Figure 3.3 Force-global deformation relation of R-UHPFRC obtained from a quasi-static tensile test

3.3.2 Results of tensile fatigue tests

Table 3.2 summarises the results of tensile fatigue tests on 12 R-UHPFRC specimens. A specimen was regarded as failed when the global deformation reading reached 2.5 mm, corresponding to strain of 10 ‰.

Table 3.2 Results of tensile fatigue tests of R-UHPFRC

Test No.		F_{max} [kN]	$F_{u,i}$ [kN]	$F_{max}/F_{u,i}$	N [×10^6]	Remarks
1	i	60.90	131.3	0.46	10.00	run-out
	ii	80.90		0.62	0.09	
2	i	67.00	125.8	0.53	13.09	run-out
	ii	72.00		0.57	17.78	run-out
	iii	77.00		0.61	0.73	
3	i	68.90	132.2	0.52	10.04	run-out
	ii	73.90		0.56	7.75	
4	i	57.90	112.6	0.51	10.20	run-out
	ii	62.90		0.56	10.00	run-out
	iii	72.90		0.65	0.46	
5		69.50	128.6	0.54	0.96	
6		78.30	138.7	0.56	4.72	
7		78.60	128.3	0.61	1.55	
8	i	74.90	122.9	0.61	10.01	run-out
	ii	84.90		0.69	0.52	
9		86.60	137.6	0.63	0.41	
10		76.90	122.2	0.63	0.31	
11		90.50	125.9	0.72	0.14	
12		75.00	121.7	0.62	1.00	

F_{max}: applied maximum fatigue force

$F_{u,i}$: estimated ultimate strength of each specimen

N: sustained number of fatigue cycles

Figure 3.4 shows the *S*-*N* diagram with the results obtained in the present study. In order to eliminate variations in material composition, specimen size and test set-up, normalized force S is used for the axis of ordinate. The ratio of maximum fatigue force F_{max} to the ultimate strength of each specimen $F_{u,i}$ was used as fatigue solicitation indicator S where $F_{u,i}$ was estimated based on the result of the single quasi-static tensile test of R-UHPFRC by using force-global deformation relation of each specimen obtained from quasi-static tensile preloading.

Ultimate strength $F_{u,i}$ was estimated by assuming that all specimens have the same strain corresponding to the yield and ultimate points (point (C) and (D) respectively in Figure 3.3 and

3.5a). These strains were determined to be 2.23 ‰ and 4.58 ‰ respectively from the quasi-static tensile test (Figure 3.5a). In addition, slope *a* of a line connecting the yield and ultimate points in the force-global deformation relation of the quasi-static tensile test (Y-U line in Figure 3.5a) was used to estimate $F_{u,i}$. In the following, the procedure to estimate the ultimate strength of each specimen is explained by using the preloading force-global deformation curve of Test 5 specimen as an example:

- As can be seen in Figure 3.3 and 3.5a, the force-global deformation relation between point (B) and (C) is almost proportional, which is assumed to be similar for all R-UHPFRC member subjected to quasi-static tensile force. By choosing two points corresponding to 0.8 ‰ and 1.0 ‰ strain (P1 and P2 respectively in Figure 3.5b) on the preloading force-global deformation curve, straight line L1 representing the slope of the proportional part is drawn (Figure 3.5b). The strain of 0.8 ‰ was chosen because it is about 30 % of the reference yield strain 2.23 ‰ while the strain of 1.0 ‰ was chosen because preloading of two specimens was stopped when global deformation readings reached 1.0 ‰ of strain.
- Then, the point corresponding to 2.23 ‰ strain on line L1 is estimated to be the yield point (P3 in Figure 3.5b).
- A straight line L2 with slope of *a* passing through the yield point P3 is then drawn (Figure 3.5b). The force corresponding to 4.58 ‰ strain on line L2 is determined to be the ultimate strength (P4 in Figure 3.5b).

In the proposed method to estimate the ultimate strength, the chosen yield and ultimate values were adopted as reference from a single quasi-static tensile test, which might be considered as a vague assumption. However, since these stress and strain values are similar to the average values determined from three formerly conducted quasi-static tensile tests [3.6], the applied method is considered to provide reliable estimated ultimate strength values.

The results shown in Figure 3.4 indicate a fatigue strength that may be expressed by a linear relation between *S* (= $F_{max}/F_{u,i}$) and Log *N*. A straight line was determined by linear regression (without considering run-outs) with a correlation coefficient of -0.66:

$$\frac{F_{max}}{F_{u,i}} = -0.065 \cdot LogN + 1 \qquad \textbf{Eq. 3.2}$$

S-value at 10 million cycles is calculated to be 0.54 from Equation 3.2. *S* = 0.54 is also the average value of fatigue solicitation indicator of the tests that reached run-out. In addition, no specimen failed due to tensile fatigue when the maximum fatigue force was smaller than 54 % of the ultimate strength. Therefore, the fatigue endurance limit at 10 million cycles may be determined to be at *S* = 0.54 (indicated with a dotted line in Figure 3.4). Consequently, the fatigue endurance limit of R-UHPFRC may be conservatively considered to be 50 % of the ultimate strength. Similar result, e.g. fatigue endurance limit at 50 % of the ultimate strength, was obtained for RC members strengthened with R-UHPFRC (RU-RC members) [3.18].

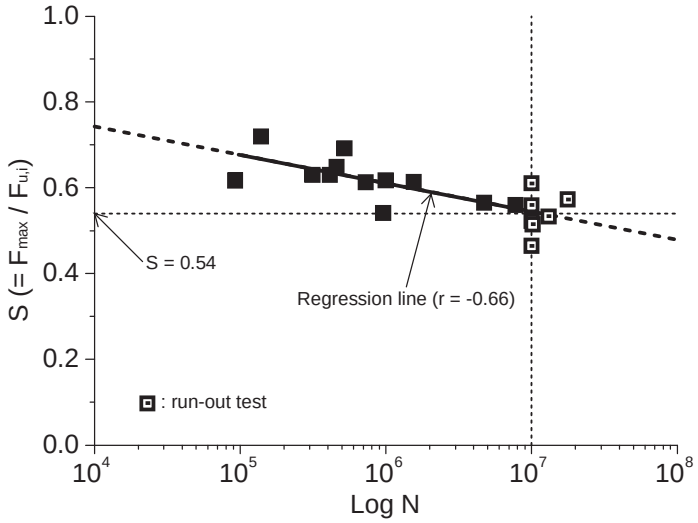

Figure 3.4 *S-N* diagram obtained from tensile fatigue tests of R-UHPFRC

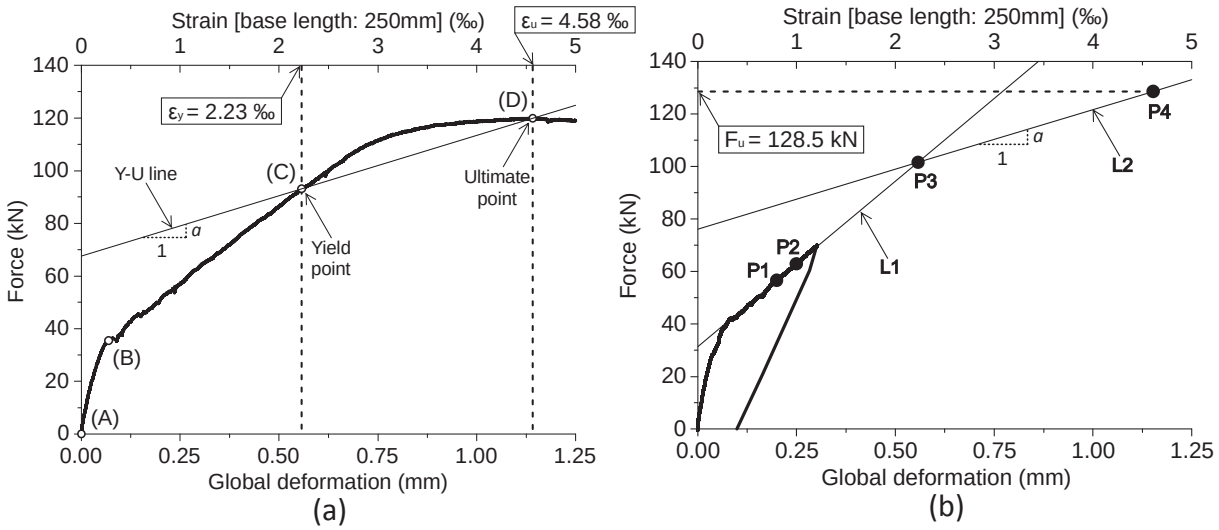

Figure 3.5 (a) Force-global deformation relation of a quasi-static tensile test defining reference points and slope of a line to (b) estimate the ultimate strength of specimens using Test 5 specimen.

3.3.3 Fatigue resistance of R-UHPFRC as expressed by the maximum fatigue force level

The fatigue resistance of R-UHPFRC may be explained in terms of fatigue solicitation indicator *S* which is categorised into three domains as follows (Figure 3.6):

1) $S \leq 0.23$

Stress in UHPFRC and steel rebars is largely below the fatigue endurance limit of both materials.

The fatigue endurance limit of monolithic UHPFRC is about 70 % of the elastic limit strength [3.19] and average ratio of the elastic limit strength to the ultimate strength of all R-UHPFRC specimens is calculated to be 0.33. Accordingly, $S = 0.23$ is obtained as 70 % of the average ratio of the elastic limit strength to the ultimate strength of R-UHPFRC. At this force

level, UHPFRC contributes more significantly to the fatigue resistance of the R-UHPFRC element than the steel rebars.

2) $0.23 < S \leq 0.54$

Stress in the UHPFRC is beyond the fatigue endurance limit, and when *S* is larger than 0.33, which is the average ratio of the elastic limit strength to the ultimate strength of all R-UHPFRC specimens, the stress in UHPFRC is in the strain-hardening domain. Stress in steel rebars is still below the fatigue endurance limit.

Although monolithic UHPFRC subjected to fatigue stress at this level would fail, deformation localisation does not occur in the R-UHPFRC specimen because of the stress distribution from UHPFRC to steel rebars. Contribution of UHPFRC and steel rebars to the fatigue resistance of R-UHPFRC is similar. The global deformation grows in the early stage of the fatigue test only and remains constant in the subsequent stage.

3) $S > 0.54$

Stress in the UHPFRC is in the strain-hardening domain and stress in steel rebars is higher than the fatigue endurance limit.

The fatigue resistance of R-UHPFRC is essentially determined by the steel rebars and the UHPFRC functions merely as a stress reducing element for the steel rebars. The global deformation grows in the beginning of the fatigue solicitation, and then remains constant until one of the three steel rebars fractures. Deformation localisation in UHPFRC is always at the same location as the fatigue fracture of steel rebars.

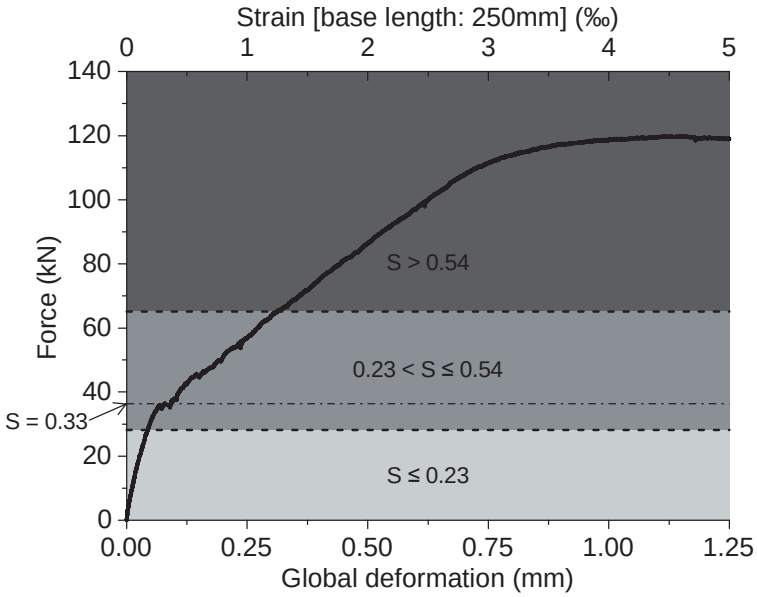

Figure 3.6 Schematic representation of fatigue solicitation indicator *S* with reference to force-global deformation relation of R-UHPFRC

3.4 Tensile fatigue behaviour of R-UHPFRC

3.4.1 Stress transfer from UHPFRC to steel rebars

It was shown in [3.20] that stress gradually transfers from UHPFRC to steel rebars in R-UHPFRC as the number of fatigue cycles increases. This is due to degradation of deformation modulus of UHPFRC. In order to verify this stress transfer, evolution of stress in the UHPFRC and steel rebars was investigated. As no direct deformation measurement on the steel rebars was performed, stress in steel rebars was calculated according to Equation 3.3 using the modulus of elasticity and global deformation measurements obtained from LVDTs on the UFPFRC surface.

$$\sigma_s = E_s \cdot \frac{\Delta \ell_g}{\ell_b} \qquad \textbf{Eq. 3.3}$$

where σ_s is the stress in steel rebar; E_s the modulus of elasticity of steel rebar (= 205 GPa); $\Delta\ell_g$ global deformation; ℓ_b base length of LVDTs. Stress in UHPFRC σ_U was then obtained by subtracting the force carried by steel rebars from applied force F according to the following equation:

$$\sigma_U = \frac{F - A_s \cdot \sigma_s}{A_U} \qquad \textbf{Eq. 3.4}$$

Figure 3.7 shows *S-N* diagram for stress range in the steel rebars as calculated according to Equation 3.3. Both the stress range at the first fatigue cycle and the largest stress range during a fatigue test are plotted. The initial fatigue test result was used to draw the *S-N* diagram in case that more than one fatigue test was conducted to a specimen.

The stress range in the steel rebars of all R-UHPFRC specimens became the largest before the number of fatigue cycles reached 500,000. Accordingly, it is understood that stress range in the steel rebars of R-UHPFRC gradually grew larger as the number of fatigue cycles increased. Considering equilibrium of internal and external forces in the R-UHPFRC specimen, stress transfer from UHPFRC to steel rebars may be inferred. Figure 3.8 shows the evolution of stress range in UHPFRC and steel rebars during Test 8-i and 10 using Equations 3.3 and 3.4, describing stress transfer from UHPFRC to steel rebars in R-UHPFRC.

Fatigue strength expressed as a linear relation between $Log\ \Delta\sigma_s$ and $Log\ N$ was determined by linear regression (without considering run-outs) for data of stress range at the first cycle and the largest stress range in the rebars with correlation coefficients of -0.89 and -0.83 respectively (Figure 3.7):

$$Log\Delta\sigma_s = -0.1 \cdot LogN + 2.86 \quad \text{(stress range at the first cycle)} \qquad \textbf{Eq. 3.5}$$

$$Log\Delta\sigma_s = -0.1 \cdot LogN + 2.92 \quad \text{(the largest stress range)} \qquad \textbf{Eq. 3.6}$$

Comparing these fatigue strength equations, it is interpreted that the more fatigue stress cycles the R-UHPFRC specimen sustains, the smaller the stress transfer from UHPFRC to steel rebars. These findings support the fact that if the stress range in the steel rebars is small, R-UHPFRC specimen survives longer in the fatigue test because steel rebars determine the fatigue behaviour of R-UHPFRC except in the early stage of the fatigue test (as explained in section 3.4.2).

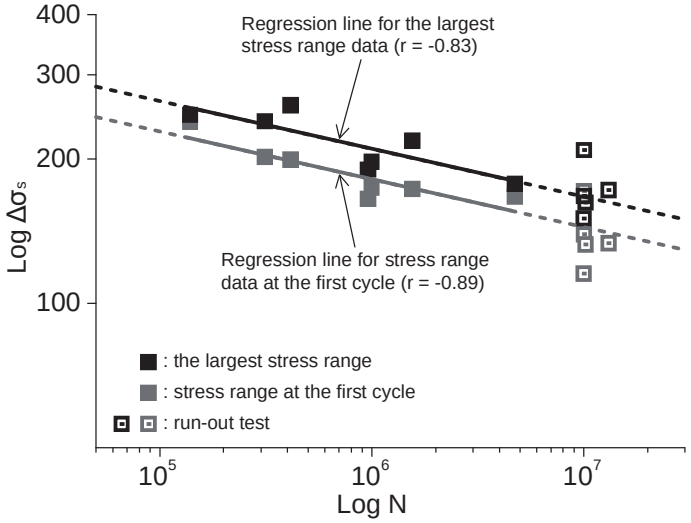

Figure 3.7 *S-N* diagram for stress range in steel rebars of R-UHPFRC

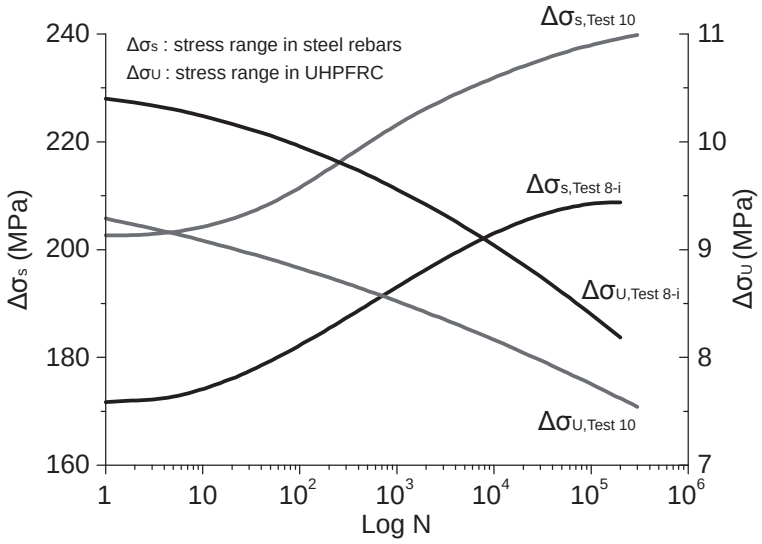

Figure 3.8 Evolution of stress range in UHPFRC and steel rebars during Test 8-i and 10

3.4.2 Fatigue deformation behaviour

Tensile fatigue testing was conducted while imposing constant maximum and minimum forces and specimen deformation as a function of fatigue cycles was recorded. Similar deformation behaviour was observed from all R-UHPFRC specimens under tensile fatigue. The recorded global deformation of R-UHPFRC is discussed in terms of three regimes of

characteristic behaviours using the example of the specimen behaviour of Test 5.

1) Small deformation growth

Global deformation of R-UHPFRC specimen grew only in the early stage of the fatigue test (up to about 500,000 cycles), and then remained approximately constant during the fatigue test until one of the steel rebars fractured (Figure 3.9a). This is attributed to stress transfer from UHPFRC to steel rebars.

In the early stage of the fatigue test, UHPFRC mainly carried fatigue stress and deformation behaviour of R-UHPFRC was strongly influenced by UHPFRC whose deformation was observed to grow under tensile fatigue [3.19]. This is why global deformation of R-UHPFRC increased in the early stage of the fatigue test. Then, fatigue stress gradually transferred to the steel rebars and steel rebars became main fatigue stress carrying element in R-UHPFRC. Consequently, deformation behaviour of R-UHPFRC was predominantly influenced by steel rebars and since steel rebars do not show any deformation growth under tensile fatigue, global deformation of the R-UHPFRC specimen was rather constant.

2) Variations in local deformation

Variations in local deformations of R-UHPFRC were measured by G1 to G5 transducers (Figure 3.9b). This may again be explained by stress transfer from UHPFRC to steel rebars.

As explained in the preceding paragraph, UHPFRC controlled the behaviour of R-UHPFRC in the early stage of the fatigue test. Under tensile fatigue stress, local deformation of UHPFRC varied which is explained by variation of material properties of UHPFRC in the hardening domain [3.19] (Figure 3.10). This UHPFRC behaviour led to variations in local deformation of R-UHPFRC in the early stage of the fatigue test. After the main fatigue stress carrying component of R-UHPFRC transferred from UHPFRC to steel rebars, these variations in local deformation persisted because deformations induced in the UHPFRC at the early stage of the fatigue test remained constant.

3) Conservation of force bearing capacity of UHPFRC

Although applied fatigue force is beyond the elastic limit strength of UHPFRC, local deformation measurements indicate that deformation did not localise in the UHPFRC. Besides, modulus of deformation of the UHPFRC part was calculated to be around 10 GPa in average for all run-out specimens using the following equation.

$$D_{U,fat,i} = \frac{\sigma_{U,max,i} - \sigma_{U,min,i}}{\varepsilon_{max,i} - \varepsilon_{min,i}} \qquad \textbf{Eq. 3.7}$$

where $D_{U,fat,i}$ is modulus of deformation of the UHPFRC part at *i*-th cycle; $\sigma_{U,max(min),i}$ maximum (minimum) fatigue stress in the UHPFRC part at *i*-th cycle calculated using Equation 3.4; $\varepsilon_{max(min),i}$ global maximum (minimum) fatigue strain of R-UHPFRC at *i*-th cycle.

From this it follows that when combined with steel rebars, UHPFRC keeps its fatigue force

bearing capacity although it is subjected to stress within the strain-hardening domain in the fatigue test.

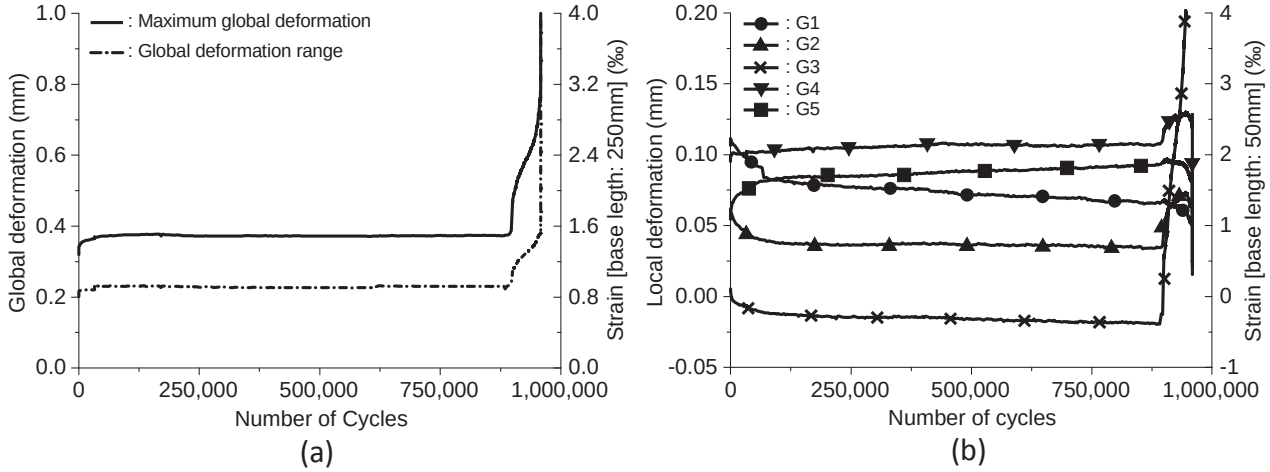

Figure 3.9 Recorded deformation growth curves during Test 5 (a) maximum global deformation and global deformation range, (b) local deformations over the specimen length

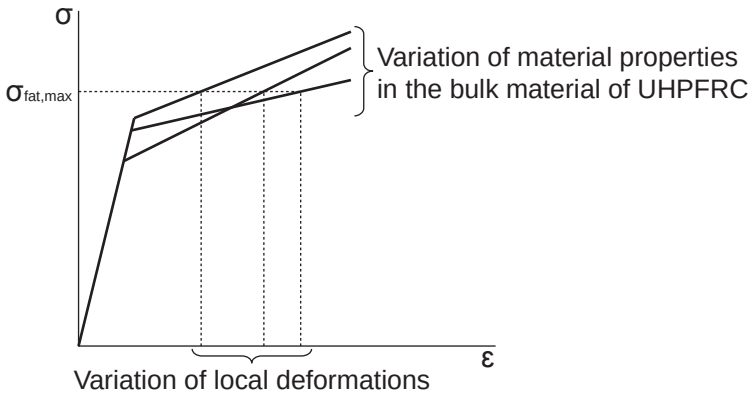

Figure 3.10 Variation of local deformation of UHPFRC at given tensile fatigue stress

3.4.3 Fracture mechanism of R-UHPFRC under tensile fatigue

By analysing fatigue fracture surfaces of R-UHPFRC specimens by visual observation, fracture mechanism of R-UHPFRC under tensile fatigue may be identified. In the following, fatigue fracture surfaces of UHPFRC and steel rebar are separately discussed.

Matrix spalling and pulverisation, smooth fracture surface area and rust-coloured powdery products are three distinct features observed on the fatigue fracture surface of the UHPFRC. These phenomena were already observed on the fatigue fracture surfaces of monolithic UHPFRC specimen subjected to tensile fatigue stress in a previous study by the authors [3.19].

Fracture surface of steel rebar clearly indicated two distinct types of fracture surfaces, i.e., smooth and rough fracture surfaces. Smooth fracture surface indicates the well-known stable fatigue crack growth in steel. Rough fracture surface is brought about by rapid final fracture of

the steel rebar when the applied fatigue stress reaches the ultimate resistance of the fatigue cracked rebar.

The characteristics of the fracture surfaces depict the chronological order of failure of the three steel rebars. The first fractured steel rebar is the one with the largest smooth fracture surface (Figure 3.11). This is because fatigue stress imposed on each steel rebar was relatively small when all three rebars carried stress and fatigue crack grew slowly making fracture surface smooth. The steel rebar with the largest rough fracture surface is the one that fractured last under relatively high applied stress concentrating on the final rebar (Figure 3.11). In addition, the last fractured steel rebar is also identified by a reduced fracture surface area due to necking (Figure 3.11).

It is noted that deformation readings did not change even when fatigue crack growth occurred in steel rebars. Change in deformation readings was recorded only when one of the three steel rebars fractured.

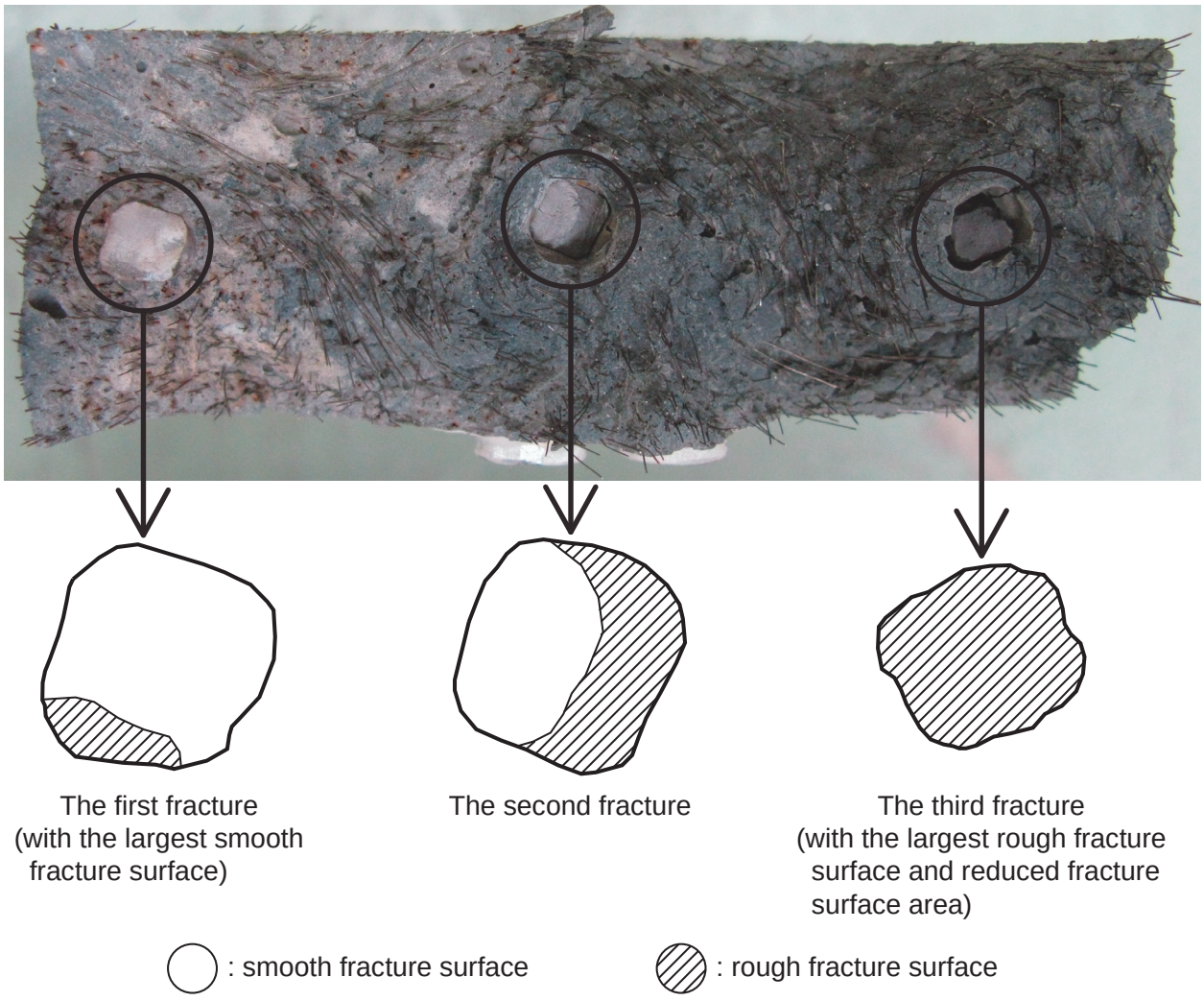

Figure 3.11 Fatigue fracture surface of specimen of Test 5 and chronological order of fracture of the three steel rebars based on the characteristics of the fracture surfaces

3.5 Conclusion

The following conclusions can be drawn regarding the tensile fatigue behaviour of R-UHPFRC as obtained from uniaxial constant amplitude tensile fatigue tests:

1) A constant amplitude fatigue endurance limit at 10 million cycles was determined to be at a solicitation level of $S = 0.54$ for S being the ratio between the maximum fatigue force and the ultimate strength of the R-UHPFRC specimen. Considering that at this force level, UHPFRC behaviour is in the strain-hardening domain, the steel rebars improve actually the fatigue force bearing capacity of UHPFRC by distributing the applied fatigue stress.

2) The respective contribution of UHPFRC and steel rebars to the fatigue resistance of R-UHPFRC depends on the maximum fatigue force level and the stage of the fatigue test. Stress distribution and transfer between UHPFRC and steel rebars enhances the fatigue capacity of both material components.

3) Fatigue deformation behaviour of R-UHPFRC depends on the stage of the fatigue test. In the early stage of the fatigue test, UHPFRC mainly determines the fatigue behaviour of R-UHPFRC. In the middle and final stages of the fatigue test, steel rebars predominantly determine the fatigue behaviour of R-UHPFRC.

4) Examination of the fatigue fracture surfaces of steel rebars revealed typical fatigue crack growth and final fracture surface. The chronological order of the fatigue failure of the three steel rebars was identified from the characteristics of the fracture surfaces.

Chapter 4

Fatigue behaviour of bridge deck slab elements strengthened with reinforced UHPFRC

Presented at *IABMAS 2012* and published in the proceedings edited by Biondini F., Frangopol D. M., Stresa, Italy, pp. 1974-1980

This page is intentionally left blank.

Fatigue behaviour of bridge deck slab elements strengthened with reinforced UHPFRC

Abstract

With the occurrence of higher and more frequent axle loads on roads, in particular bridge deck slabs are more severely solicitated by fatigue loading. To avoid heavy interventions for strengthening of bridge deck slabs, an improved building material is used, namely Ultra-High Performance Fibre Reinforced Concrete containing steel rebars (= R-UHPFRC). By adding a thin (30 to 50 mm) layer of R-UHPFRC on top of the deck slab, the required fatigue resistance and load carrying capacity may be restored and improved. In addition, the R-UHPFRC layer is waterproof which provides improved durability. This paper presents results of fatigue tests for the determination of the fatigue behaviour of reinforced concrete (RC) slab-like beams strengthened with R-UHPFRC leading to RU-RC beams. The experimental results show high fatigue resistance of RU-RC beams indicating a significant potential for strengthening of RC bridge deck slabs. For the application, rules are deduced for the design of the RU-RC member and the corresponding fatigue safety verification. Finally, an application of this novel technology is briefly described demonstrating that improvement of bridge deck slabs using UHPFRC is a relatively gentle intervention with limited intervention costs. There is a potential inherent with this novel construction method to limit the duration of the working site and thus to reduce the user costs as well as life cycle costs.

Keywords: fatigue strengthening, reinforced UHPFRC, bridge deck slab, fatigue endurance limit, fatigue deformation behaviour, fracture process

4.1 Introduction

The development of economic activity has accelerated the increase of traffic volume since the late 20th century. In order to keep up with this increase, transportation infrastructures are required to improve their traffic and load bearing capacities. As for the improvement of load bearing capacity, it is usually carried out by exchanging existing structural members or adding new structural members. If one operation of such maintenance works is the only intervention during the service life, it is desirable in terms of life cycle maintenance strategy to follow Strategy A according to Figure 4.1 implying enhanced durability. In this context, the concept of application of Ultra-High Performance Fibre Reinforced Concrete reinforced with steel rebars (R-UHPFRC) to improve existing concrete members was conceived. UHPFRC has eminent properties such as relatively high compressive and tensile strength, low permeability, strain-hardening behaviour in tension.

The objectives of the present paper are to describe the bending fatigue behaviour of R-UHPFRC reinforced concrete composite member (RU-RC member) and demonstrate the

effectiveness of fatigue strengthening of existing RC bridge deck slabs using R-UHPFRC. The experimental set-up represents a strip of RC bridge deck cantilever strengthened with R-UHPFRC (circled part in Figure 4.2). The experimental tests are detailed and the test results are analysed. Design rules for the RU-RC member and the corresponding fatigue safety verification are then proposed. In the final part of the present paper, an on-site application of R-UHPFRC layer to RC bridge deck slab is described.

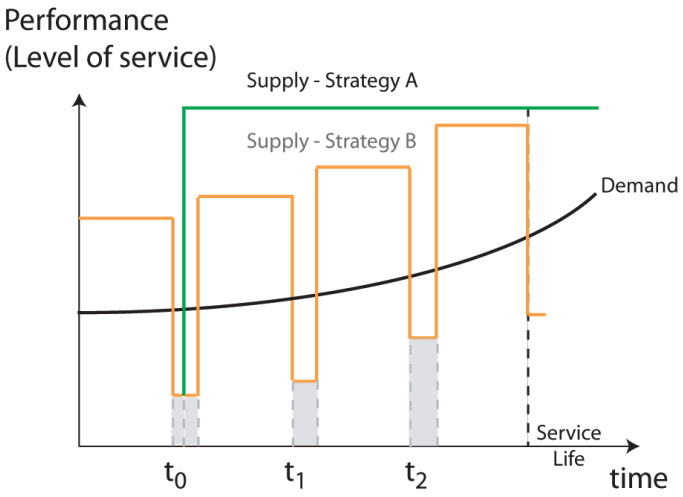

Figure 4.1 Life cycle maintenance strategies [4.1]

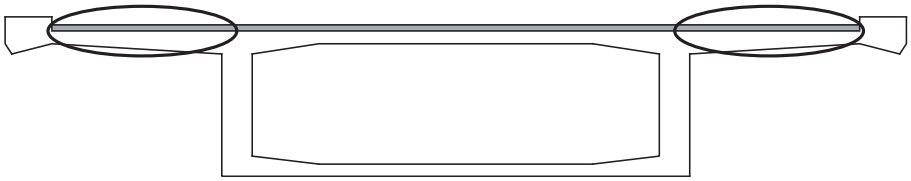

Figure 4.2 RC bridge slab improved with R-UHPFRC layer

4.2 Behaviour of UHPFRC under quasi-static tension

The tensile behaviour of UHPFRC is characterised by three domains as observed in quasi-static tensile tests:

- The elastic domain is governed by the behaviour of the matrix until it reaches its tensile strength, called the elastic limit strength. Microcracks start to form at this stress level.
- These microcracks are bridged and controlled by fibres. After entering into the strain-hardening domain, more microcracks develop in the whole specimen volume. A considerable reduction in modulus of deformation, i.e. the ratio of stress to strain, is observed. The strain-hardening extends until the ultimate resistance or tensile strength is reached in the weakest section of the specimen.
- In the strain-softening domain beyond ultimate resistance, a discrete macrocrack forms in

this weakest section and becomes eventually visible. Consequently, deformation localizes in the macrocrack zone while the zones outside are unloaded. Finally the specimen fails in two parts at the end of softening.

In the present paper microcrack is defined as a crack which is not visible to the naked eye and its width is commonly much smaller than 0.05 mm. Macrocrack is defined as a crack which is visible to the naked eye and its width is larger than 0.05 mm.

4.3 Experimental tests

4.3.1 Specimens, test set-up and instrumentation

The specimen is a 1,900 mm long slab-like beam with a cross section of 400 mm × 220 mm (Figure 4.3). Thickness of R-UHPFRC layer is 50 mm using an in-house developed UHPFRC mix called HIFCOM 13. This mix is characterised by 3.0 vol.-% content of steel fibres 13 mm long with a diameter of 0.16 mm and by the use of CEM III/B type cement which contains a high percentage of blast furnace slag (66 % to 80 %). Although the static strength of UHPFRC in tension depends on casting procedure and element configuration [4.2], the average elastic limit strength and ultimate strength were determined from quasi-static uniaxial tensile tests using monolithic UHPFRC plates to be around 10 MPa and 12 MPa each. Four steel rebars of 10 mm diameter were arranged in the UHPFRC layer with a spacing of 100 mm.

Concrete in the RC part was C30/37 grade with a maximum aggregate size of 16 mm. The average tested concrete cylinder compressive strength was 64.5 MPa after 180 days. Four steel rebars of 16 mm and 10 mm diameter were arranged in the top and bottom of the RC part with a spacing of 100 mm.

All of steel rebars used in the experimental tests were of Grade B500B and had a nominal yielding strength of 500 MPa.

The RC part was first cast, and 28 days later the UHPFRC layer was cast on the top surface of the RC part which was roughened with hydro-jetting to obtain monolithic bond between UHPFRC and concrete. (Neither any adhesion products nor any shear connector was used for the bonding.)

Linear Variable Differential Transducer (LVDT) was set to measure the specimen deflection at the position of the jack (Figure 4.3). Seven displacement transducers with a base length of 100 mm were set at the transversal centre of the top surface of R-UHPFRC layer to measure the R-UHPFRC deformation (Figure 4.3). The displacement transducers were intended to cover the area where the largest negative bending moment acted.

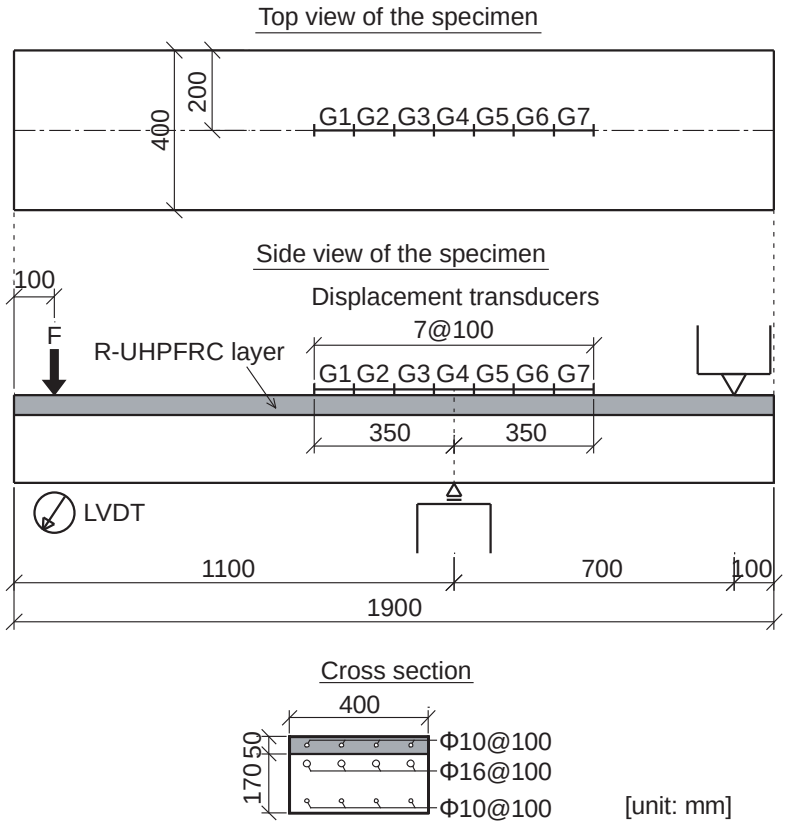

Figure 4.3 Specimen geometry, measuring devices and test set-up

4.3.2 Testing program

Maximum fatigue force F_{max} was varied between 40 % and 60 % of the ultimate static strength F_u of the specimen. F_u was determined to be 90 kN from one static test with the same specimen type as used in the fatigue tests. Applied minimum fatigue force F_{min} was always 10 % of maximum force. When a specimen sustained more than 10 million fatigue cycles, the test was regarded as "run-out" and the new fatigue test was continued at a higher fatigue force level.

In the present paper the fatigue limit is defined as a normalised force (i.e. the ratio $S = F_{max}/F_u$) below which no fatigue failure occurs after 10 million fatigue cycles. In fact, 10 million is not a large number of cycles when considering actual numbers of axle load cycles occurring on bridge deck slabs. However, as limited time is available for the experimental campaign, 10 million is considered as representative for estimation of the fatigue limit in the high cycle fatigue domain.

Fatigue force was applied manually during the first 10 cycles; then sinusoidal fatigue force cycles were imposed at 8 Hz using hydraulic actuator. Force was measured by the load cell installed just below the force applying jack.

Deflection, deformation and force data were recorded with a frequency of 160 Hz. The initial and final phases of the tests were recorded permanently, while between these phases data was recorded for 1 second every 480 cycles.

4.4 Results and discussion of experimental results

4.4.1 Fatigue limit

Table 4.1 summarises the results of bending fatigue tests of RU-RC beams. When the whole testing system became unstable due to reduction of stiffness of the specimen and force could no longer be applied, the fatigue test was stopped and specimen was regarded as failed.

Figure 4.4 shows the *S*-*N* diagram as obtained in the present study from the RU-RC beam specimens. In order to eliminate variations in material composition, specimen size and testing set-up, normalised force *S* is used for vertical axis. Scatter in the results may be explained by differences in static strength and age of specimens. As material properties of UHPFRC depend on fibre distribution and orientation [4.2], this might have influenced the variety of the static strength of the RU-RC beam in the present case. The fatigue limit may be estimated to be at a level of S = 0.5 or 50 % of F_u.

Table 4.1 Results of bending fatigue tests of RU-RC composite beam

Test No.		F_{max} [kN]	S	N [×10^6]	Remarks
1	i	36.0	0.40	10.13	run-out
	ii	45.0	0.50	1.04	
2	i	40.5	0.45	20.00	run-out
	ii	45.0	0.50	1.97	
3	i	45.0	0.50	23.94	run-out
	ii	49.5	0.55	10.00	run-out
	iii	54.0	0.60	2.10	
4		49.5	0.55	6.99	
5		49.5	0.55	0.99	

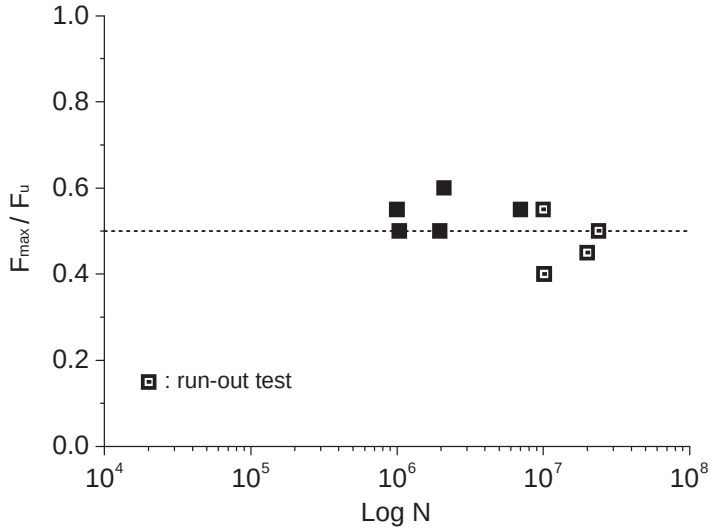

Figure 4.4 *S*-*N* diagram

4.4.2 Characteristic behaviour

All the RU-RC beams showed similar behaviour until failure under bending fatigue. The characteristic behaviour is discussed by looking at the behaviour of Test 2 specimen. First, deformation of R-UHPFRC layer is explained; then, the behaviour of the RU-RC beam is mentioned chronologically focusing on failure mechanism.

4.4.2.1 Deformation of R-UHPFRC layer

Distribution and evolution of deformation of R-UHPFRC layer during Test 2-i is displayed in Figure 4.5. G1 to G7 on the horizontal axis indicate the displacement transducers on the top surface of R-UHPFRC layer (Figure 4.3). Dashed line in Figure 4.5 shows calculated deformation and its distribution almost follows acting moment distribution. When compared with the calculated deformation, measured deformation was significantly different from the beginning of the test and that difference became larger as the number of cycles increased. This is explained from the two viewpoints as follows.

1) Variation of material properties

Variation of material properties of UHPFRC in the hardening domain may have a significant effect on observed deformation. For a given fatigue stress level, large range of local UHPFRC deformations may be obtained as shown in Figure 4.6 leading to the large variation in local deformation values as measured by G1 to G7 transducers.

2) Reduction of UHPFRC stiffness

Stiffness of UHPFRC was reduced due to micro- and macrocracking caused by fatigue stress as the number of cycles increased. Therefore, deformation of R-UHPFRC developed gradually under the same acting moment. In the case of Test 2-i, it was observed that several macrocracks intensively developed at G3 zone, which led to reduction of UHPFRC stiffness locally and the deformation of G3 zone thus increased significantly (Figure 4.5). Approaching the end of the test, these macrocracks coalesced into one distinct macrocrack (Figure 4.7).

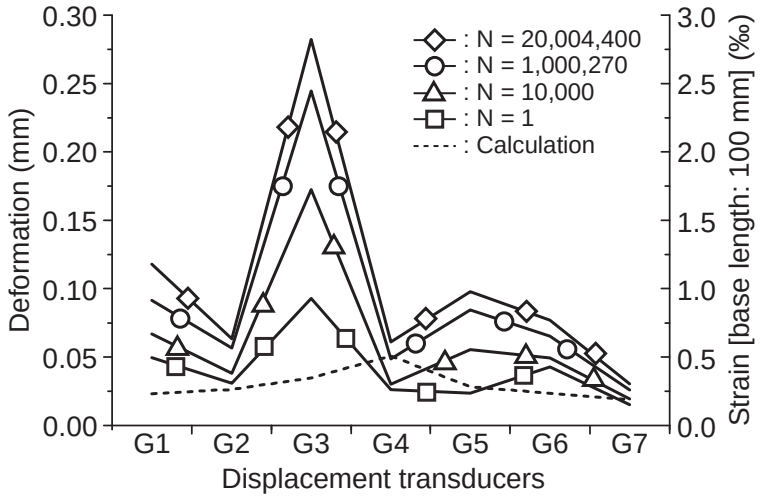

Figure 4.5 Distribution and evolution of deformation of R-UHPFRC layer during Test 2-i

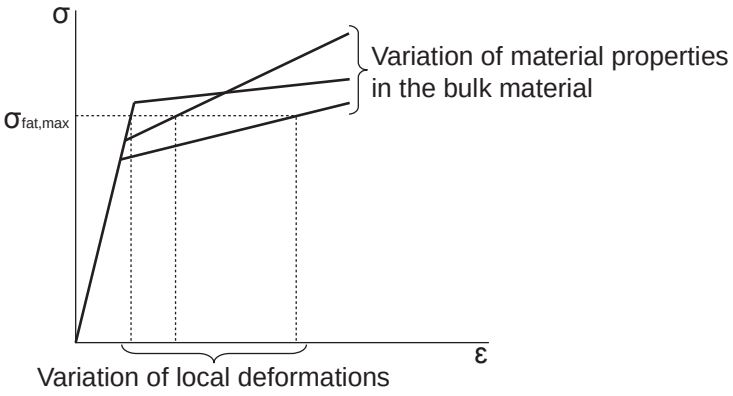

Figure 4.6 Variation of local deformation of UHPFRC under constant tensile fatigue stress

4.4.2.2 Chronological behaviour of RU-RC beam

i. During the first 10 cycles a few vertical macrocracks developed crossing the interface between R-UHPFRC layer and RC part on the side surface of the specimen (G3 zone, Figure 4.7). Tensile stress in top steel rebars of RC part was about 30 MPa corresponding to 0.15 ‰ strain, which caused macrocracking of the concrete. The presence of R-UHPFRC layer cannot prevent but reduce this macrocracking in concrete.

ii. As for the run-out test (Test 2-i), growth rate of deflection and deformation of R-UHPFRC layer became moderate after about 1 million cycles (Figure 4.8). Further macrocrack development on the top surface of R-UHPFRC layer and the side surface of the specimen didn't occur.

iii. As for the test showing fatigue failure (Test 2-ii), one of the four rebars in R-UHPFRC layer fractured at around 828,000 cycles (① in Figure 4.9b). As a consequence, deformation of R-UHPFRC layer and its growth rate increased and deformation localised in a macrocrack on R-UHPFRC layer. Deflection also increased slightly, but its growth rate was only slightly higher than before (① in Figure 4.9a).

iv. One of the remaining three rebars then fractured at about 1,764,000 cycles. Growth rate of deflection and localised deformation on R-UHPFRC layer became significantly large (② in Figure 4.9).

v. After sustaining additional about 168,000 cycles one of the remaining two rebars fractured at about 1,932,000 cycles (③ in Figure 4.9); then the final rebar in UHPFRC fractured at about 1,952,000 cycles (④ in Figure 4.9). Fracture of the fourth rebar was due to exhausting of resistance rather than due to fatigue.

vi. Since applied maximum fatigue bending moment was almost at the same level as the moment resistance of RC part, the RU-RC beam failed and lost its load bearing capacity soon after the fracture of R-UHPFRC layer.

All the four rebars in R-UHPFRC layer fractured almost at the same cross section causing one fracture plane in the R-UHPFRC layer perpendicular to the longitudinal axis of the RU-RC

beam (Figure 4.7).

The R-UHPFRC layer, in particular the steel rebars in the layer determine the behaviour of the RU-RC beam under bending fatigue. Stress amplitude in the steel rebars in R-UHPFRC layer is thus the most relevant factor for the fatigue behaviour of the RU-RC beam. UHPFRC carries stress and contributes to reduction of the stress in the rebars; however, stress in UHPFRC transfers to the rebars gradually as deformation (crack opening) of UHPFRC increases due to fatigue.

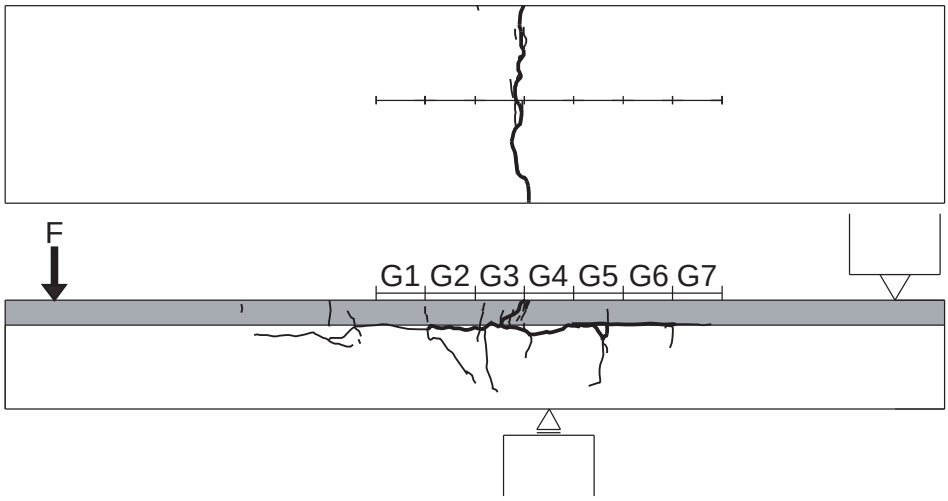

Figure 4.7 Final crack pattern of Test 2 specimen

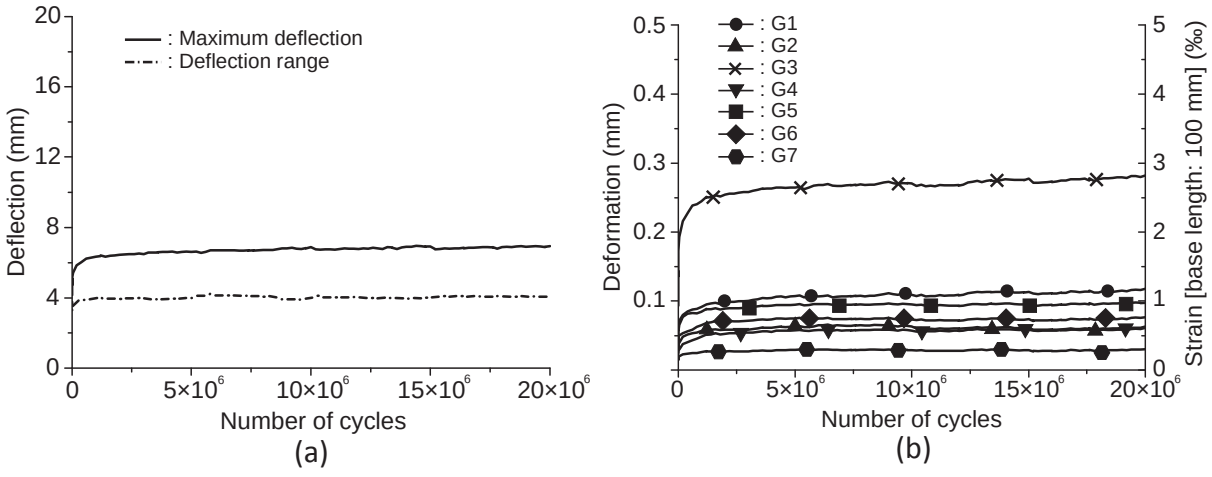

Figure 4.8 (a) Deflection and (b) deformation growth curves of Test 2-i showing no fatigue failure after 20 million cycles (run-out)

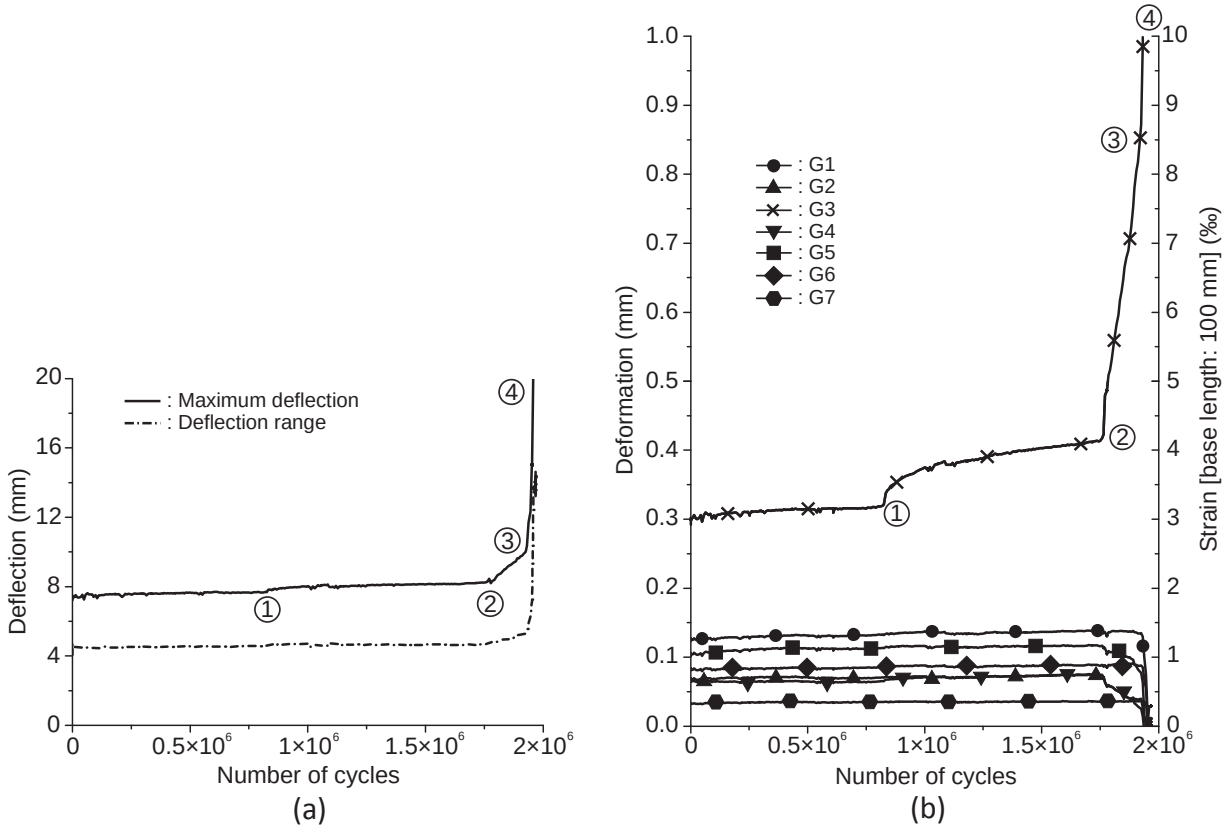

Figure 4.9 (a) Deflection and (b) deformation growth curves of Test 2-ii

4.5 Fatigue design rules for RU-RC composite members under bending fatigue

On the basis of the present experimental test results, design rules for RU-RC member under bending fatigue are proposed.

The fatigue safety of a structural member is investigated by checking if the following condition is satisfied:

$$n_{fat} = \frac{R_{d,fat}}{E_{d,fat}} \geq 1.0 \qquad \textbf{Eq. 4.1}$$

where n_{fat} is fatigue safety index; $R_{d,fat}$ examination value for the fatigue resistance; $E_{d,fat}$ examination value for the fatigue action effect. In the present case of RU-RC members, bending moment is used as examination value. As indicated in section 4.4.1, the fatigue limit of the RU-RC beam is 50 % of the ultimate static strength. Consequently, RU-RC member needs to be designed to satisfy the following condition:

$$n_{fat} = \frac{0.5 \cdot M_{Rd}}{M_{d,fat}} \geq 1.0 \qquad \textbf{Eq. 4.2}$$

where M_{Rd} is examination value of moment resistance of the RU-RC member; $M_{d,fat}$ examination value of maximum acting moment due to fatigue loading.

Since R-UHPFRC layer determines the fatigue behaviour of RU-RC member, the fatigue safety of the R-UHPFRC needs to be verified, which is done separately for both the steel rebars and the UHPFRC.

For the steel rebars, a fatigue safety check with respect to the fatigue limit is performed in a first approximation:

$$\Delta\sigma_{sd}(Q_{fat}) \leq \Delta\sigma_{sd,D} \qquad \textbf{Eq. 4.3}$$

where $\Delta\sigma_{sd}$ is examination value for stress range due to fatigue; Q_{fat} characteristic value of fatigue loading; $\Delta\sigma_{sd,D}$ examination value for fatigue limit of straight steel rebars. According to the current design codes, $\Delta\sigma_{sd,D}$ = 115 MPa for straight steel rebars of diameter smaller than 20 mm is often used.

For UHPFRC under tensile fatigue, the following criteria are proposed based on experimental tests [4.3] for maximum tensile fatigue stress and strain with respect to a fatigue limit check:

$$\sigma_{U,fat,max} \leq 0.3 \cdot (f_{Ue} + f_{Uu}) \qquad \textbf{Eq. 4.4}$$

$$\varepsilon_U \leq 0.7 \cdot \varepsilon_{Uu} \qquad \textbf{Eq. 4.5}$$

where $\sigma_{U,fat,max}$ is maximum fatigue stress in UHPFRC; f_{Ue} elastic limit strength of UHPFRC; f_{Uu} tensile strength of UHPFRC; ε_U strain in the UHPFRC due to fatigue and eventual restrained conditions in the RU-RC composite system; ε_{Uu} strain of UHPFRC corresponding to tensile strength of UHPFRC.

4.6 Application

UHPFRC and R-UHPFRC have been applied to concrete structures such as road bridges and buildings for improvement of load bearing capacity and durability [4.1, 4.4, 4.5]. A case of practical application of UHPFRC is described in this section.

Massive RC slab bridge built in 1963 with six supporting columns was improved by applying UHPFRC and R-UHPFRC to its whole deck surface including the sidewalks in autumn 2011. The bridge located near Lausanne, Switzerland, is part of a road with heavy traffic (Figure 4.10). Load bearing capacity of the bridge was found to be insufficient for today's and future vehicles. Besides, its deck slab was deteriorated due to chloride induced corrosion of steel rebars. UHPFRC layer of 25 mm thickness was designed for strengthening and waterproofing the deck except the area above columns where 65 mm-thick UHPFRC layer with steel rebars of 18 and 22 mm diameter was designed for improving bending and punching shear resistance (Figure 4.12).

The UHPFRC mix contained cement, limestone filler, silica fume, quartz sand, 4.5 % steel fibres by volume and superplasticiser. Limestone filler was used because it leads to a more economic, workable and environmentally friendly UHPFRC [4.6]. The UHPFRC material was prepared on site and about 300 litres were mixed per batch.

RC top surface of 20 to 40 mm depth was first treated with high pressure water jet. UHPFRC was then cast with standard and simple tools (Figure 4.11). Bituminous pavement was finally applied on a bituminous emulsion on the UHPFRC surface after more than three days of curing. Traffic in both directions was kept in service on one traffic lane during the works.

Figure 4.10 RC slab bridge improved with UHPFRC

Figure 4.11 Handling of UHPFRC with simple tool

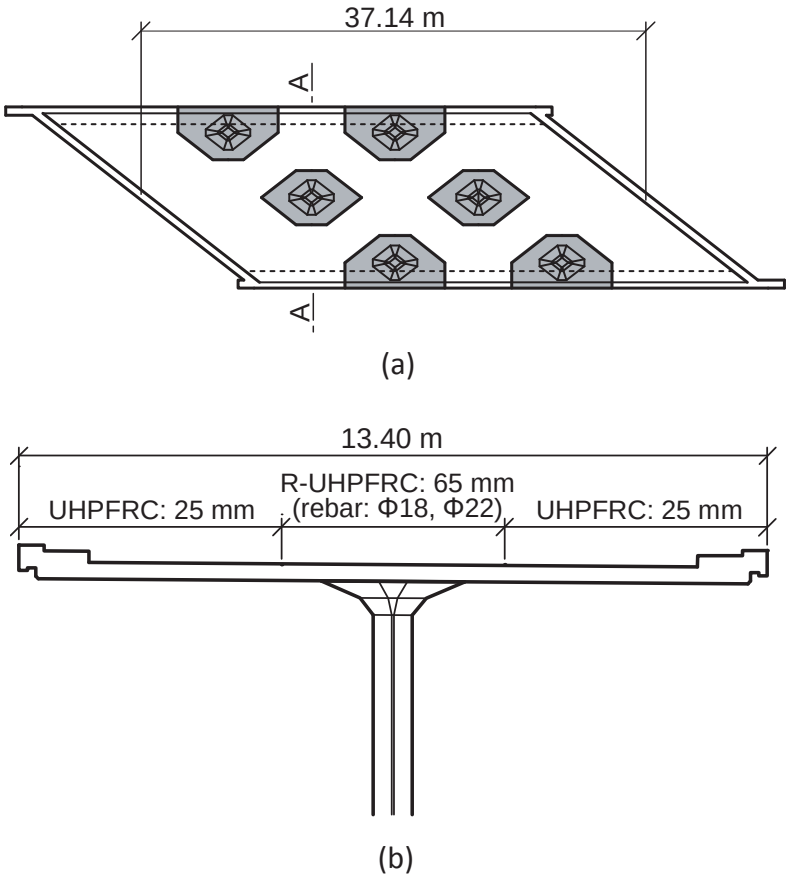

Figure 4.12 (a) Plan and (b) cross section at A-A of the RC slab bridge

4.7 Conclusion

The following conclusions are obtained from the bending fatigue tests of RU-RC beams.

1) *S-N* diagram was obtained from bending fatigue tests on RU-RC beams. Although some scatter was observed in the test results, fatigue limit at 10 million cycles was estimated to be at a solicitation level of about 50 % of the ultimate static strength of the RU-RC beam.

2) All the RU-RC beams showed similar behaviour until fatigue failure. Differences in deformation of R-UHPFRC layer between calculation and measurement is explained to be due the variation of UHPFRC material properties. Growth of the deformation of R-UHPFRC was attributed to stiffness degradation of UHPFRC caused by microcracking in the hardening domain.

3) Fatigue fracture process of RU-RC beams was determined by fatigue fracture of steel rebars in the R-UHPFRC layer. Fatigue stress amplitude in steel rebars in the R-UHPFRC layer is thus the most relevant parameter for the fatigue resistance of the RU-RC beam.

4) Fatigue design rules for RU-RC members under bending fatigue were proposed for fatigue safety check with respect to the fatigue limit. Fatigue safety needs to be checked for RU-RC member as well as for steel rebars and UHPFRC fatigue resistances.

This page is intentionally left blank.

Chapter 5

Damage models for UHPFRC and R-UHPFRC tensile fatigue behaviour

Submitted to *Engineering Structures* (version after revisions)

This page is intentionally left blank.

Damage models for UHPFRC and R-UHPFRC tensile fatigue behaviour

Abstract

Ultra-High Performance Fibre Reinforced Composites (UHPFRC) is a cementitious material showing relatively high tensile strength and significant tensile strain-hardening behaviour (given a certain volume of fibres). Adding a layer of UHPFRC or UHPFRC combined with steel rebars (R-UHPFRC) to structural members is an efficient method for strengthening of reinforced concrete structures. This paper presents empirical fatigue damage models for UHPFRC and R-UHPFRC. Tensile fatigue behaviour of UHPFRC is analysed based on elementary damage mechanics theory. Constant damage evolution rate to fatigue fracture is considered to be due to the capacity of UHPFRC to redistribute local deformation increases. Difference in damage evolution between fatigue fracture test and run-out fatigue test is highlighted, and it is understood that significant damage is caused in UHPFRC in the early stage of the fatigue life when UHPFRC fractures due to tensile fatigue. An average curve of damage evolution curves of fatigue fracture tests is proposed as a bi-linear damage evolution model of UHPFRC. The damage evolution model is used to determine the remaining fatigue life of UHPFRC by correlating damage-fatigue strain relationship for UHPFRC. Considering that stress transfer from UHPFRC to steel rebars is characteristic of R-UHPFRC tensile fatigue behaviour and is caused by fatigue damaging of the UHPFRC part, evolution of modulus of deformation, i.e. the ratio of stress to strain of the UHPFRC part of the R-UHPFRC specimens is investigated. Similar behaviour is observed in fatigue damaging curves of deformation modulus of the UHPFRC part among all the R-UHPFRC specimens. An empirical relationship between modulus of deformation of the UHPFRC part in the R-UHPFRC element and the number of fatigue cycles is proposed to characterise the R-UHPFRC tensile fatigue behaviour.

Keywords: Ultra-High Performance Fibre Reinforced Composites (UHPFRC), UHPFRC with steel rebars, tensile fatigue, damage mechanics, damage evolution, empirical relationship

5.1 Introduction

Ultra-High Performance Fibre Reinforced Composites (UHPFRC) is a cementitious material which has a compressive strength of more than 150 MPa and a tensile strength of more than 7 MPa, while developing pronounced strain-hardening (given a certain volume of fibres) and strain-softening behaviour in tension. UHPFRC also has a very low permeability for fluids providing thus high durability. Unlike conventional concrete with maximum grain size larger than 4 mm and containing no fibres, UHPFRC (with maximum aggregate sizes of less than 1 mm) carries significant tensile stress because of its relatively high tensile strength and tensile strain-hardening behaviour. For instance, overlaying UHPFRC or UHPFRC combined with steel rebars (R-UHPFRC) on the top surface of bridge deck slabs made of reinforced concrete is an

efficient intervention for increasing the ultimate resistance and improving the serviceability and durability, in particular, in parts where UHPFRC essentially carries tensile stress caused by wheel loading (Figure 5.1). In this case, repeated tensile stress cycles are imposed on the UHPFRC (R-UHPFRC) layer and sufficient fatigue resistance of UHPFRC needs to be verified in the design process. In addition, comprehension of the tensile fatigue behaviour contributes to more focused application of UHPFRC to fatigue vulnerable parts of structures like bridges.

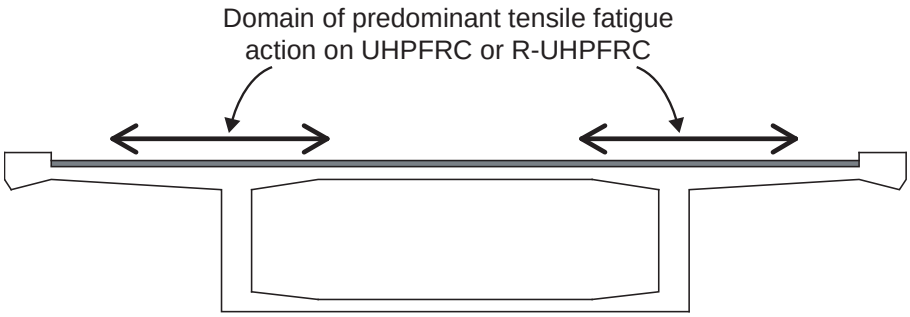

Figure 5.1 Bridge deck slab improved with UHPFRC or R-UHPFRC layer

According to [5.1], models describing the fatigue behaviour of fibre reinforced polymer composites are divided into three categories. This dividing is also applicable to fatigue models for cementitious materials. The first category refers to fatigue life models using *S-N* diagram, Goodman diagram or Palmgren-Miner rule; the second category refers to phenomenological models dealing with variation of physical quantities either directly measured by material testing or deduced from measurements; the third category refers to progressive damage models which describe the mechanism of damage progress (e.g. crack propagation).

Fatigue life models may be established from experimental test results where imposed fatigue stress (or strain) and the number of fatigue cycles are the main parameters. The actual damage caused in the material is however not taken into account in these models. For instance, from *S-N* diagram, specific relationship between applied stress and number of fatigue cycles is established enabling an estimation of fatigue life corresponding to a given applied fatigue stress.

Phenomenological models are also based on experiments, describing the variation of physical quantities such as deformation and apparent modulus of elasticity in relation to the number of fatigue cycles. Paris-Erdogan law dealing with fatigue crack growth is a model belonging to this category. Phenomenological models may be used to estimate the residual fatigue life from the change of physical quantities.

Developing of progressive damage models requires setting up a hypothesis for damage progressing mechanisms at the micro- or meso-levels and validating the models by means of experiments. Micromechanics based models dealing with constitutive relationships of the material at the meso-level and damage mechanics are representative of this category.

In the present paper, phenomenological models for UHPFRC and R-UHPFRC under tensile fatigue are proposed based on experimental results. The UHPFRC tensile fatigue behaviour is

analysed based on elementary damage mechanics theory [5.2, 5.3, 5.4, 5.5, 5.6] and characteristics of fatigue damage evolution in UHPFRC are implemented. A bi-linear damage evolution model is proposed for UHPFRC under tensile fatigue stress, with which the remaining fatigue life of UHPFRC is determined by correlating damage-fatigue strain relationship for UHPFRC. In order to describe stress transfer from UHPFRC to steel rebars which is a characteristic behaviour of R-UHPFRC [5.7], fatigue damaging of deformation modulus (the ratio of stress to strain) of the UHPFRC part of R-UHPFRC is investigated and empirical relationship between the modulus of deformation of the UHPFRC part and the number of fatigue cycles is obtained.

5.2 Literature review

There are several studies about the fatigue behaviour of the bulk UHPFRC material [5.8, 5.9, 5.10, 5.11, 5.12, 5.13, 5.14], but few literature investigating the fatigue behaviour of R-UHPFRC is available [5.15]. Regarding the fatigue behaviour of UHPFRC, several models have been developed so far.

By applying the concept of multi-layer model, Lappa [5.11] developed a progressive damage model describing the deformation growth of extreme tensile fibre of the UHPFRC beam under bending fatigue, following the methodology proposed by Hordijk [5.16] who used the multi-layer model to study the bending fatigue behaviour of conventional concrete. In the proposed model, the UHPFRC beam was subdivided into multiple layers over its height. Deformation of extreme tensile fibre of the UHPFRC beam was determined to meet the condition of force equilibrium in the cross section. Normal force and bending moment were calculated by using a constitutive fatigue damaging law and Euler-Bernoulli beam theory. Decrease of the tensile strength and modulus of elasticity was considered as fatigue damaging of the material constitutive law, which was based on the fatigue model for conventional concrete under tensile fatigue proposed by Kessler-Kramer [5.17].

Fitik [5.13, 5.14] proposed fatigue life models derived from *S*-*N* diagram and Goodman diagram and phenomenological models concerning fatigue deformation growth. Both models deal with uniaxial tensile and fully reversed tension-compression fatigue behaviour of Ultra-High Performance Concrete (UHPC) which has similar properties to UHPFRC. Four different mixes were used in the experimental tests. Fatigue life models derived from *S*-*N* diagram were proposed to describe the fatigue strength of UHPC under fully reversed tension-compression fatigue stress for different applied tensile fatigue stress in the following form:

$$LogN = b_0 + b_1 \cdot \frac{\sigma_c}{f_{cm}} \qquad \textbf{Eq. 5.1}$$

where N is the number of fatigue cycles until failure; σ_c is the applied maximum compressive

fatigue stress; f_{cm} is the average compressive strength of UHPC; b_0 and b_1 are coefficients determined by regression analysis. It was shown that UHPC fatigue strength increased with decreasing tensile fatigue stress.

Expressions of fatigue deformation growth were deduced for each combination of fatigue stresses in the following form:

$$\varepsilon = a^m \cdot (\frac{n}{N} + b)^m + c \cdot \frac{n}{N} + e \qquad \textbf{Eq. 5.2}$$

where ε is fatigue strain; n is the number of fatigue cycles; a, b, c, e and m are coefficients determined by experimental tests. Coefficient b was fixed to be -0.5 for numerical reasons.

5.3 Experimental results

Experimental campaign was conducted to investigate the tensile fatigue behaviour of UHPFRC and R-UHPFRC where tensile strain-hardening UHPFRC was used. Details of the experiments are reported in [5.18] for UHPFRC and [5.7] for R-UHPFRC. In the following, main findings from tensile fatigue tests of UHPFRC and R-UHPFRC are summarised.

5.3.1 Tensile fatigue test of UHPFRC

Monolithic UHPFRC specimens with a rectangular cross section were used for the tensile fatigue tests (Figure 5.2a). UHPFRC mix was characterised by 3.0 vol.-% content of steel fibres 13 mm long with a diameter of 0.16 mm and by the use of CEM III/B type cement which contains a high percentage of blast furnace slag (66 % to 80 %). The specimens were 750mm long with a cross section of 150 mm × 40 mm. In order to cause fracture within the 250 mm-long central zone of the specimen, aluminium plates (250 mm long, 150 mm wide and 2 mm thick) were glued to both surfaces of the specimen end parts as strengthening elements. Two 250 mm-long Linear Variable Differential Transducers (LVDTs) and five displacement transducers with a 50mm measurement length were used to measure the specimen deformation (Figure 5.2a). LVDTs were set up on both of specimen sides to measure global specimen deformation $\Delta\ell_g$. The five displacement transducers were set up on the specimen surface to measure local specimen deformation $\Delta\ell_l$ in five consecutive zones.

Three quasi-static tensile tests were performed using the same UHPFRC specimens as used in the tensile fatigue tests. The specimens of the quasi-static tensile tests were fabricated from the same batch of UHPFRC mix as for the S1 series tensile fatigue test (S1 series is explained in the following paragraph). Average of the elastic limit and ultimate strength of UHPFRC (f_e and f_u) was determined to be 8.2 MPa and 9.4 MPa, respectively, where strain-hardening capacity was 1.33 ‰ (Figure 5.3).

Force-controlled constant amplitude tensile fatigue tests consisting of three test series were conducted at various imposed stress levels as characterized by maximum applied fatigue

stress σ_{max} and pre-applied deformation. Each fatigue test series was characterised as follows, referring to the quasi-static stress-strain curve according to Figure 5.2b:

- S1 series: maximum fatigue stress high in the elastic domain
- S2 series: initial application of deformation entering into the strain-hardening domain followed by fatigue testing
- S3 series: initial application of deformation entering into the strain-softening domain followed by fatigue testing

From the test results plotted in the *S-N* diagrams, the fatigue endurance limit at 10 million cycles was determined to be at about 70 %, 55 to 65 % and 45 % of the elastic limit strength for the S1, S2 and S3 series, respectively (Figure 5.4). 10 million fatigue cycles were chosen because it is a realistic number for representing axles loading in heavily trafficked bridges, and it is also considered as a lower bound of the very high cycle fatigue domain. Measured global and local specimen deformations were plotted against the number of fatigue cycles *N* for each test (Figure 5.5a and b). Fatigue deformation as recorded from the S1 series showed four distinct characteristic behaviours, that is, redistribution of localised deformation, variations in local deformation, change in deformation range and a particular relationship between modulus of deformation and global specimen deformation. Since deformation caused by preloading was relatively high in the S2 and S3 series, residual deformation was predominant on the fatigue deformation readings and hence noteworthy fatigue deformation behaviour wasn't observed.

All the quasi-static and fatigue tests in this experimental campaign were performed in the mode of uniaxial tension. Since there was a possibility that asymmetric micro- and macrocracks were formed leading to concomitant bending of the UHPFRC specimen, by setting up displacement transducers on both surfaces of several specimens (five displacement transducers on each surface), the formation of asymmetric micro- and macrocracks was monitored. Deflection of the specimens wasn't explicit in measurements of the displacement transducers and thus applied tensile force was regarded as uniaxial.

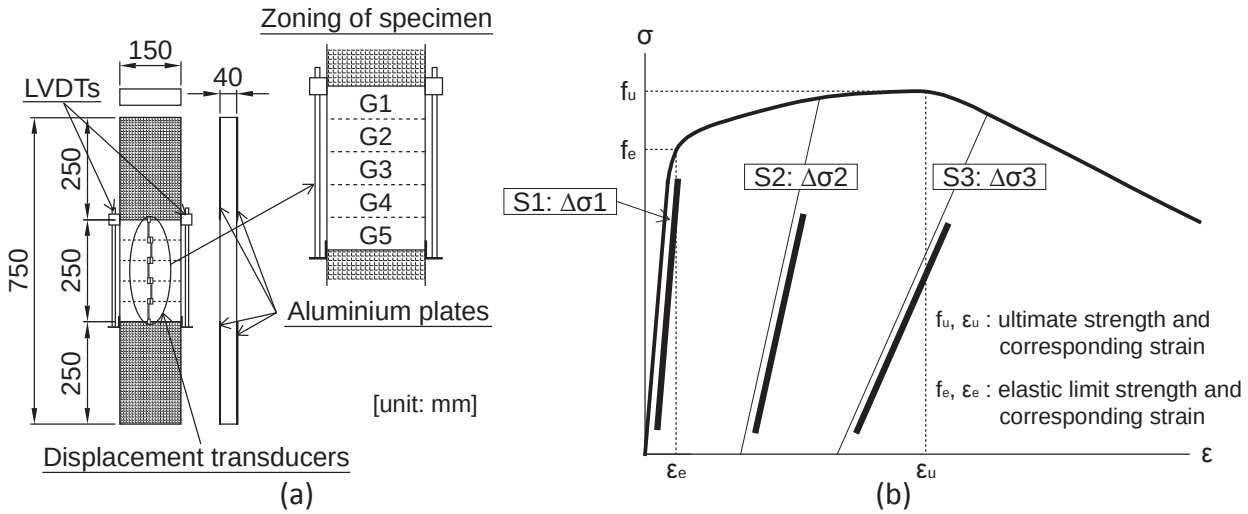

Figure 5.2 (a) UHPFRC specimen geometry and measuring instruments and (b) schematic representation of quasi-static tensile response of UHPFRC and definition of fatigue test series

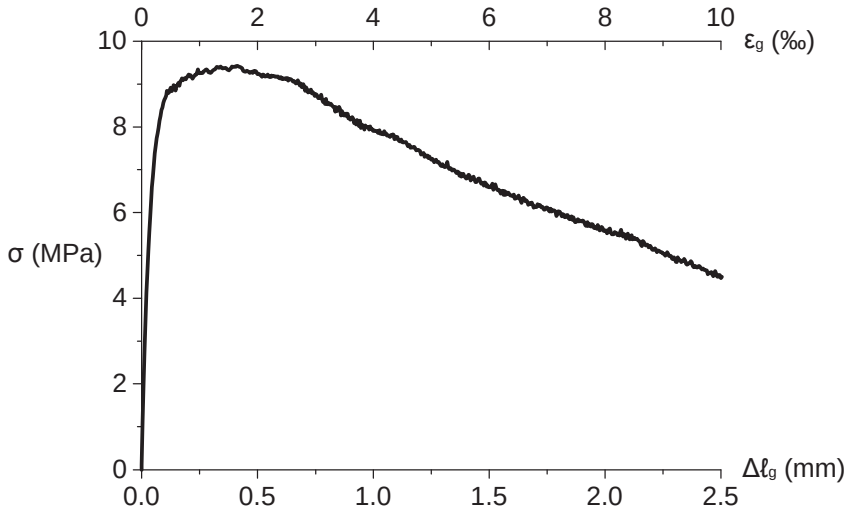

Figure 5.3 Average stress-strain curve obtained from three quasi-static tensile tests of UHPFRC

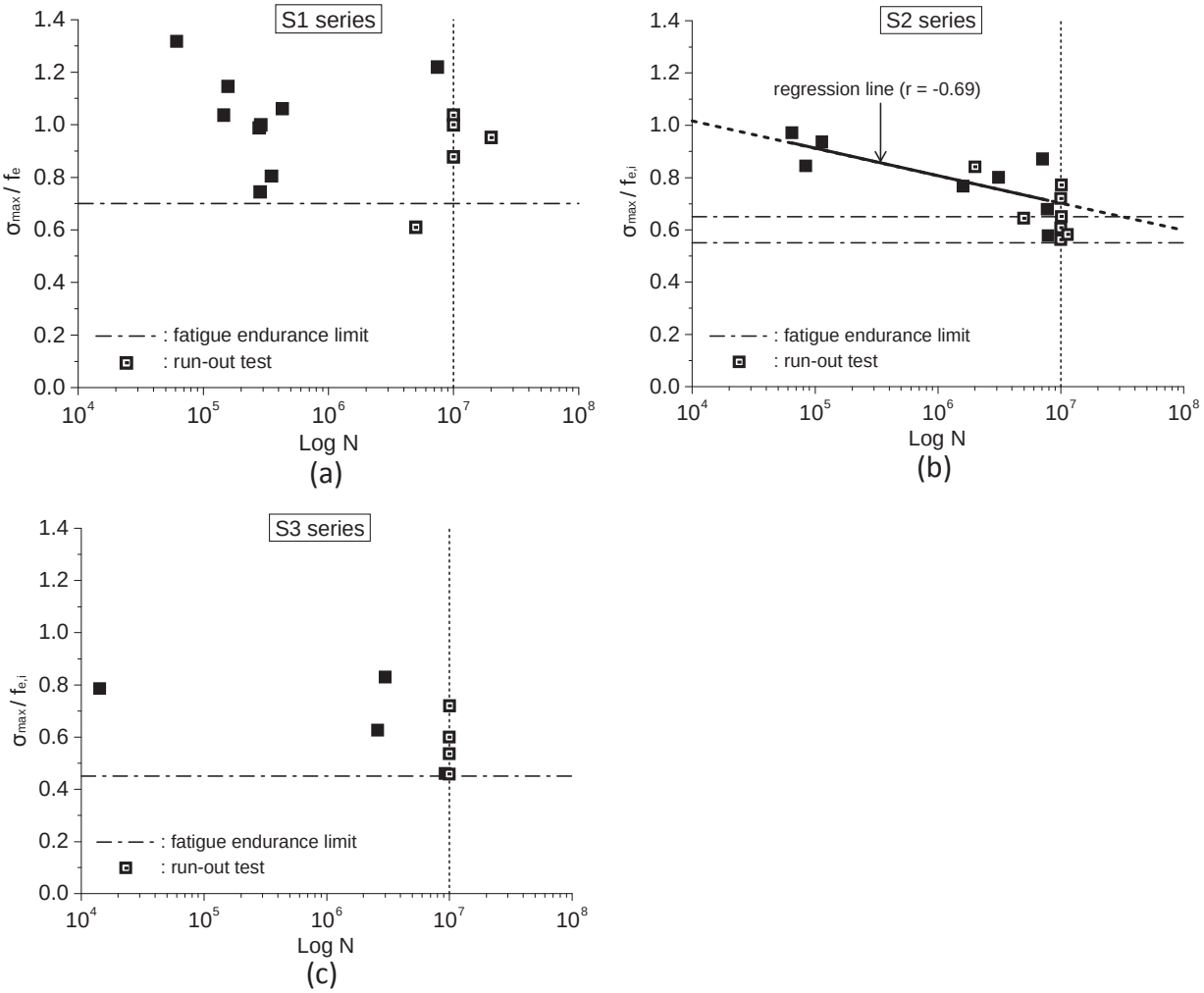

Figure 5.4 *S-N* diagrams of (a) S1 series, (b) S2 series and (c) S3 series

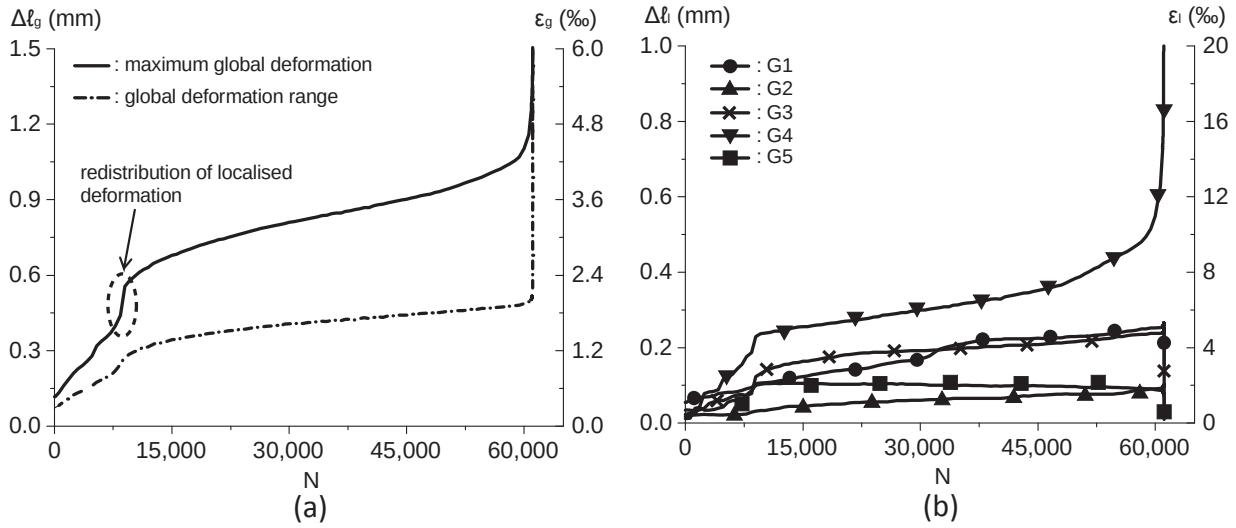

Figure 5.5 Deformation growth during a tensile fatigue test of UHPFRC leading to fracture (a) global specimen deformation and (b) local specimen deformation

5.3.2 Tensile fatigue test of R-UHPFRC

Dog-bone shaped R-UHPFRC specimens were used for the tensile fatigue tests (Figure 5.6). The same UHPFRC mix was used as the tensile fatigue testing of bulk UHPFRC and three steel rebars of Grade B500B with a diameter of 8 mm (nominal yield strength of 500 MPa) were combined. Maximum fatigue force F_{max} was determined so as to cause stress range in the steel rebars between 170 and 230 MPa. Constant amplitude tensile fatigue force was applied to the specimens. Global and local specimen deformation was measured with two LVDTs and five displacement transducers in the central part of the specimens (Figure 5.6).

Test results were plotted in the *S*-*N* diagram from which the fatigue endurance limit at 10 million cycles was determined to be at about 54 % of the estimated ultimate static strength F_u (Figure 5.7). Considering that at this fatigue force level UHPFRC behaviour is in the strain-hardening domain, steel rebars improved actually the fatigue resistance of UHPFRC by distributing the imposed fatigue stress. Fatigue deformation behaviour of R-UHPFRC was dependent on the stage during the fatigue test. In the early stage of the fatigue test, UHPFRC mainly determined the fatigue deformation behaviour of R-UHPFRC whereas in the intermediate and final stages of the fatigue test, steel rebars predominantly determined the fatigue deformation behaviour of R-UHPFRC. Stress transfer from UHPFRC to steel rebars characterised the R-UHPFRC behaviour in terms of fatigue resistance and deformation growth (Figure 5.8). Steel rebars fractured one by one, and chronological order of the steel rebar fracture was determined from characteristics of fracture surfaces of the steel rebars.

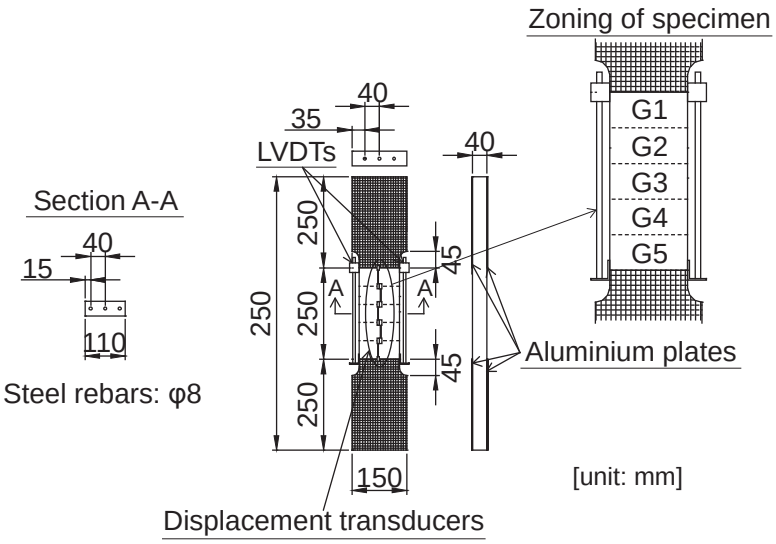

Figure 5.6 R-UHPFRC specimen geometry and measuring instruments

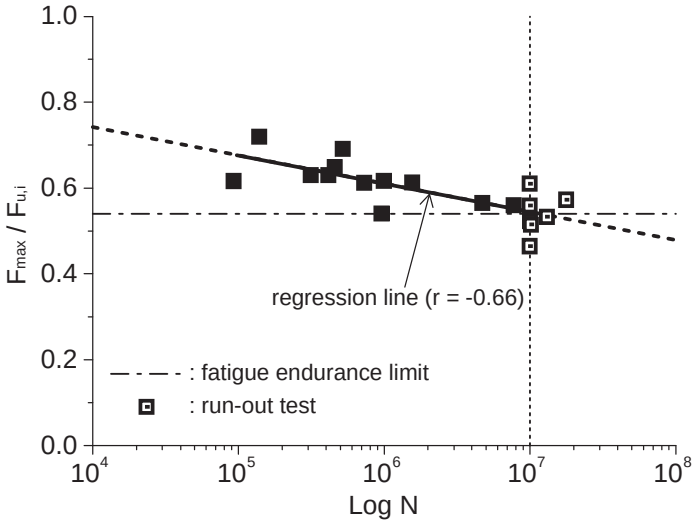

Figure 5.7 *S-N* diagram obtained from tensile fatigue tests of R-UHPFRC

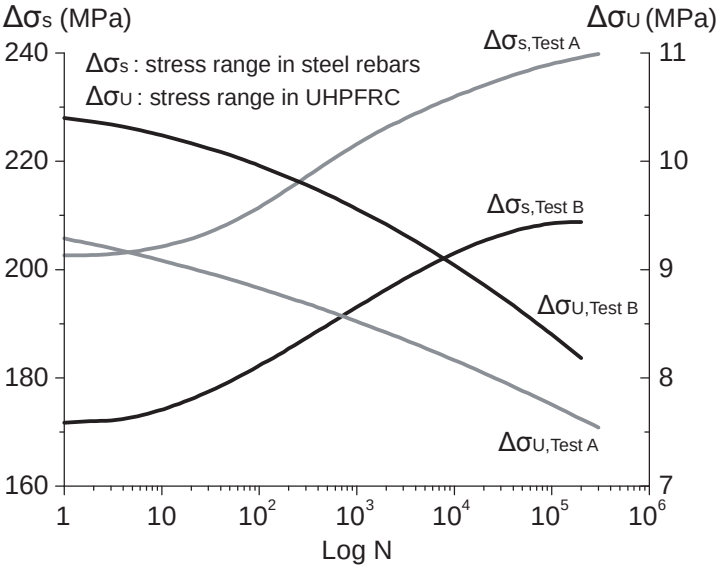

Figure 5.8 Stress transfer from UHPFRC to steel rebars in R-UHPFRC as a function of fatigue cycles obtained from two experimental tests

5.4 Fatigue damaging of UHPFRC

Fatigue fracture of materials occurs as a result of damage accumulation in the materials. If the degree of damage in materials can be represented by a physical quantity, the probability of occurrence of fatigue fracture of the materials may be expressed quantitatively. In this section, damage evolution in UHPFRC under tensile fatigue is described based on elementary damage mechanics theory [5.2, 5.3, 5.4, 5.5, 5.6]. Damage is supposed to develop because of the presence of defects such as microflaws and microvoids leading to stress concentrations with subsequent increase of these defects. Damage manifests itself macroscopically as a reduction of modulus of deformation or strength. In the present study, damage is macroscopically dealt with and its evolution is investigated by using the modulus of deformation of UHPFRC as obtained from experimental results. Fatigue damage in UHPFRC is characterised by anisotropic phenomena because of variations in local deformation as observed in the tensile fatigue tests (Figure 5.5b). However, for simplicity, UHPFRC is regarded as isotropic in the present study until deformation localisation takes place.

5.4.1 Damage variables

Damage state of UHPFRC is represented by damage variables which are defined by using a rectangular cuboid (Figure 5.9). The damage variable characterised by modulus of deformation is derived based on elementary concepts of damage mechanics according to [5.6, 5.19].

Consider the isotropic damage state of a surface element dA in a rectangular cuboid (Figure 5.9). Assume that fatigue damage is produced by the development of microscopic voids and the total voids area in dA is dA_D. The net area carrying the applied force on the surface element dA is expressed as:

$$d\tilde{A} = dA - dA_D \qquad \textbf{Eq. 5.3}$$

where $d\tilde{A}$ is the effective area. It is understood from Equation 5.3 that as the damage increases in the surface element dA, i.e. dA_D increases, $d\tilde{A}$ gradually decreases, and consequently, force carrying capacity also decreases.

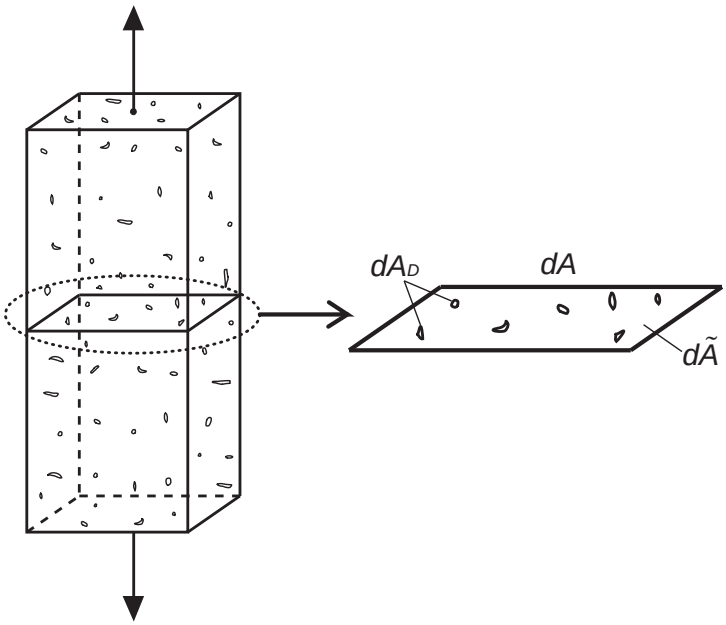

Figure 5.9 Microscopic voids as damage and effective area (after [5.6])

Equation 5.3 is now converted by introducing the damage variable *D*:

$$d\tilde{A} = (1-D)dA \quad \text{with} \quad D = \frac{dA_D}{dA} \qquad \textbf{Eq. 5.4}$$

The damage variable *D* is specified as:

$D = 0$: initial undamaged state

$D = D_c$: final fractured state

where D_c is maximum value of damage. If the definition of damage variable is followed strictly, when D_c is equal to 1, stress carrying capacity is completely lost and fracture of the material occurs. However, failure of structural members occurs before *D* becomes 1, i.e. dA_D reaches *dA*. In fact, tensile fatigue fracture of UHPFRC occurs before a fatigue macrocrack propagates over full sectional area of the member as the applied maximum fatigue stress needs to be carried by the uncracked sectional area. When the maximum fatigue stress reaches the ultimate resistance of the uncracked remaining cross section, the specimen fails [5.18].

When tensile force *dF* is applied to a surface element *dA* in a rectangular cuboid (Figure 5.10b), the stress σ is written as:

$$\sigma = \frac{dF}{dA} \qquad \textbf{Eq. 5.5}$$

Due to damage, applied force *dF* is actually carried by effective area $d\tilde{A}$ (Figure 5.10c). The stress induced in the effective area is obtained as:

$$\tilde{\sigma} = \frac{dF}{d\tilde{A}} = \frac{dF}{(1-D)dA} = \frac{\sigma}{1-D} \qquad \textbf{Eq. 5.6}$$

where $\tilde{\sigma}$ is the effective stress. It is supposed that the damaged rectangular cuboid subjected to tensile force *dF* with the cross sectional area *dA* (Figure 5.10b) is mechanically equivalent to a fictitious undamaged rectangular cuboid subjected to the same tensile force *dF* with the cross sectional area $d\tilde{A}$ (Figure 5.10c). Accordingly, strain ε in the fictitious undamaged rectangular cuboid caused by stress $\tilde{\sigma}$ is identical to that in damaged rectangular cuboid caused by stress σ (Figure 5.10b and c). σ and $\tilde{\sigma}$ are written as:

$$\sigma = E\varepsilon, \quad \tilde{\sigma} = E_0\varepsilon \qquad \textbf{Eq. 5.7}$$

where *E* is the modulus of deformation at the damaged state; E_0 is the modulus of deformation at the initial undamaged state. Subsequently, effective stress $\tilde{\sigma}$ is given by:

$$\tilde{\sigma} = \frac{E_0}{E}\sigma \qquad \textbf{Eq. 5.8}$$

From Equations 5.6 and 5.8, the damage variable *D* characterised by modulus of deformation is obtained as:

$$D = 1 - \frac{E}{E_0} \qquad \textbf{Eq. 5.9}$$

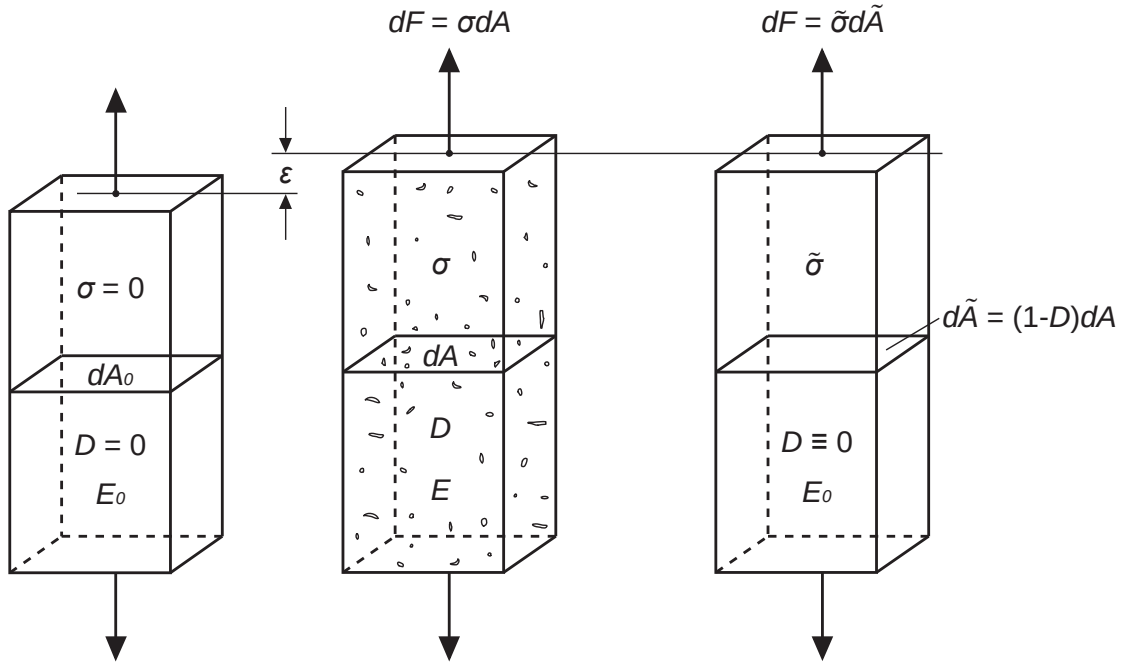

(a) undamaged state (b) damaged state (c) fictitious undamaged state

Figure 5.10 Deformation and damage of a rectangular cuboid under tensile force (after [5.6])

5.4.2 Damage analysis of tensile fatigue behaviour of UHPFRC

5.4.2.1 Definition of parameters

Modulus of deformation of UHPFRC under tensile fatigue stress at *i*-th cycle $E_{U,fat,i}$ is determined as follows:

$$E_{U,fat,i} = \frac{\sigma_{max} - \sigma_{min}}{\varepsilon_{max,i} - \varepsilon_{min,i}} \quad \textbf{Eq. 5.10}$$

where σ_{max} and σ_{min} are the applied maximum and minimum fatigue stresses (being constant); $\varepsilon_{max,i}$ and $\varepsilon_{min,i}$ are maximum and minimum measured global strain at *i*-th cycle. Dividing $E_{U,fat,i}$ by the initial modulus of deformation of a specimen $E_{U,fat,0}$ yields normalised modulus of deformation $E_{U,fat,n}$ as:

$$E_{U,fat,n} = \frac{E_{U,fat,i}}{E_{U,fat,0}} \quad \textbf{Eq. 5.11}$$

By inserting Equation 5.11 into Equation 5.9, expression of fatigue damage of UHPFRC is obtained as:

$$D = 1 - E_{U,fat,n} \quad \textbf{Eq. 5.12}$$

In order to analyse fatigue damage evolution of all specimens along the same time base, damage variables were plotted against normalised number of fatigue cycles N_n which is calculated as:

$$N_n = \frac{N}{N_f} \quad \textbf{Eq. 5.13}$$

where N is the number of fatigue cycles; N_f is the sustained number of fatigue cycles to failure. In the following, tensile fatigue behaviour of UHPFRC is analysed in terms of damage by using the experimental results of S1 series tensile fatigue test of UHPFRC.

5.4.2.2 Constant damage evolution

Figure 5.11 shows the damage evolution curves of five specimens of S1 series obtained from five fatigue tests in which the specimens fractured (called 'fracture tests' hereafter) and three run-out tests, where among five specimens, two specimens reached run-out once and twice, respectively. When a specimen sustained 10 million cycles, this result was regarded as "run-out" and the subsequent test was continued with an increased fatigue stress.

For all fracture tests, damage variables increase approximately linearly with similar rate between N_n = 0.2 and 0.9 in spite of the fact that among these five specimens, initial damage states before fracture tests vary depending on each testing history, i.e. with or without preceding run-out tests, and damage variables vary during fracture tests. In this range, average

damage evolution rate dD/dN_n is determined to be 0.33. Constant damage evolution rate dD/dN_n irrespective of damage degree may be explained by the capacity of UHPFRC to redistribute local deformation increases due to damage concentration.

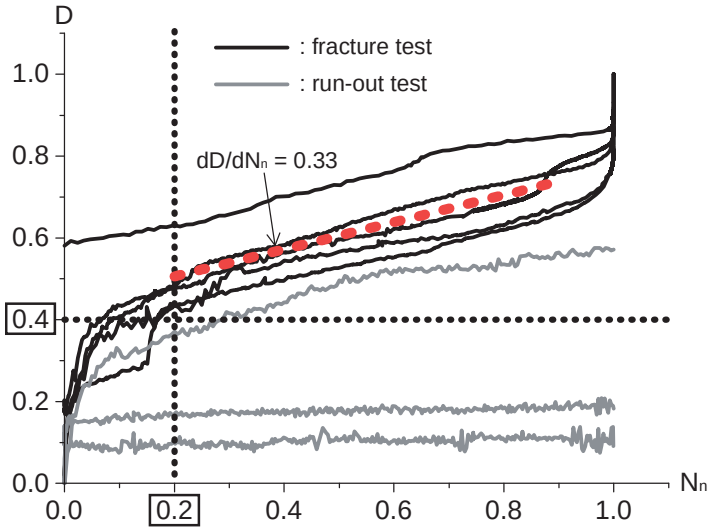

Figure 5.11 Damage evolution curves of UHPFRC under tensile fatigue

5.4.2.3 Significant damaging at the early stage of the fatigue life

In order to understand the difference in damage evolution between fracture tests and run-out tests, damage evolution of run-out tests and its evolution rate were investigated. In Figure 5.12, damage evolution curves of two (out of five) specimens obtained from run-out tests and subsequent fracture tests are shown. Since Specimen 1 reached run-out twice, there are two damage evolution curves obtained from the run-out tests of Specimen 1.

During the run-out tests, damage in Specimen 1 increased slightly (Figure 5.12a), while damage in Specimen 2 increased until about N_n = 0.55 in a similar way like specimens which fractured in the first fatigue test: rapid increase during the first 20 % of the fatigue life followed by moderate and constant damage evolution (Figure 5.12b). There are two reasons for Specimen 2 to reach run-out despite the fact that its damage evolution was similar to that of fracture specimens.

One reason is that dD/dN_n of Specimen 2 became smaller after N_n = 0.55. Between N_n = 0.2 and 0.55, dD/dN_n of Specimen 2 was 0.42, and after N_n = 0.55 it became 0.13. This was caused by a change of stress carrying behaviour of UHPFRC due to redistribution of deformation localisation, which was confirmed by local deformation measurements (Figure 5.13).

A second reason is that increase of damage during the first 20 % of the fatigue life was less significant than that of fracture specimens. At N_n = 0.2, damage values of fracture specimens were larger than 0.4, whereas those of run-out specimens were smaller than 0.4 (Figure 5.11). From this follows that more than 40 % of the bulk UHPFRC material is damaged in the early stage of fatigue stress application when UHPFRC fractures due to tensile fatigue.

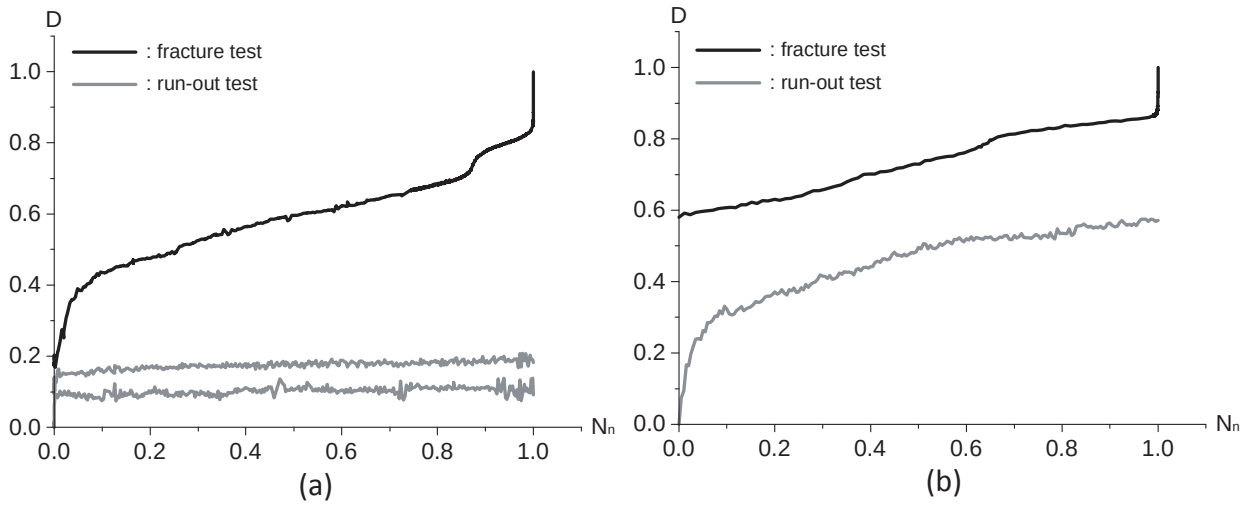

Figure 5.12 Comparison of damage evolution between run-out tests and fracture tests (a) Specimen 1 undergoing run-out twice and (b) Specimen 2 undergoing run-out once

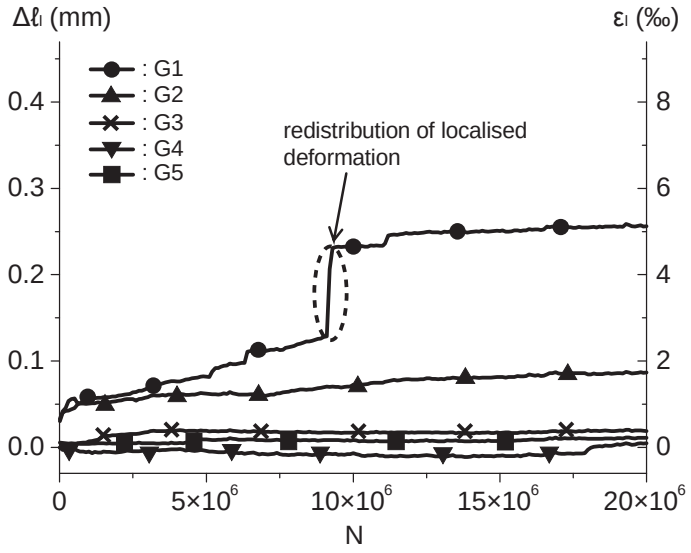

Figure 5.13 Local deformation growth during run-out test of Specimen 2

5.4.3 Fatigue damage modelling of UHPFRC

5.4.3.1 Damage evolution model of UHPFRC

From the damage evolution curves obtained from five fracture tests, damage evolution model of UHPFRC was deduced as a simplified form (Figure 5.14). It is represented as a bi-linear curve and expressed as:

$$D = 2.53 \cdot N_n \quad \text{for} \quad 0 \le N_n < 0.2 \qquad \textbf{Eq. 5.14}$$

$$D = 0.33 \cdot N_n + 0.44 \quad \text{for} \quad 0.2 \le N_n \le 1 \qquad \textbf{Eq. 5.15}$$

As discussed in section 5.4.2.2, between N_n = 0.2 and 0.9, the damage evolution curves of all fracture tests are roughly linear and the slope of those curves are similar. The damage evolution model between N_n = 0.2 and 0.9 was determined as an average linear curve of the damage evolution curves of five fracture tests. The average linear curve was extended to describe the damage evolution between N_n = 0.9 and 1. For N_n of 0 to 0.2, the damage evolution model was determined by connecting the origin of coordinates with a point on the average linear curve at N_n = 0.2.

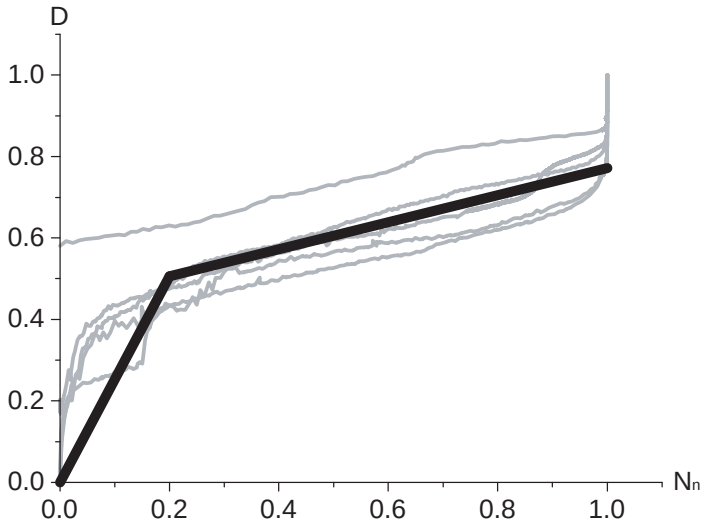

Figure 5.14 Damage evolution model of UHPFRC

5.4.3.2 Damage-fatigue strain relationship

When damage variable was plotted against maximum fatigue global strain for the same five specimens as dealt with in section 5.4.2, all curves showed a similar behaviour (Figure 5.15). Obviously, these curves are equivalent to the inverse of relationship between modulus of deformation and maximum fatigue global strain as discussed in [5.18]. By taking the average of these curves, an expression is determined for the relationship between damage variable and maximum fatigue global strain as:

$$D = -1.37 \cdot e^{-\frac{\varepsilon_{g,max}}{0.36}} - 0.28 \cdot e^{-\frac{\varepsilon_{g,max}}{4.87}} + 1 \qquad \textbf{Eq. 5.16}$$

where $\varepsilon_{g,max}$ is maximum fatigue global strain of UHPFRC. By using this relationship, damage degree in UHPFRC under tensile fatigue is derived from maximum fatigue strain.

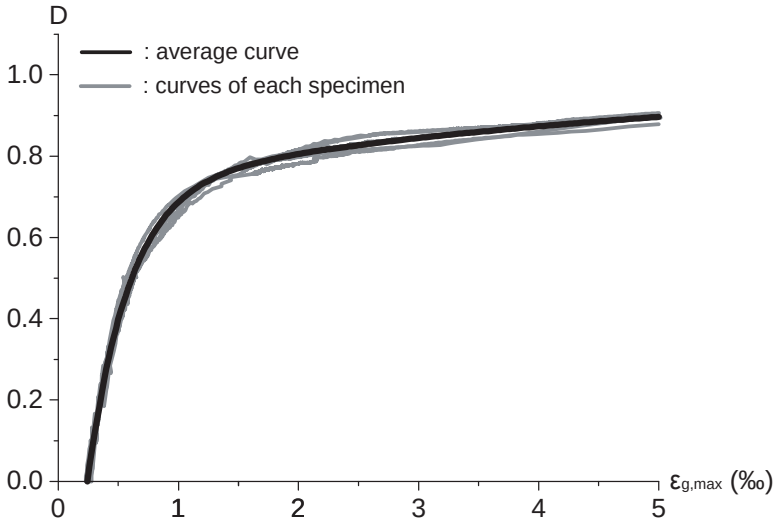

Figure 5.15 Relationship between damage variable and maximum fatigue global strain

5.4.3.3 Determination of the remaining fatigue life

By combining the proposed damage evolution model with damage-fatigue strain relationship, the remaining fatigue life of UHPFRC is determined. An example is explained in the following.

Assuming that maximum fatigue strain of UHPFRC is 0.8 ‰. At this strain value, damage variable is obtained to be 0.62 from Equation 5.16. When damage variable is 0.62, normalised number of cycles is calculated to be 0.53 from Equation 5.15. Consequently, it is understood that 47 % of the fatigue life for UHPFRC is remaining.

Since determined remaining fatigue life is represented in a relative expression, it is necessary to convert it into an absolute expression to obtain the remaining fatigue life in terms of number of cycles. The conversion is performed by using an expression representing fatigue strength of UHPFRC:

$$Log N = -9.55 \cdot \frac{\sigma_{max}}{f_e} + 13.72 \qquad \textbf{Eq. 5.17}$$

This expression was determined from the *S-N* diagram of S2 series tensile fatigue test of UHPFRC by regression analysis without considering run-out tests. Since in the S2 series, deformation entering into the strain-hardening domain was statically imposed on the specimens before fatigue testing and thus the specimens were initially damaged, the fatigue life determined from Equation 5.17 is rather conservative for UHPFRC which is not subjected to stress beyond the elastic limit before fatigue stress application.

This method is applicable to UHPFRC of elements in existing structures where the strain in the UHPFRC due to maximum fatigue loading is measured and subsequently maximum fatigue stress σ_{max} determined.

5.5 Fatigue damage relationship for R-UHPFRC

The tensile fatigue behaviour of R-UHPFRC is characterised by stress transfer from UHPFRC to steel rebars [5.7]. This stress transfer is described in the following by considering decrease of deformation modulus of the UHPFRC due to fatigue assuming that applied fatigue stress is carried by UHPFRC and steel rebars depending on their moduli of deformation or elasticity, respectively. While the modulus of elasticity of steel rebar E_s is constant (= 205 GPa), modulus of deformation of UHPFRC in R-UHPFRC depends on fatigue damage and is obtained as follows. Firstly fatigue stress at *i*-th cycle carried by steel rebars $\sigma_{s,fat,i}$ is calculated according to Equation 5.18 using global deformation at *i*-th cycle $\Delta\ell_{g,i}$ obtained from LVDTs on the UFPFRC surface. This calculation is needed because no direct deformation measurements on the steel rebars were carried out.

$$\sigma_{s,fat,i} = E_s \cdot \frac{\Delta\ell_{g,i}}{\ell_b} \qquad \textbf{Eq. 5.18}$$

where ℓ_b is base length of LVDTs. Fatigue stress at *i*-th cycle in UHPFRC $\sigma_{RU,fat,i}$ is then obtained by subtracting the force carried by steel rebars from applied fatigue force F_{fat} according to Equation 5.19.

$$\sigma_{RU,fat,i} = \frac{F_{fat} - A_s \cdot \sigma_{s,fat,i}}{A_U} \qquad \textbf{Eq. 5.19}$$

where A_s is the sectional area of three steel rebars; A_U is the sectional area of UHPFRC. Finally modulus of deformation of UHPFRC in R-UHPFRC at *i*-th cycle $E_{RU,fat,i}$ is calculated by inserting maximum and minimum fatigue stress at *i*-th cycle in UHPFRC (as obtained by Equation 5.19) into Equation 5.21 with global strain at *i*-th cycle ε_i calculated as:

$$\varepsilon_i = \frac{\Delta\ell_{g,i}}{\ell_b} \qquad \textbf{Eq. 5.20}$$

$$E_{RU,fat,i} = \frac{\sigma_{RU,max,i} - \sigma_{RU,min,i}}{\varepsilon_{max,i} - \varepsilon_{min,i}} \qquad \textbf{Eq. 5.21}$$

Figure 5.16 shows moduli of deformation of UHPFRC $E_{RU,fat}$ as determined from nine test specimens (out of twelve) plotted against log-scaled number of fatigue cycles. Only the first fatigue test result was used to draw the fatigue decreasing curve of $E_{RU,fat}$ in cases where more than one fatigue test was conducted on a specimen. This is because decrease of $E_{RU,fat}$ due to fatigue wasn't observed in the second and third fatigue tests conducted on specimens reaching run-out, which is supposed to be due to the change of the main stress carrying element in R-UHPFRC from UHPFRC to steel rebars in the early stage of the first fatigue test (until about 500,000 cycles).

UHPFRC mainly carried fatigue stress in the early stage of the first fatigue test and deformation behaviour of R-UHPFRC was strongly influenced by UHPFRC whose deformation

was observed to grow under tensile fatigue [5.18]. Thus, decrease of $E_{RU,fat}$ due to fatigue occurred in the early stage of the first fatigue test. Then, fatigue stress gradually transferred to steel rebars due to fatigue damaging of UHPFRC and steel rebars became the main fatigue stress carrying element in R-UHPFRC. Consequently, deformation behaviour of R-UHPFRC was predominantly influenced by steel rebars and since steel rebars do not show any deformation growth under tensile fatigue, global deformation of the R-UHPFRC specimen was rather constant. Accordingly, decrease of $E_{RU,fat}$ due to fatigue didn't occur after the early stage of the first fatigue test. In the subsequent second and third fatigue tests, steel rebars were the main fatigue stress carrying element from the beginning and thus $E_{RU,fat}$ didn't decrease further.

Since all specimens were preloaded to a level subjecting UHPFRC to a solicitation in the strain-hardening domain (in order to determine the maximum force for subsequent fatigue testing), $E_{RU,fat}$ at the first fatigue cycle was already reduced compared to the original state of the UHPFRC.

Although the specimens showed different $E_{RU,fat}$ at the first fatigue cycle, all specimens revealed similar trends in decrease of $E_{RU,fat}$ due to fatigue: it slowly decreased until about 30 cycles, and then its decrease rate increased while keeping its rate constant until about 30,000 cycles. Finally the decrease rate again became small and it stopped decreasing at about 500,000 cycles.

In order to deduce a curve describing decreasing behaviour of $E_{RU,fat}$ due to fatigue, each decreasing curve of Figure 5.16 was normalised with respect to the modulus of deformation at the first cycle $E_{RU,fat,1}$, eliminating thus the influence of preloading. Figure 5.17 shows normalised fatigue decreasing curves of $E_{RU,fat}$ as a function of the number of fatigue cycles. Damaging process is subdivided into three stages, namely slow damaging in the first and third stages while relatively rapid damaging in the second stage (Figure 5.17). It is understood that regardless of applied fatigue force level, decrease of $E_{RU,fat}$ due to fatigue stops at about 500,000 cycles when $E_{RU,fat}$ has reduced by about 30 %. Expression for normalised fatigue decreasing curve of deformation modulus of UHPFRC $E_{RU,fat,n}$ is finally obtained from the average curve of all normalised fatigue decreasing curves as follows:

$$E_{RU,fat,n} = 0.68 + 0.32 \cdot \sin^2\left(\frac{LogN + 5.7}{11.4}\pi\right) \quad \text{for} \quad N \leq 500{,}000 \qquad \textbf{Eq. 5.22}$$

This relationship is valid only for R-UHPFRC members subjected to constant amplitude tensile fatigue force imposing stress in the strain-hardening domain on UHPFRC. In addition, it is assumed in Equation 5.22 that stress transfer from UHPFRC to steel rebars takes place until 500,000 cycles and then stress range in steel rebars remains constant until one of the steel rebars fails due to fatigue fracture.

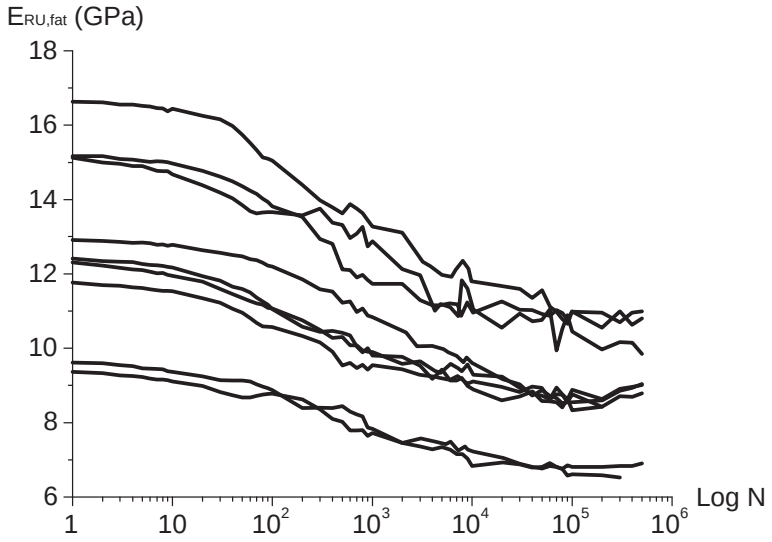

Figure 5.16 Fatigue damaging curves of deformation modulus of UHPFRC in R-UHPFRC

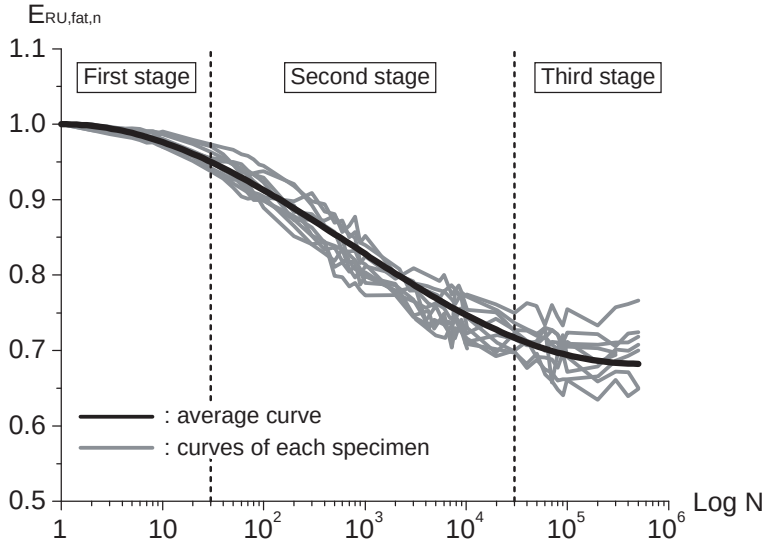

Figure 5.17 Normalised fatigue damaging curves of deformation modulus of UHPFRC in R-UHPFRC and the average curve

5.6 Conclusion

The following conclusions are drawn from the present study.

1) Regardless of imposed fatigue stress level, initial damage states and testing history, damage in UHPFRC under tensile fatigue stress develops with constant rate during most of the fatigue life when it fractures due to tensile fatigue. This may be attributed to the capacity of UHPFRC to redistribute local deformation increases due to damage concentration.

2) When UHPFRC fractures under constant tensile fatigue stress, significant damage is caused in the bulk UHPFRC in the early stage of the fatigue stress application.

3) A bi-linear damage evolution model is proposed for bulk UHPFRC under tensile fatigue stress. By using the damage evolution model together with damage-fatigue strain relationship, the remaining fatigue life is determined for UHPFRC of elements in existing structures.

4) Fatigue damaging of UHPFRC leads to stress transfer from UHPFRC to steel rebars in R-UHPFRC members. An empirical relationship between modulus of deformation of UHPFRC in R-UHPFRC and the number of fatigue cycles was deduced.

Chapter 6

Modelling of fatigue behaviour of bridge deck slab elements strengthened with reinforced UHPFRC

Submitted to *IABMAS 2014*

This page is intentionally left blank.

Modelling of fatigue behaviour of bridge deck slab elements strengthened with reinforced UHPFRC

Abstract

With the occurrence of higher and more frequent axle loads on roads, in particular bridge deck slabs are more severely solicitated by fatigue loading. To avoid heavy interventions for strengthening of deck slabs, an improved building material is used, namely Ultra-High Performance Fibre Reinforced Concrete with steel reinforcing bars (reinforced UHPFRC = R-UHPFRC). By adding a thin (30 to 50 mm) layer of R-UHPFRC on top of the bridge deck slab, the required fatigue resistance and load carrying capacity may be restored and improved. In addition the R-UHPFRC layer is waterproof which provides durability. This paper presents a model to describe the fatigue behaviour of reinforced concrete (RC) slab-like beams strengthened with R-UHPFRC leading to RU-RC beams. The model determines stress and deformation evolution in components of the RU-RC beam by considering decrease of UHPFRC stiffness due to fatigue. Comparison with available experimental results shows that the model can accurately represent the beam behaviour. Force distribution among components of the RU-RC beam reveals efficient fatigue resistant behaviour of the RU-RC beam, by which R-UHPFRC is demonstrated to be an effective member for fatigue strengthening of RC member.

Keywords: Ultra-High Performance Fibre Reinforced Concrete, bridge deck slabs, strengthening, fatigue behaviour, Palmgren-Miner rule

6.1 Introduction

Maintenance of bridge deck slabs is one of the most demanding tasks in management of road infrastructures because intervention of bridge deck slabs causing traffic disruptions should be avoided as much as possible considering its large impact on economic activities heavily relying on road transportation. Bridge deck slabs are the most solicitated structural members making up road infrastructures due to severe actions such as wheel loading. Effective technologies optimising the life cycle maintenance of bridge deck slabs are called for by bridge owners.

Overlay of Ultra-High Performance Fibre Reinforced Concrete combined with steel rebars (R-UHPFRC) on top of concrete bridge deck slab is a promising method to establish an efficient life cycle maintenance strategy due to UHPFRC's properties such as high compressive and tensile strength (≥ 180 and 10 MPa respectively), tensile strain-hardening behaviour and low permeability. Besides, high workability makes UHPFRC easy-to-handle material on site.

R-UHPFRC has been applied to concrete structures such as road bridges and buildings for improvement of load bearing capacity and durability [6.1, 6.2] (Figure 6.1). Structural behaviour of reinforced concrete members strengthened with R-UHPFRC leading to RU-RC

members has been investigated in detail with respect to ultimate resistance (e.g. [6.3, 6.4]) and the findings from the researches have been utilised in practical applications for safety check of ultimate limit states of RU-RC members. However, there were few investigations about the structural behaviour of RU-RC members in fatigue [6.5] and safety check of fatigue limit states of RU-RC members in practical application had relied on limited knowledge. In order to understand the structural behaviour of RU-RC members in fatigue in more detail and establish systematic UHPFRC application methodology for improving fatigue safety of concrete structures, fatigue behaviour of UHPFRC, R-UHPFRC and RU-RC members has been investigated by the authors [6.6, 6.7, 6.8].

This paper presents a model to describe the fatigue behaviour of RU-RC beams as a final product of a series of studies about UHPFRC as a fatigue strengthening material for concrete structures. Fatigue damaging relationship of R-UHPFRC member obtained from the tensile fatigue tests of R-UHPFRC plates is modified and adopted to consider stress transfer from UHPFRC to steel rebars in the R-UHPFRC layer of the RU-RC beam. Evolution of deformation range of the R-UHPFRC layer is obtained and compared with experimental measurements for verification of the proposed model. By using calculated stress range in steel rebar in the R-UHPFRC layer which determines the fatigue behaviour of the RU-RC beam, whether Palmgren-Miner rule is applicable for predicting the fatigue fracture of steel rebar is investigated. Subsequently, distribution of fatigue force range among components of the RU-RC beam is analysed and fatigue resistant behaviour of the RU-RC beam is explained.

Figure 6.1 Overlaying of UHPFRC on top surface of RC bridge deck slab by cast-in-place in Geneva, Switzerland in autumn 2010

6.2 Fatigue behaviour of RU-RC beam

Experimental campaign was conducted to investigate the bending fatigue behaviour of RU-RC beams. Details of the experiments are reported in [6.6]. In the following, main findings from bending fatigue tests of the RU-RC beam are summarised.

The specimen was a 1,900 mm long slab-like beam with a cross section of 400 mm × 220 mm (Figure 6.2). Thickness of R-UHPFRC layer was 50 mm using UHPFRC mix characterised by 3.0 vol.-% content of steel fibres 13 mm long with a diameter of 0.16 mm and by the use of CEM III/B type cement which contains a high percentage of blast furnace slag (66 % to 80 %). Four steel rebars of 10 mm diameter were arranged in the R-UHPFRC layer with a spacing of 100 mm. Concrete in the RC part was C30/37 grade with a maximum aggregate size of 16 mm. Four steel rebars of 16 mm and 10 mm diameter were arranged in the top and bottom of the RC part with a spacing of 100 mm. All steel rebars used in the experimental tests were of Grade B500B. UHPFRC was cast on the top surface of the RC part which was roughened with hydro-jetting to obtain monolithic bond between UHPFRC and concrete. (Neither any adhesion products nor any shear connector was used for the bonding.) Specimen deflection and R-UHPFRC deformation were measured at the position of the jack and the transversal centre of the top surface of R-UHPFRC layer, respectively (Figure 6.2).

All the RU-RC beams showed similar behaviour until failure under bending fatigue. Difference between measured and calculated deformation of the R-UHPFRC layer was observed and became larger as the number of fatigue cycles increased, which was attributed to local variation of material properties of UHPFRC in the strain-hardening domain and fatigue damaging of R-UHPFRC. It was concluded that steel rebars in the R-UHPFRC layer determines fatigue fracture process of the RU-RC beam and fatigue stress amplitude in the steel rebars is thus the most relevant parameter for the fatigue behaviour of the RU-RC beam.

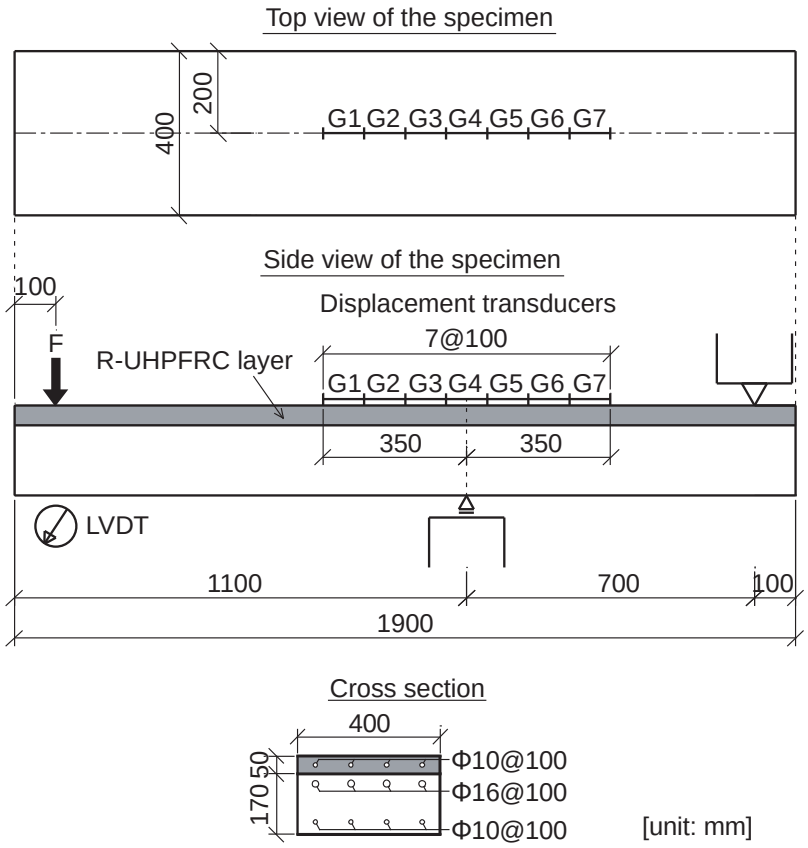

Figure 6.2 Specimen geometry, measuring devices and test set-up

6.3 Modelling of RU-RC beam in bending fatigue

It was understood from experimental tests that the behaviour of RU-RC beam under bending fatigue is predominantly determined by steel rebars arranged in R-UHPFRC layer on tensile side of the beam. In this structural system, the role of UHPFRC is to reduce fatigue stress in steel rebars by carrying a part of imposed fatigue stress. Fatigue stress in UHPFRC gradually decreases and transfers to steel rebars as the number of fatigue cycles increases. This is caused by fatigue damaging of deformation modulus of UHPFRC $E_{U,fat,i}$ expressed as:

$$E_{U,fat,i} = \frac{\sigma_{U,max,i} - \sigma_{U,min,i}}{\varepsilon_{max,i} - \varepsilon_{min,i}} \qquad \textbf{Eq. 6.1}$$

where $E_{U,fat,i}$ is modulus of deformation of the UHPFRC part at *i*-th cycle; $\sigma_{U,max(min),i}$ maximum (minimum) fatigue stress in the UHPFRC part at *i*-th cycle; $\varepsilon_{max(min),i}$ maximum (minimum) fatigue strain of R-UHPFRC at *i*-th cycle. In order to describe the fatigue behaviour of the RU-RC beam, decrease of $E_{U,fat}$ due to fatigue needs to be considered properly, by which stress range in steel rebars in the R-UHPFRC layer is calculated and subsequently fatigue fracture of the steel rebars might be predicted using Palmgren-Miner rule for damage accumulation in the steel rebars.

In the following, a model for the RU-RC beam under bending fatigue is proposed. Dealt

with is the specific case that maximum fatigue bending moment is sufficiently high such that UHPFRC is solicitated by tensile stress within the strain-hardening domain from the first fatigue cycle and amplitude of the fatigue bending moment is constant. Firstly, decrease of $E_{U,fat}$ due to fatigue in R-UHPFRC member is explained and modification of fatigue curve of normalised $E_{U,fat}$ obtained from tensile fatigue tests of R-UHPFRC plate is performed to represent the behaviour of the R-UHPFRC layer of the RU-RC beam. Secondly, calculation of stress and deformation of components of the RU-RC beam is performed until the first fracture of four steel rebars in the R-UPFRC layer occurs. Lastly, calculated deformation range of the R-UHPFRC layer $\Delta\ell_{RU}$ is compared with experimental measurements to validate the proposed model. In addition, accumulated damage in steel rebars in the R-UHPFRC layer is estimated using calculated stress range in the steel rebars and applicability of Palmgren-Miner rule for predicting the fatigue fracture of steel rebar is investigated.

6.3.1 Empirical relationship for fatigue of R-UHPFRC

Stress transfer from UHPFRC to steel rebars is a characteristic behaviour of R-UHPFRC member under tensile fatigue, which is effectuated by reduction of $E_{U,fat}$ [6.8]. In the experimental campaign, when R-UHPFRC plates were subjected to such a high tensile fatigue force as to impose stress within the strain-hardening domain on UHPFRC, similar trend was observed in fatigue behaviour of $E_{U,fat}$ regardless of varied fatigue force level. By normalising each fatigue curve of $E_{U,fat}$ with the modulus of deformation at the first cycle $E_{U,fat,1}$, normalised expression for fatigue of deformation modulus of UHPFRC $E_{U,fat,n}$ was determined as:

$$E_{U,fat,n} = 0.68 + 0.32 \cdot \sin^2\left(\frac{LogN + 5.7}{11.4}\pi\right) \quad \text{for} \quad N \le 500{,}000 \qquad \textbf{Eq. 6.2}$$

where N is the number of fatigue cycles.

In Equation 6.2, $E_{U,fat,n}$ is defined to stop decreasing at 500,000 cycles based on observations during the tensile fatigue tests of the R-UHPFRC plates, and consequently, stress doesn't transfer from UHPFRC to steel rebars after 500,000 cycles, resulting in constant deformation of R-UHPFRC. On the other hand, deformation readings of the R-UHPFRC layer during bending fatigue tests of the RU-RC beams continued to grow even after the number of fatigue cycles exceeding 500,000 cycles. Besides, growth rate of strain of the R-UHPFRC layer was larger than that of the R-UHPFRC plate. In order to describe the fatigue behaviour of the RU-RC beam by considering fatigue of the R-UHPFRC layer, Equation 6.2 needs to be modified.

It was supposed that discrepancy in fatigue deformation behaviour between the R-UHPFRC plate and the R-UHPFRC layer of the RU-RC beam is due to the difference of steel rebar ratio ρ_s of R-UHPFRC member and decreasing degree of $E_{U,fat}$ due to fatigue is in inverse proportion to ρ_s of R-UHPFRC member. In other words, the smaller ρ_s of R-UHPFRC member is, the more significantly decrease of $E_{U,fat}$ due to fatigue occurs. In Equation 6.2 coefficient of sine-squared function (= 0.32) determines decreasing degree of $E_{U,fat,n}$. By multiplying the coefficient of sine-squared function of Equation 6.2 by the ratio of $\rho_{s,pl}$ to $\rho_{s,lyr}$, where $\rho_{s,pl}$ is steel rebar ratio

of the UHPFRC plate (= 3.43 %) and $\rho_{s,lyr}$ steel rebar ratio of the UHPFRC layer of the RU-RC beam (= 1.57 %) (Figure 6.3), decreasing degree of $E_{U,fat,n}$ due to fatigue is increased. The ratio of $\rho_{s,pl}$ to $\rho_{s,lyr}$ is calculated as:

$$\frac{\rho_{s,pl}}{\rho_{s,lyr}} = \frac{3.43\%}{1.57\%} = 2.18 \qquad \textbf{Eq. 6.3}$$

Using the 'amplification factor' obtained by Equation 6.3, Equation 6.2 is modified with the boundary condition that $E_{U,fat,n}$ is equal to 1 at the first cycle as:

$$E_{U,fat,n} = 0.30 + 0.70 \cdot \sin^2\left(\frac{LogN + 5.7}{11.4}\pi\right) \quad \text{for} \quad N \le 500{,}000 \qquad \textbf{Eq. 6.4}$$

One more modification to describe continuing fatigue deformation growth of the R-UHPFRC layer after 500,000 cycles is carried out by extending $E_{U,fat,n}$ curve. A tangent of the $E_{U,fat,n}$ curve at 100,000 cycles is proposed as an extension of $E_{U,fat,n}$ curve. Consequently, modified $E_{U,fat,n}$ curve for fatigue of the R-UHPFRC layer of the RU-RC beam is expressed as:

$$E_{U,fat,n} = 0.30 + 0.70 \cdot \sin^2\left(\frac{LogN + 5.7}{11.4}\pi\right) \quad \text{for} \quad N \le 100{,}000 \qquad \textbf{Eq. 6.5}$$

$$E_{U,fat,n} = -7.25 \cdot 10^{-2} \cdot LogN + 0.69 \quad \text{for} \quad 100{,}000 < N \qquad \textbf{Eq. 6.6}$$

Figure 6.4 shows fatigue curve of $E_{U,fat,n}$ determined from tensile fatigue tests of R-UHPFRC plates (represented by Equation 6.2) and modified fatigue curve of $E_{U,fat,n}$ for R-UHPFRC layer of RU-RC beam (represented by Equations 6.5 and 6.6). With modified fatigue curve of $E_{U,fat,n}$, reproduction of fatigue behaviour of the RU-RC beams is performed in the following section.

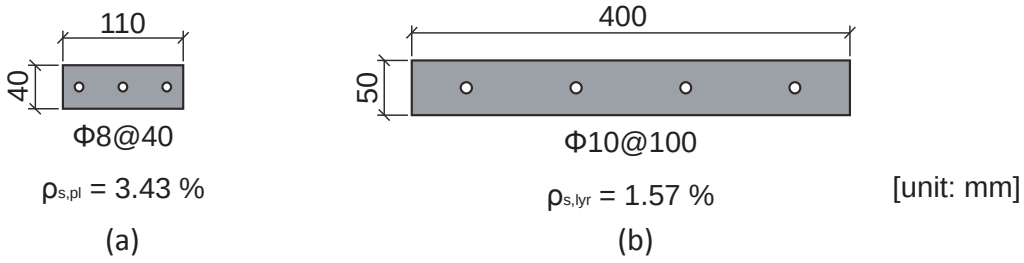

Figure 6.3 Comparison of cross section: (a) R-UHPFRC plate and (b) R-UHPFRC layer of RU-RC beam

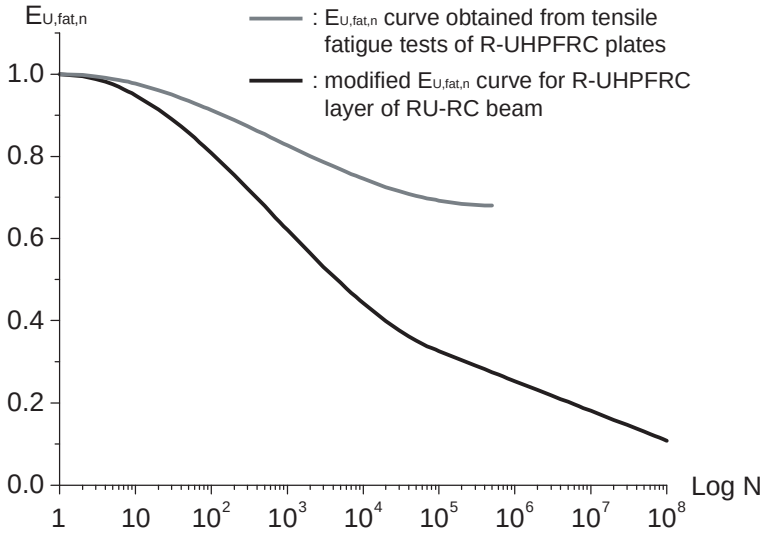

Figure 6.4 Normalised fatigue curves of deformation modulus of UHPFRC of R-UHPFRC member

6.3.2 Assumptions and conditions in calculation of stress and deformation

Stress and deformation of three components of the RU-RC beam, namely UHPFRC, steel rebar and concrete, are calculated based on Euler-Bernoulli beam theory for each fatigue cycle. Because bond strength between UHPFRC and steel rebars is high (= 44 MPa) [6.3], UHPFRC and steel rebars in the R-UHPFRC layer are assumed to deform together until steel rebar fractures. Concrete in tension isn't taken into account because a few macrocracks were observed in the tensile side of the RC part just after the first fatigue cycle and contribution of tensile fatigue strength of concrete to bending fatigue resistance of the RU-RC beams is negligible.

In the experimental campaign, bending fatigue tests were conducted on five specimens. Although three of the five specimens were subjected to more than one fatigue test (as these three specimens reached run-out at the first fatigue test), stress and deformation during the initial fatigue test are solely reproduced. As for fatigue tests in which the specimens failed, stress and deformation are calculated until the first fracture of the four steel rebars in the R-UHPFRC layer. Because acting bending moment and specimen material properties were different depending on local zone of the RU-RC beam which was bounded by the position of displacement transducers (G1 to G7), variations in measured deformation were observed. In the modelling, a local zone of each specimen whose measured deformation was the largest among all the local zones is focused on and stress and deformation of the three components of the RU-RC beam at the focused local zone are calculated. Summary of experimental test parameters and results are listed in Table 6.1. In fatigue tests reaching run-out, obviously no steel rebars fractured.

Figure 6.5 shows constitutive laws of the three components of the RU-RC beam. The behaviour of UHPFRC in tension is divided into three domains, namely elastic, strain-hardening and strain-softening domains. In the modelling, UHPFRC is assumed to enter and remain in the

strain-hardening domain and the behaviour of UHPFRC in tension is represented by a bi-linear stress-strain curve until the ultimate strength. Steel (rebar) has the same behaviour in tension and compression and its behaviour is represented by a bi-linear elastic-plastic stress-strain curve. The behaviour of concrete in compression is represented by a linear stress-strain curve until the ultimate strength.

Table 6.2 lists material properties of UHPFRC used in the modelling. Initial modulus of deformation of UHPFRC $E_{U,0}$ is a variable and determined by iteration to be an integer which yields deformation range of R-UHPFRC best fitting measured deformation range of R-UHPFRC during the first ten cycles. Other material properties of UHPFRC (elastic limit strength of UHPFRC f_{Ue}, strain corresponding to elastic limit strength of UHPFRC ε_{Ue}, ultimate strength of UHPFRC f_{Uu}, strain corresponding to ultimate strength of UHPFRC ε_{Uu}) are either constant or obtained by using $E_{U,0}$ or other property. Material properties of steel rebar and concrete used in the modelling are constant for all the cases: modulus of elasticity of steel rebar E_s = 205 GPa, yield strength of steel rebar f_{sy} = 500 MPa, yield strain of steel rebar ε_{sy} = 2.43 ‰, ultimate strength of steel rebar f_{su} = 500 MPa, modulus of elasticity of concrete E_c = 33 GPa, compressive strength of concrete f_{ck} = 30 MPa and strain of concrete corresponding to the compressive strength ε_{ck} = 0.90 ‰.

Table 6.1 Summary of test parameters and results

Test No.	F_{max} [kN]	Local zone	$M_{G\text{-}i,max}$ [kN·m]	N_f [×10^6]	N_{1st} [×10^6]	Notes
1-i	36.0	G2	28.8	10.13	-	run-out
2-i	40.5	G3	36.5	20.00	-	run-out
3-i	45.0	G2	36.0	23.94	-	run-out
4	49.5	G3	44.6	6.99	6.11	
5	49.5	G3	44.6	0.99	0.88	

F_{max}: maximum fatigue force (minimum fatigue force is 10 % of F_{max})

$M_{G\text{-}i,max}$: maximum fatigue moment at focused local G-*i* zone

N_f: sustained number of fatigue cycles

N_{1st}: number of fatigue cycles at which the first fracture of four steel rebars in the R-UHPFRC layer occurred

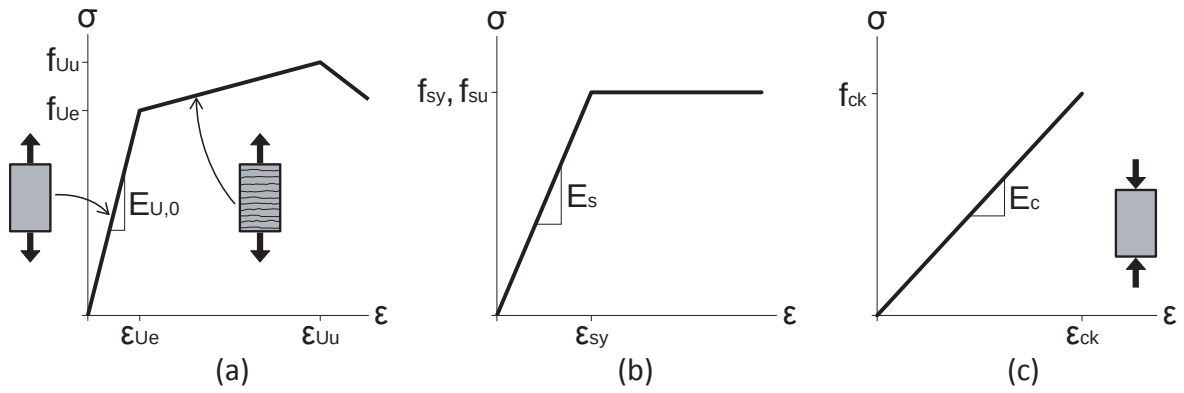

Figure 6.5 Constitutive laws of components of the RU-RC beam: (a) UHPFRC in tension (until reaching ultimate strength), (b) steel rebar and (c) concrete in compression

Table 6.2 Material properties of UHPFRC used in modelling

Test No.	$E_{U,0}$ [GPa]	f_{Ue} [MPa]	ε_{Ue} [‰]	f_{Uu} [MPa]	ε_{Uu} [‰]
1-i	28.0	4.87	0.17	5.97	4.58
2-i	39.0	6.79		8.32	
3-i	36.0	6.26		7.68	
4	51.0	8.87		10.88	
5	53.0	9.22		11.30	

$f_{Ue} = \varepsilon_{Ue} \cdot E_{U,0}$

ε_{Ue} is determined as an average of thirteen R-UHPFRC plate specimens

$f_{Uu} = f_{Ue} \cdot R_{U,sh}$*

ε_{Uu} is determined from an R-UHPFRC plate specimen

*$R_{U,sh}$ is strain-hardening ratio of UHPFRC and defined as the ratio of f_{Uu} to f_{Ue}. In this modelling, $R_{U,sh}$ is obtained to be 1.225 from results of quasi-static tensile tests of monolithic UHPFRC specimens.

6.3.3 Model validation

Based on assumptions and conditions explained in section 6.3.2 with consideration of decrease of $E_{U,fat,n}$ due to fatigue as defined in section 6.3.1, evolution of stress and deformation of the three components of the RU-RC beam were obtained. Figure 6.6 provides the plots of evolution of the measured and calculated $\Delta\ell_{RU}$ at focused local zone. There is a good agreement between the theoretical and the experimental $\Delta\ell_{RU}$. Consequently, by choosing appropriate $E_{U,0}$ value, the fatigue behaviour of RU-RC beam is predicted properly with the proposed model. Modified fatigue curve of $E_{U,fat,n}$ represents the fatigue behaviour of the R-UHPFRC layer of the RU-RC beam well, and it is indirectly demonstrated from this successful modification that steel rebar ratio of R-UHPFRC member determines the decreasing degree of $E_{U,fat}$ due to fatigue of R-UHPFRC member.

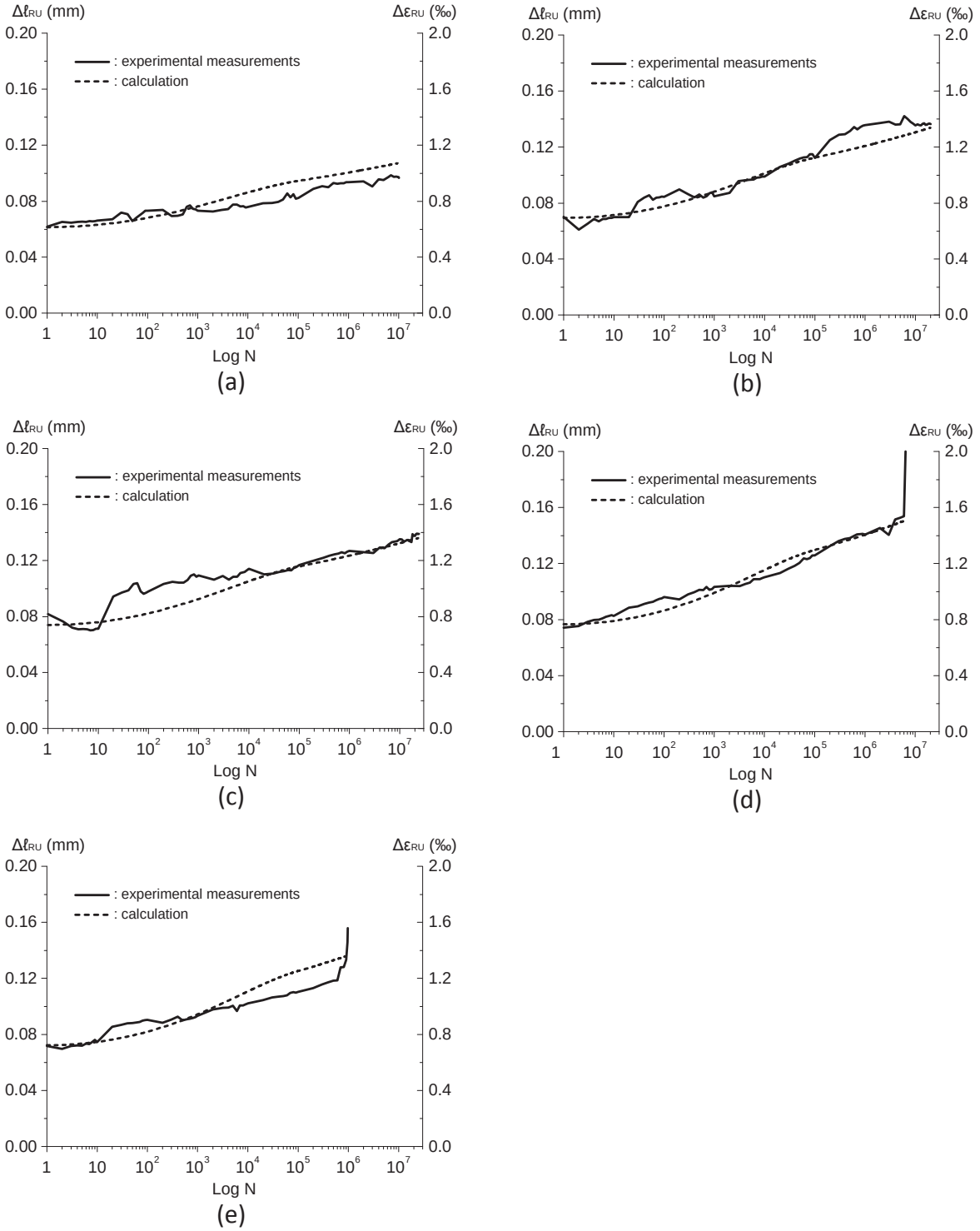

Figure 6.6 Comparison of measured and calculated deformation range of the R-UHPFRC layer of the RU-RC beams (a) G2 zone of Test 1-i [run-out], (b) G3 zone of Test 2-i [run-out], (c) G2 zone of Test 3-i [run-out], (d) G3 zone of Test 4 [fracture] and (e) G3 zone of Test 5 [fracture]

6.3.4 Applicability of Palmgren-Miner rule

Accumulated damage in steel rebars in the R-UHPFRC layer is estimated by using calculated stress range of the steel rebars based on Palmgren-Miner rule or the linear cumulative fatigue damage rule. According to this rule, applying n_i fatigue cycles with a stress range $\Delta\sigma_{s,i}$ and a

corresponding fatigue life N_i is equivalent to inducing n_i/N_i of fatigue damage in steel rebar. If imposed $\Delta\sigma_{s,i}$ varies, total accumulated damage D is calculated as:

$$D = \sum \frac{n_i}{N_i} \qquad \textbf{Eq. 6.7}$$

Fatigue fracture of steel rebar is supposed to occur when D is equal to 1.

Figure 6.7a shows calculated stress range of components in tension of the RU-RC beam for Test 4. As can be seen, stress range of steel rebars in the R-UHPFRC layer grows as the number of fatigue cycles increases and takes a different value for each cycle. n_i/N_i needs to be calculated for each cycle. n_i is always equal to 1, while N_i is determined for each $\Delta\sigma_{s,i}$ from S-N curve obtained from bending fatigue tests of Grade B500B steel rebar (Figure 6.8).

Table 6.3 lists calculated D-values for steel rebars in the R-UHPFRC layer of the RU-RC beams used in five fatigue tests. Test 1-i and 2-i (with no steel rebar fracture) rigorously follow Palmgren-Miner rule, while D-value of Test 4 (= 0.88), where fatigue fracture of steel rebar occurred, might be considered within a tolerance domain for Palmgren-Miner rule. In fact, Miner proposed this linear cumulative fatigue damage rule based on experimental results in which he found D-values varying from 0.61 to 1.45 [6.9, 6.10].

Although Test 3-i reached run-out and Test 5 resulted in fracture, calculated D-values of those tests are much higher and lower than 1, respectively. Considering that proposed model can describe the fatigue behaviour of the RU-RC beam properly as verified in section 6.3.3, D-values of those tests different from 1 might be attributed to inherent shortcomings of Palmgren-Miner rule, e.g. dependence on sequence of varying fatigue force [6.10] or uncertainty of S-N curve for steel rebar used in the present study.

It is concluded that fatigue fracture of steel rebar is predicted with reliability of about 60 %.

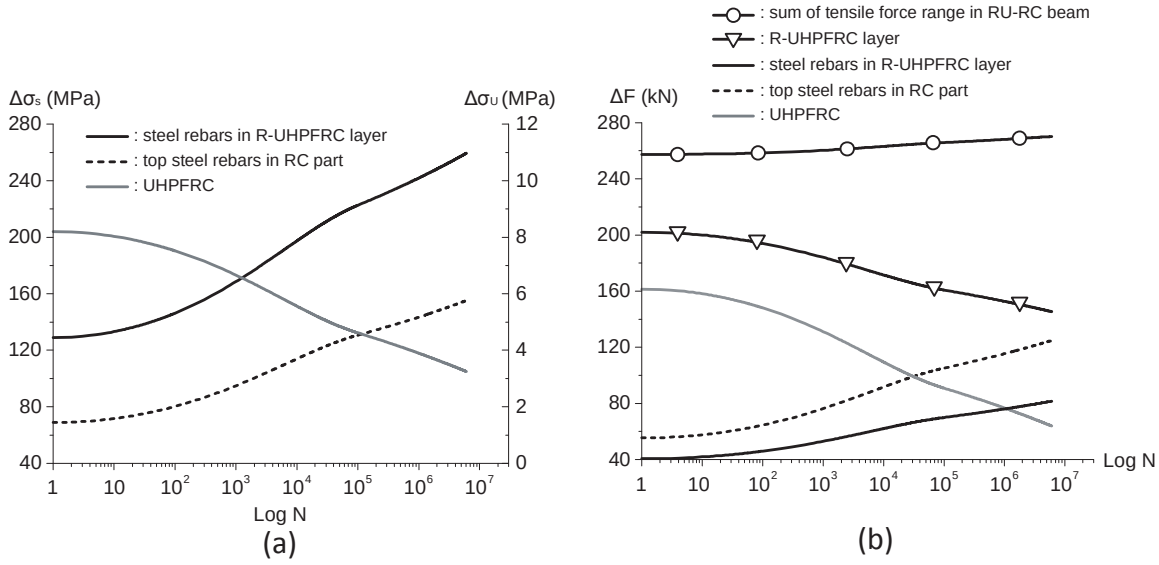

Figure 6.7 Evolution of calculated (a) stress range and (b) force range in steel rebar in R-UHPFRC layer, top steel rebar in RC part and UHPFRC of Test 4

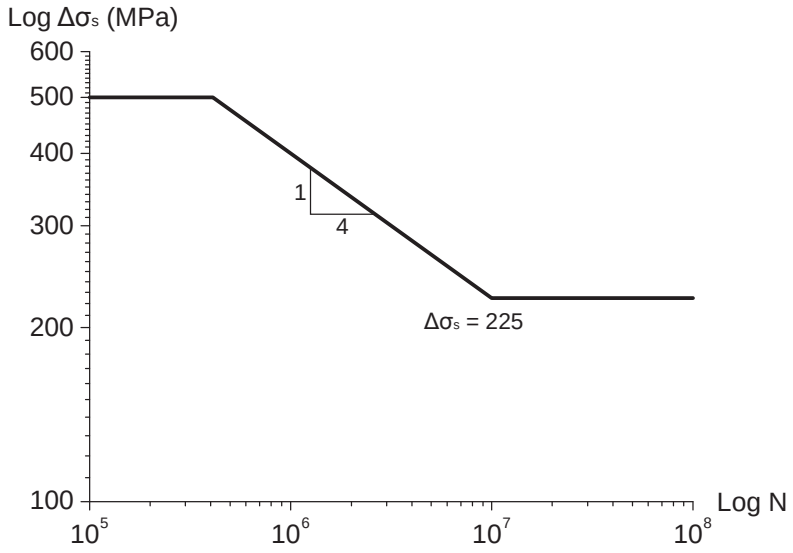

Figure 6.8 *S-N* curve of Grade B500B steel rebar [6.11]

Table 6.3 Accumulated damage

Test No.	*D*	N_{1st} [×10^6]	N_f [×10^6]
1-i	0.00	run-out	10.13
2-i	0.41	run-out	20.00
3-i	2.00	run-out	23.94
4	0.88	6.11	6.99
5	0.05	0.88	0.99

6.4 Fatigue behaviour of RU-RC member

In this chapter, distribution of fatigue force in the RU-RC beam is discussed by examining calculated force range *ΔF* in components of the RU-RC beam of Test 4 (Figure 6.7b). As results of the discussion, fatigue behaviour of RU-RC member is described and effectiveness of R-UHPFRC as a fatigue strengthening element is demonstrated.

Looking at components of the RU-RC beam in terms of contribution to tensile fatigue force resistance of the RU-RC beam, UHPFRC was the most contributing component at the beginning of the fatigue test. As the number of fatigue cycles increased, tensile fatigue force gradually transferred to steel rebars in the R-UHPFRC layer and top steel rebars in the RC part. At about 30,000 cycles the main tensile fatigue force carrying element changed from the UHPFRC to the top steel rebars in the RC part, and at about 1 million cycles tensile fatigue force carried by the UHPFRC became smaller than that by the steel rebars in the R-UHPFRC layer. The degree of contribution of each component to tensile fatigue force resistance of the RU-RC beam changes as the number of fatigue cycles increases where the point at which the change occurs depends on applied fatigue force level. It is noted that although stress range in the steel rebars in the R-UHPFRC layer was higher than that in the top steel rebars in the RC part (Figure 6.7a), force

range in the top steel rebars in the RC part was higher than that in the steel rebars in the R-UHPFRC layer (Figure 6.7b), which is obviously attributed to the difference of cross sectional area of the steel rebars. The top steel rebars in the RC part contribute more to tensile fatigue force resistance of the RU-RC beam than the steel rebars in the R-UHPFRC layer if cross sectional area of the top steel rebars in the RC part is larger than that of the steel rebars in the R-UHPFRC layer.

Thus, this is a favourable structural system in terms of redundancy because two functions are distributed between the components: the UHPFRC or the steel rebars in the RC part carry the largest tensile fatigue force in the RU-RC beam, while the steel rebars in the R-UHPFRC layer determines the fatigue behaviour of the RU-RC beam.

As outlined in [6.8], UHPFRC functions as a fatigue stress reducing element for steel rebars in R-UHPFRC member. This is understood from the fact that $E_{U,fat}$ decreases as the number of fatigue cycles increases and fatigue stress/force gradually transfers from the UHPFRC to the steel rebars in the R-UHPFRC layer shown in Figure 6.7a and b. Similar to this, fatigue force transfers from the R-UHPFRC layer to the top steel rebars in the RC part in the RU-RC beam. In Figure 6.7b, as the number of fatigue cycles increases, tensile fatigue force range in the R-UHPFRC layer gradually decreases, while tensile fatigue force range in the top steel rebars in the RC part becomes larger. From this follows that the R-UHPFRC layer functions as fatigue force reducing element for the top steel rebars in the RC part, indicating that application of R-UHPFRC is an effective method for fatigue strengthening of RC member.

6.5 Conclusion

The following conclusions are drawn:

1) Fatigue behaviour of RU-RC beam is properly described by considering fatigue damaging of R-UHPFRC layer. Deformation range of R-UHPFRC layer of the RU-RC beam under bending fatigue is analysed based on Euler-Bernoulli beam theory.

2) Fatigue damaging of UHPFRC in R-UHPFRC member depends on the steel rebar ratio. The smaller steel rebar ratio of R-UHPFRC member, the more significant is fatigue of UHPFRC.

3) Fatigue fracture of steel rebar is predicted with fair reliability by applying Palmgren-Miner rule in spite of the fact that there are some inherent shortcomings with this rule.

4) Due to fatigue damaging of UHPFRC, the degree of contribution of each component to tensile fatigue force resistance of the RU-RC beam changes as the number of fatigue cycles increases.

5) Main fatigue force carrying element in RU-RC beam is either UHPFRC or top steel rebars in RC part, while the fatigue behaviour of RU-RC beam is determined by steel rebars in the R-UHPFRC layer. Two essential functions for the RU-RC beam are allocated between the components and thus the RU-RC beam becomes an efficient structural system.

6) It is understood from fatigue force distribution among components of RU-RC beam that R-UHPFRC reduces fatigue stress in top steel rebars in RC part. Thus, RC member is effectively strengthened for fatigue by applying R-UHPFRC.

Chapter 7

Conclusion

This page is intentionally left blank.

Conclusion

The conclusions of this thesis are presented for fatigue behaviour of UHPFRC, R-UHPFRC and RU-RC members, respectively. Subsequently, future works are outlined.

7.1 Fatigue behaviour of UHPFRC

1) UHPFRC shows a fatigue endurance limit under constant amplitude tensile fatigue stress with respect to 10 million cycles. The fatigue endurance limit was determined for three fatigue test series and to be at solicitation levels of (1) S = 0.70 for fatigue testing in the elastic domain, (2) S = 0.60 for fatigue testing with pre-applied deformation in the strain-hardening domain and (3) S = 0.45 for fatigue testing with pre-applied deformation in the strain-softening domain, where S is the ratio between the maximum fatigue stress and the elastic limit strength of the UHPFRC specimen.

2) Rather large differences were observed in local deformations of UHPFRC specimens subjected to a given tensile stress. This is due to variations in material properties, in particular elastic limit strength and strain hardening behaviour. Significant stress and deformation redistribution capacity is given to the UHPFRC bulk material by these local variations in material properties, enhancing thus the fatigue stress bearing behaviour of UHPFRC.

3) Clear signs of matrix spalling and pulverisation were shown on the fatigue fracture surface of UHPFRC. Spalling of matrix might occur when fibres are partially or fully pulled out of the matrix in a direction other than fibre axis. Pulverisation of matrix might be due to abrasion of spalled matrix, while the irregular faces of the rough fracture surface are subjected to fretting and grinding under fatigue force.

4) Fatigue fracture surface of UHPFRC shows features of fatigue fracture surface of steel because it has a distinct area where the surface is smooth and only few fibres exist when compared to the rest of the fatigue fracture surface. This smooth area coincides with the fatigue fracture initiation. Fatigue fracture mechanisms of UHPFRC and steel are similar despite the fact that fatigue crack propagation behaviour of UHPFRC and steel is dissimilar due to the difference in material structure at meso-level.

5) Smooth fracture surface areas were covered with rust-coloured powdery products which were identified to be corrosion products from fibres by EDS and SEM analysis. Tribocorrosion is considered to cause corrosion of the fibres subjected to pull-out – slip-back movement that leads to wear of fibres with matrix.

6) Analysis of the tensile fatigue behaviour of UHPFRC based on elementary damage mechanics theory demonstrated that fatigue damage in UHPFRC develops with constant rate until its fracture regardless of imposed fatigue stress level, initial damage states and testing history. This is attributed to the capacity of UHPFRC to redistribute local deformation increases due to damage concentration.

7) Evolution of damage in UHPFRC under tensile fatigue stress is different between fatigue fracture test and run-out fatigue test. By examining the difference, it was understood that damage degree of UHPFRC exceeds 40 % before reaching 20 % of the expected fatigue life when UHPFRC fractures under constant tensile fatigue stress.

8) For UHPFRC under tensile fatigue stress, a bi-linear damage evolution model is proposed. By using the damage evolution model together with damage-fatigue strain relationship, the remaining fatigue life is determined for UHPFRC of elements in existing structures.

7.2 Fatigue behaviour of R-UHPFRC

1) A fatigue endurance limit of R-UHPFRC under constant amplitude tensile fatigue force was determined to be at a solicitation level of $S = 0.54$ with respect to 10 million cycles where S is the ratio between the maximum fatigue force and the ultimate strength of the R-UHPFRC specimen. In view of the fact that this force level is sufficiently high such that UHPFRC is solicitated by tensile stress within the strain-hardening domain, the steel rebars improve actually the fatigue stress bearing capacity of UHPFRC by distributing the imposed fatigue stress.

2) Depending on the maximum fatigue force level, the respective contribution of UHPFRC and steel rebars to the fatigue resistance of R-UHPFRC varies and is defined by referring to a solicitation level S as follows. (1) $S \leq 0.23$: UHPFRC contributes more than steel rebars, (2) $0.23 < S \leq 0.54$: UHPFRC and steel rebars contributes equally and (3) $0.54 < S$: steel rebars contribute more than UHPFRC. Stress distribution and transfer between UHPFRC and steel rebars enhance the fatigue stress bearing capacity of both material components.

3) Fatigue deformation behaviour of R-UHPFRC depends on the stage of the fatigue test. In the early stage of the fatigue test, UHPFRC mainly determines the fatigue deformation behaviour of R-UHPFRC and deformation of R-UHPFRC grows with local variations. In the middle and final stages of the fatigue test, steel rebars predominantly determine the fatigue deformation behaviour of R-UHPFRC and deformation of R-UHPFRC keeps almost constant.

4) Examination of the fatigue fracture surfaces of steel rebars in R-UHPFRC revealed two distinct types of fracture surfaces, i.e., smooth surface caused by stable fatigue crack growth and rough surface caused by rapid final fracture. The characteristics of the fracture surfaces identify the chronological order of the fatigue fracture of steel rebars in R-UHPFRC.

5) Stress transfer from UHPFRC to steel rebars in R-UHPFRC is brought about by fatigue damaging of the UHPFRC part. Among all R-UHPFRC specimens of the tensile fatigue tests, similar behaviour was observed in fatigue damaging curves of deformation modulus of UHPFRC. An empirical relationship was deduced between modulus of deformation of UHPFRC in R-UHPFRC and the number of fatigue cycles.

6) Depending on the steel rebar ratio, degree of fatigue damaging of UHPFRC in R-UHPFRC member changes. The smaller steel rebar ratio of R-UHPFRC member, the more significant is fatigue damaging of UHPFRC.

7.3 Fatigue behaviour of RU-RC members

1) *S-N* diagram was obtained from bending fatigue tests on RU-RC beams. Although some scatter was observed in the test results, a fatigue endurance limit of RU-RC beams under constant amplitude bending fatigue was determined to be at a solicitation level of $S = 0.50$ with respect to 10 million cycles where S is the ratio between the maximum fatigue force and the ultimate strength of the RU-RC beam

2) Similar behaviour was observed on all the RU-RC beams until failure due to bending fatigue. Differences in deformations of the R-UHPFRC layer between calculation and measurement are explained to be due to the variations of UHPFRC material properties in the elastic limit strength and strain-hardening behaviour. Deformation growth of the R-UHPFRC layer is attributed to fatigue damaging of the UHPFRC part caused by microcracking in the strain-hardening domain.

3) Fatigue fracture process of the RU-RC beams is determined by fatigue fracture of steel rebars in the R-UHPFRC layer. Fatigue stress amplitude in steel rebars in the R-UHPFRC layer is thus the most relevant parameter for the fatigue behaviour of the RU-RC beam.

4) Behaviour of the RU-RC beam under bending fatigue is properly modelled by considering fatigue damaging of the R-UHPFRC layer adopting the empirical relationship deduced from the tensile fatigue tests of R-UHPFRC plates. Growth of deformation range of the R-UHPFRC layer under bending fatigue was reproduced well by calculation based on

Euler-Bernoulli beam theory.

5) Fatigue damaging of UHPFRC changes the degree of contribution of each component to fatigue resistance of the RU-RC beam as the number of fatigue cycles increases.

6) Examination of fatigue force distribution among components of the RU-RC beam demonstrated that the R-UHPFRC layer reduces fatigue stress in top steel rebars in the RC part. Thus, application of R-UHPFRC element to RC member is an effective fatigue strengthening method.

7) Design rules for RU-RC members under bending fatigue are proposed for the fatigue safety verification with respect to the fatigue endurance limit. The fatigue safety verification consists of two-level check: macro- and meso-level check.

   At macro-level, moment resistance of RU-RC member needs to be checked according to:

$$n_{fat} = \frac{0.5 \cdot M_{Rd}}{M_{d,fat}} \geq 1.0 \qquad \textbf{Eq. 7.1}$$

   where n_{fat} is fatigue safety index; M_{Rd} examination value of moment resistance of RU-RC member; $M_{d,fat}$ examination value of maximum acting moment due to fatigue loading.

   At meso-level, stress range in steel rebars in the R-UHPFRC layer needs to be checked according to:

$$\Delta\sigma_{sd}(Q_{fat}) \leq \Delta\sigma_{sd,D} \qquad \textbf{Eq. 7.2}$$

   where $\Delta\sigma_{sd}$ is examination value of stress range in the steel rebars due to fatigue; Q_{fat} characteristic value of fatigue loading; $\Delta\sigma_{sd,D}$ examination value for fatigue endurance limit of straight steel rebars. According to the current design codes, $\Delta\sigma_{sd,D}$ = 115 MPa for straight steel rebar of diameter smaller than 20 mm is often used. Considering that UHPFRC reduces its modulus of deformation due to fatigue damaging and thus stress in the steel rebars in the R-UHPFRC layer increases because stress transfers from the UHPFRC to the steel rebars, stress range in the steel rebars in the R-UHPFRC layer needs to be checked for the long-term fatigue safety.

   When UHPFRC is not reinforced with steel rebars and applied for waterproofing of RC members, stress in the UHPFRC layer needs to be checked according to:

$$\sigma_{U,fat,max}(Q_{fat}) \leq 0.3 \cdot (f_{Ue} + f_{Uu}) \qquad \textbf{Eq. 7.3}$$

   where $\sigma_{U,fat,max}$ is maximum fatigue stress in the UHPFRC layer; Q_{fat} characteristic value of fatigue loading; f_{Ue} elastic limit strength of UHPFRC; f_{Uu} ultimate strength of UHPFRC.

7.4 Future works

1) The experimental study in the present thesis is limited to the behaviour of UHPFRC and R-UHPFRC under constant amplitude tensile fatigue and RU-RC beam under constant amplitude negative bending fatigue. In real structures, amplitude of fatigue loading is often variable. Moreover, fully reversed fatigue actions, i.e. tension-compression fatigue and negative-positive bending fatigue, are loading conditions that occur on bridge deck slab. The behaviour of UHPFRC, R-UHPFRC and RU-RC members under variable amplitude and fully reversed fatigue are subjects of further research.

2) UHPFRC with tensile strain-hardening behaviour (SH-UHPFRC) is used in this thesis. Since tensile strain-hardening improves the deformation and energy absorption capacity of SH-UHPFRC under static tension, it is inferred that tensile fatigue resistance of SH-UHPFRC is higher than that of UHPFRC without tensile strain-hardening behaviour, which, however, is not clearly demonstrated by experimental results in this doctoral thesis. Influence of the tensile strain-hardening property on the tensile fatigue behaviour of UHPFRC is necessary to be examined.

3) In this thesis, the fatigue behaviour of RU-RC members is investigated by means of RU-RC beams subjected to fatigue force applied at a fixed point. The RU-RC beam represents a strip of RC bridge deck slab strengthened with R-UHPFRC layer and the fatigue behaviour of RU-RC members as slab is not understood in detail. Fatigue tests of RU-RC slab should be performed using moving wheel-type force and the fatigue behaviour of RU-RC slab in a practical situation needs to be studied.

4) When UHPFRC and R-UHPFRC are overlaid on top of bridge deck slab, no waterproofing is necessary to be carried out because UHPFRC has a waterproof function due to its low permeability. Then, one may question if fatigue resistance of submerged UHPFRC is the same as that of dried UHPFRC. The tensile fatigue behaviour of UHPFRC should be investigated by changing its moisture condition.

5) The tensile fatigue behaviour of UHPFRC is analysed macroscopically in this thesis. In order to understand the tensile fatigue behaviour of UHPFRC in more detail (e.g. fatigue fracture crack propagation, development of multiple microcracks under tensile fatigue), micromechanics based analysis and modelling are anticipated.

This page is intentionally left blank.

References

This page is intentionally left blank.

References

Chapter 1

[1.1] Brühwiler E., Denarié E., (2013) “Rehabilitation and strengthening of concrete structures using Ultra-High Performance Fibre Reinforced Concrete”, Structural Engineering International, Vol. 23, No. 4, pp. 450-457

[1.2] Habel K., (2004) “Structural behaviour of elements combining Ultra-High Performance Fibre Reinforced Concretes (UHPFRC) and reinforced concrete”, Doctoral thesis No. 3036, École Polytechnique Fédérale de Lausanne (EPFL), Switzerland
http://infoscience.epfl.ch/record/33507

[1.3] Kamen, A., (2007) “Comportement au jeune âge et différé d'un BFUP écrouissant sous les effets thermomécaniques”, Doctoral thesis No. 3827, École Polytechnique Fédérale de Lausanne (EPFL), Switzerland
http://infoscience.epfl.ch/record/104117

[1.4] Wuest J., (2007) “Comportement structural des bétons de fibres ultra performants en traction dans des éléments composés”, Doctoral thesis No. 3987, École Polytechnique Fédérale de Lausanne (EPFL), Switzerland
http://infoscience.epfl.ch/record/114755

[1.5] Herwig A., (2008) “Reinforced concrete bridges under increased railway traffic loads – fatigue behaviour and safety measures”, Doctoral thesis No. 4010, École Polytechnique Fédérale de Lausanne (EPFL), Switzerland
http://infoscience.epfl.ch/record/114778

[1.6] Oesterlee C., (2010) “Structural response of reinforced UHPFRC and RC composite members”, Doctoral thesis No. 4848, École Polytechnique Fédérale de Lausanne (EPFL), Switzerland
http://infoscience.epfl.ch/record/150553

[1.7] Switek A. E., (2011) “Time-dependent response of Ultra High Performance Fibre Reinforced Concrete (UHPFRC) under low to high tensile stresses”, Doctoral thesis No. 4899, École Polytechnique Fédérale de Lausanne (EPFL), Switzerland
http://infoscience.epfl.ch/record/153013

[1.8] Noshiravani T., (2012) “Structural response of R-UHPFRC – RC composite members subjected to combined bending and shear”, Doctoral thesis No. 5246, École Polytechnique Fédérale de Lausanne (EPFL), Switzerland
http://infoscience.epfl.ch/record/169623

[1.9] Kazemi-Kamyab M., (2013) “Autogenous shrinkage and hydration kinetics of SH-UHPFRC under moderate to low temperature curing conditions”, Doctoral thesis No. 5681, École Polytechnique Fédérale de Lausanne (EPFL), Switzerland
http://infoscience.epfl.ch/record/185995

[1.10] Behloul M., Chanvillard G., Pimienta P., (2005) “Fatigue flexural behavior of pre-cracked specimens of special UHPFRC”, Proceedings of Seventh International Symposium on the Utilization of High-Strength/High-Performance Concrete, ACI Symposium Publication 228, pp. 1253-1268

[1.11] Farhat F. A., Nicolaides D., Kanellopoulos A., Karihaloo B. L., (2007) “High performance fibre-reinforced cementitious composite (CARDIFRC) – Performance and application to retrofitting”, Engineering Fracture Mechanics, Vol. 74, Issue 1-2, pp. 151-167

[1.12] Parant E., Rossi P., Boulay C., (2007) “Fatigue behaviour of a multi-scale cement composite”, Cement and Concrete Research, Vol. 37, Issue 2, pp. 264-269

[1.13] Lappa E. S., (2007) “High Strength Fibre Reinforced Concrete Static and fatigue behaviour in bending”, Doctoral thesis, Delft University of Technology
http://repository.tudelft.nl/view/ir/uuid%3A0f7ea161-1bbe-4d6b-b2bd-9adfae98323c/

[1.14] Fitik B., (2012) “Ermüdungsverhalten von ultrahochfestem Beton (UHPC) bei zyklischen Beanspruchungen im Druck-Zug-Wechselbereich”, Doctoral thesis, Technical University of Munich
http://mediatum.ub.tum.de/node?id=1006912

[1.15] Bache H. H., (1990) “Compact Reinforced Composite”, United States Patent, Patent No. 4979992, Date of patent: 25 December, 1990

[1.16] Cornelissen H.A.W., (1984) “Fatigue failure of concrete in tension”, Heron, Vol. 29, No. 4, pp. 1-68

Chapter 2

[2.1] Denarié E., Brühwiler E., (2006) “Structural rehabilitations with Ultra High Performance Fibre Reinforced Concretes”, International Journal for Restoration of Buildings and Monuments, Vol. 12, No. 5 and 6, pp. 453-465.

[2.2] Brühwiler E., Denarié E., (2008) “Rehabilitation of concrete Structures using Ultra-High Performance Fibre Reinforced Concrete”, Proceedings of the Second International Symposium on Ultra High Performance Concrete, Ed. by Fehling E., Schmidt M., Stürwald S., Kassel, Germany, pp. 895-902

[2.3] Brühwiler E., (2009) “Rehabilitation of bridges using Ultra-High Performance Fiber Reinforced Concrete”, Proceedings of 5th New York City Bridge Conference, New York City, United States of America

[2.4] Brühwiler E., (2010) “Ultra-High Performance Fiber Reinforced Concrete improves concrete structures”, Structural concrete in Switzerland, Swiss national group of the international federation for structural concrete, pp. 145-149

[2.5] Lappa E. S., René Braam C., Walraven J. C., (2006) “Flexural fatigue of high and ultra high strength fiber reinforced concrete”, Proceedings of International RILEM Workshop on High Performance Fiber Reinforced Cementitious Composites in Structural Applications, Ed. by Fischer G. and Li V. C., Honolulu, United States of America, pp. 509-518

[2.6] Behloul M., Chanvillard G., Pimienta P., (2005) “Fatigue flexural behavior of pre-cracked specimens of special UHPFRC”, Proceedings of Seventh International Symposium on the Utilization of High-Strength/High-Performance Concrete, ACI Symposium Publication 228, pp. 1253-1268

[2.7] Farhat F. A., Nicolaides D., Kanellopoulos A., Karihaloo B. L., (2007) “High performance fibre-reinforced cementitious composite (CARDIFRC) – Performance and application to retrofitting”, Engineering Fracture Mechanics, Vol. 74, Issue 1-2, pp. 151-167

[2.8] Parant E., Rossi P., Boulay C., (2007) “Fatigue behaviour of a multi-scale cement composite”, Cement and Concrete Research, Vol. 37, Issue 2, pp. 264-269

[2.9] Fitik B., Niedermeier R., Zilch K., (2009) “Fatigue behaviour of ultra high performance concrete under cyclic stress reversal loading”, Proceedings of the 11th Annual International *fib* Symposium - Concrete: 21st Century Superhero, Ed. by Denton S. and Clark G., London, Great Britain

[2.10] Fitik B., Niedermeier R., Zilch K., (2010) “Fatigue behaviour of ultra-high performance concrete under cyclic stress reversal loading”, Proceedings of the Third International *fib* Congress incorporating the PCI Annual Convention and Bridge Conference, Washington D.C., United States of America, pp. 5393-5402

[2.11] Cornelissen H.A.W., (1984) “Fatigue failure of concrete in tension”, Heron, Vol. 29, No. 4, pp. 1-68

[2.12] Sadananda K., Vasudevan A.K., Phan N., (2007) “Analysis of endurance limits under very high cycle fatigue using a unified damage approach” International Journal of Fatigue, Vol. 29, Issue 9-11, pp. 2060-2071

[2.13] Wuest J., (2007) “Comportement structural des bétons de fibres ultra performants en traction dans des éléments composés”, Doctoral thesis No. 3987, École Polytechnique Fédérale de Lausanne (EPFL), Switzerland
http://infoscience.epfl.ch/record/114755

[2.14] Oesterlee C., Sadouki H., Brühwiler E., (2008) “Structural analysis of a composite bridge girder combining UHPFRC and reinforced concrete”, Proceedings of the Second International Symposium on Ultra High Performance Concrete, Ed. By Fehling E., Schmidt M., Stürwald S., Kassel, Germany, pp. 647-654

[2.15] Habel K., (2004) “Structural behaviour of elements combining Ultra-High Performance Fibre Reinforced Concretes (UHPFRC) and reinforced concrete”, Doctoral thesis No. 3036, École Polytechnique Fédérale de Lausanne (EPFL), Switzerland
http://infoscience.epfl.ch/record/33507

[2.16] ASM Handbook Committee, (1987) “ASM Handbook Volume 12: Fractography”, ASM International

[2.17] Brandt A.M., (1985) “On the optimal direction of short metal fibres in brittle matrix composites”, Journal of Materials Science, Vol. 20, Issue 11, pp. 3831-3841

[2.18] Li V. C., Backer S., (1990) “Effect of inclining angle, bundling and surface treatment on synthetic fibre pull-out from a cement matrix”, Composites, Vol. 21, Issue 2, pp. 132-140

[2.19] Anderson T. L., (2005) “Fracture mechanics: fundamentals and applications, Third Edition”, CRC Press

[2.20] Johansson U., (2004) “Fatigue tests and analysis of reinforced concrete bridge deck models”, Licentiate thesis, Royal Institute of Technology, Sweden
http://urn.kb.se/resolve?urn=urn:nbn:se:kth:diva-1820

[2.21] Zhang J., Stang H., Li V.C., (2001) “Crack bridging model for fibre reinforced concrete under fatigue tension”, International Journal of Fatigue, Vol. 23, Issue 8, pp. 655-670

[2.22] ASM Handbook Committee, (1987) “ASM Handbook Volume 13: Corrosion”, ASM International

[2.23] Landolt D., (2007) “Corrosion and surface chemistry of metals“, EPFL Press

[2.24] Schijve J., (2009) “Fatigue of Structures and Materials“, Springer

Chapter 3

[3.1] Wuest J., Denarié E., Brühwiler E., (2007) “Measurement and modelling of fibre distribution and orientation in UHPFRC”, Proceedings of Fifth International RILEM Workshop on High Performance Fiber Reinforced Cement Composites (HPFRCC5), Ed. by Reinhardt H. W., Naaman A. E., Mainz, Germany

[3.2] Brühwiler E., Denarié E., (2013) “Rehabilitation and strengthening of concrete structures using Ultra-High Performance Fibre Reinforced Concrete”, Structural Engineering International, Vol. 23, No. 4, pp. 450-457

[3.3] Jungwirth J., Muttoni A., (2004) “Structural behavior of tension members in UHPC”, Proceedings of International Symposium on Ultra-High Performance Concrete, Ed. by Schmidt M., Fehling E., Geisenhanslüke C., Kassel, Germany, pp. 533-544

[3.4] Redaelli D., Muttoni A., (2007) “Tensile behaviour of reinforced Ultra-High Performance Fiber Reinforced Concrete elements”, Proceedings of *fib* Symposium: Concrete Structures – Stimulators of Development, Ed. by Radić J., Dubrovnik, Croatia

[3.5] Leutbecher T., Fehling E., (2008) “Crack formation and tensile behaviour of UHPC reinforced with a combination of rebars and fibres”, Proceedings of the Second International Symposium on Ultra-High Performance Concrete, Ed. by Fehling E., Schmidt M., Stürwald S., Kassel, Germany, pp. 497-504

[3.6] Oesterlee C., (2010) “Structural response of reinforced UHPFRC and RC composite members”, Doctoral thesis No. 4848, École Polytechnique Fédérale de Lausanne (EPFL), Switzerland
http://infoscience.epfl.ch/record/150553

[3.7] Bache H. H., (1990) “Compact Reinforced Composite”, United States Patent, Patent No. 4979992, Date of patent: 25 December, 1990

[3.8] Behloul M., Chanvillard G., Pimienta P., (2005) “Fatigue flexural behavior of pre-cracked specimens of special UHPFRC”, Proceedings of Seventh International Symposium on the Utilization of High-Strength/High-Performance Concrete, ACI Symposium Publication 228, pp. 1253-1268

[3.9] Farhat F. A., Nicolaides D., Kanellopoulos A., Karihaloo B. L., (2007) “High performance fibre-reinforced cementitious composite (CARDIFRC) – Performance and application to retrofitting”, Engineering Fracture Mechanics, Vol. 74, Issue 1-2, pp. 151-167

[3.10] Lappa E. S., René Braam C., Walraven J. C., (2005) “Flexural fatigue of high and ultra high strength fiber reinforced concrete”, Proceedings of International RILEM Workshop on High Performance Fiber Reinforced Cementitious Composites in Structural Applications, Ed. by Fischer G. and Li V. C., Honolulu, United States of America, pp. 509-518

[3.11] Parant E., Rossi P., Boulay C., (2007) “Fatigue behaviour of a multi-scale cement composite”, Cement and Concrete Research, Vol. 37, Issue 2, pp. 264-269

[3.12] Fitik B., Niedermeier R., Zilch K., (2009) “Fatigue behaviour of ultra high performance concrete under cyclic stress reversal loading”, Proceedings of the 11th Annual International *fib* Symposium - Concrete: 21st Century Superhero, Ed. by Denton S. and Clark G., London, Great Britain

[3.13] Tilly G. P., (1979) “Fatigue of Steel Reinforcement Bars in Concrete: A Review”, Fatigue & Fracture of Engineering Materials and Structures, Vol. 2, Issue 3, pp. 251–268

[3.14] Zheng H., Abel A. A., (1999) “Fatigue Properties of Reinforcing Steel Produced by TEMPCORE Process”, Journal of Materials in Civil Engineering, Vol. 11, Issue 2, pp. 158-165

[3.15] Rocha M., Brühwiler E., (2012) “Prediction of fatigue life of reinforced concrete bridges using Fracture Mechanics”, Proceedings of 6th International Conference on Bridge Maintenance, Safety and Management (IABMAS 2012), Ed. by Biondini F., Frangopol D. M., Stresa, Italy, pp. 3755-3760

[3.16] Schläfli M., Brühwiler E., (1998) “Fatigue of existing reinforced concrete bridge deck slabs”, Engineering Structures, Vol. 20, No. 11, pp. 991-998

[3.17] Sadananda K., Vasudevan A.K., Phan N., (2007) “Analysis of endurance limits under very high cycle fatigue using a unified damage approach” International Journal of Fatigue, Vol. 29, Issue 9-11, pp. 2060-2071

[3.18] Makita T., Brühwiler E., (2012) “Fatigue behaviour of bridge deck slab elements strengthened with reinforced UHPFRC”, Proceedings of 6th International Conference on Bridge Maintenance, Safety and Management (IABMAS 2012), Ed. by Biondini F., Frangopol D. M., Stresa, Italy, pp. 1974-1980

[3.19] Makita T., Brühwiler E., (2013) “Tensile fatigue behaviour of ultra-high performance fibre reinforced concrete (UHPFRC)”, Materials and Structures, Published online: 23 April, 2013

[3.20] Herwig A., (2008) “Reinforced concrete bridges under increased railway traffic loads – fatigue behaviour and safety measures”, Doctoral thesis No. 4010, École Polytechnique Fédérale de Lausanne (EPFL), Switzerland
http://infoscience.epfl.ch/record/114778

Chapter 4

[4.1] Denarié E., Brühwiler E., (2006) “Structural rehabilitations with Ultra High Performance Fibre Reinforced Concretes”, International Journal for Restoration of Buildings and Monuments, Vol. 12, No. 5 and 6, pp. 453-465.

[4.2] Wuest J., (2007) “Comportement structural des bétons de fibres ultra performants en traction dans des éléments composés”, Doctoral thesis No. 3987, École Polytechnique Fédérale de Lausanne (EPFL), Switzerland
http://infoscience.epfl.ch/record/114755

[4.3] Makita T., Brühwiler E., (2013) “Tensile fatigue behaviour of ultra-high performance fibre reinforced concrete (UHPFRC)”, Materials and Structures, Published online: 23 April, 2013

[4.4] Brühwiler E., Denarié E., (2008) “Rehabilitation of Concrete Structures using Ultra-High Performance Fibre Reinforced Concrete”, Proceedings of UHPC-2008: the Second International Symposium on Ultra High Performance Concrete, Ed. By Fehling E., Schmidt M., Stürwald S., Kassel, Germany, pp. 895-902

[4.5] Brühwiler E, (2009) “Rehabilitation of bridges using Ultra-High Performance Fibre Reinforced Concrete”, Proceedings of 5th New York City Bridge Conference

[4.6] Denarié E., Kazemi-Kamyab M., Brühwiler E., Haddad B., Nendaz S., (2011) “Béton fibré ultra performant pour la maintenance, un nouvel élan”, Tracés, Vol. 137, Issue 12, pp. 20-23.

Chapter 5

[5.1] Degrieck J., Van Paepegem W. (2001) “Fatigue Damage Modelling of Fiber-reinforced Composite Materials: Review”, Applied Mechanics Reviews, Vol. 54, Issue 4, pp.279-300

[5.2] Rabotnov Y. N. (1968) “Creep rupture”, Proceedings of the Twelfth International Congress of Applied Mechanics, Ed. by Hetenyi M. and Vincenti M., Stanford University, United States of America, pp. 342–349

[5.3] Rabotnov Y. N. (1969) “Creep problems in structural members”, North-Holland Series in Applied Mathematics and Mechanics Vol. 7, North-Holland Publishing Company

[5.4] Kachanov L. M. (1986) “Introduction to continuum damage mechanics”, Springer

[5.5] Kachanov L. M. (1999) “Rupture time under creep conditions (translated from Izvestia Akademii Nauk SSSR, Otdelenie tekhnicheskich nauk, No. 8, 1958, pp. 26–31, in Russian)” International Journal of Fracture, Vol. 97, Issue 1-4, pp. 11-18

[5.6] Murakami S. (2012) “Continuum Damage Mechanics: A Continuum Mechanics Approach to the Analysis of Damage and Fracture”, Springer, pp.15-20

[5.7] Makita T., Brühwiler E. (2014) “Tensile fatigue behaviour of Ultra-High Performance Fibre Reinforced Concrete combined with steel rebars (R-UHPFRC)”, International Journal of Fatigue, Vol. 59, pp. 145-152

[5.8] Behloul M., Chanvillard G., Pimienta P., (2005) “Fatigue flexural behavior of pre-cracked specimens of special UHPFRC”, Proceedings of Seventh International Symposium on the Utilization of High-Strength/High-Performance Concrete, ACI Symposium Publication 228, pp. 1253-1268

[5.9] Farhat F. A., Nicolaides D., Kanellopoulos A., Karihaloo B. L., (2007) “High performance fibre-reinforced cementitious composite (CARDIFRC) – Performance and application to retrofitting”, Engineering Fracture Mechanics, Vol. 74, Issue 1-2, pp. 151-167

[5.10] Lappa E. S., René Braam C., Walraven J. C., (2006) “Flexural fatigue of high and ultra high strength fiber reinforced concrete”, Proceedings of International RILEM Workshop on High Performance Fiber Reinforced Cementitious Composites in Structural Applications, Ed. by Fischer G. and Li V. C., Honolulu, United States of America, pp. 509-518

[5.11] Lappa E. S., (2007) “High Strength Fibre Reinforced Concrete Static and fatigue behaviour in bending”, Doctoral thesis, Delft University of Technology
http://repository.tudelft.nl/view/ir/uuid%3A0f7ea161-1bbe-4d6b-b2bd-9adfae98323c/

[5.12] Parant E., Rossi P., Boulay C., (2007) “Fatigue behaviour of a multi-scale cement composite”, Cement and Concrete Research, Vol. 37, Issue 2, pp. 264-269

[5.13] Fitik B., Niedermeier R., Zilch K., (2010) “Fatigue behaviour of ultra-high performance concrete under cyclic stress reversal loading”, Proceedings of the Third International *fib* Congress incorporating the PCI Annual Convention and Bridge Conference, Washington D.C., United States of America, pp. 5393-5402

[5.14] Fitik B., (2012) “Ermüdungsverhalten von ultrahochfestem Beton (UHPC) bei zyklischen Beanspruchungen im Druck-Zug-Wechselbereich”, Doctoral thesis, Technical University of Munich
http://mediatum.ub.tum.de/node?id=1006912

[5.15] Bache H. H., (1990) “Compact Reinforced Composite”, United States Patent, Patent No. 4979992, Date of patent: 25 December, 1990

[5.16] Hordijk D. A., (1991) “Local approach to fatigue of concrete”, Doctoral thesis, Delft University of Technology
http://repository.tudelft.nl/view/ir/uuid%3Afa87147b-8201-47ed-83d7-b812b09c5fbb/

[5.17] Kessler-Kramer C., (2002) “Zugtragverhalten von Beton unter Ermüdungsbeanspruchung”, Doctoral thesis, Karlsruhe Institute of Technology
http://digbib.ubka.uni-karlsruhe.de/volltexte/20522002

[5.18] Makita T., Brühwiler E., (2013) “Tensile fatigue behaviour of Ultra-High Performance Fibre Reinforced Concrete (UHPFRC)” Materials and Structures, Published online: 23 April, 2013
http://link.springer.com/article/10.1617/s11527-013-0073-x

[5.19] Gross D., Seelig T., (2011) “Fracture Mechanics: With an Introduction to Micromechanics Mechanical Engineering Series”, Springer, pp.301-316

Chapter 6

[6.1] Brühwiler E., (2009) "Rehabilitation of bridges using Ultra-High Performance Fibre Reinforced Concrete", Proceedings of 5th New York City Bridge Conference

[6.2] Brühwiler E., Denarié E., (2013) "Rehabilitation and strengthening of concrete structures using Ultra-High Performance Fibre Reinforced Concrete", Structural Engineering International, Vol. 23, No. 4, pp. 450-457

[6.3] Oesterlee C., (2010) "Structural response of reinforced UHPFRC and RC composite members", Doctoral thesis No. 4848, École Polytechnique Fédérale de Lausanne (EPFL), Switzerland
http://infoscience.epfl.ch/record/150553

[6.4] Noshiravani T., (2012) "Structural response of R-UHPFRC – RC composite members subjected to combined bending and shear", Doctoral thesis No. 5246, École Polytechnique Fédérale de Lausanne (EPFL), Switzerland
http://infoscience.epfl.ch/record/169623

[6.5] Herwig A., (2008) "Reinforced concrete bridges under increased railway traffic loads – fatigue behaviour and safety measures", Doctoral thesis No. 4010, École Polytechnique Fédérale de Lausanne (EPFL), Switzerland
http://infoscience.epfl.ch/record/114778

[6.6] Makita T., Brühwiler E., (2012) "Fatigue behaviour of bridge deck slab elements strengthened with reinforced UHPFRC", Proceedings of 6th International Conference on Bridge Maintenance, Safety and Management (IABMAS 2012), Ed. by Biondini F., Frangopol D. M., Stresa, Italy, pp. 1974-1980

[6.7] Makita T., Brühwiler E., (2013) "Tensile fatigue behaviour of ultra-high performance fibre reinforced concrete (UHPFRC)", Materials and Structures, Published online: 23 April, 2013

[6.8] Makita T., Brühwiler E. (2014) "Tensile fatigue behaviour of Ultra-High Performance Fibre Reinforced Concrete combined with steel rebars (R-UHPFRC)", International Journal of Fatigue, Vol. 59, pp. 145-152

[6.9] Miner M. A., (1945) "Cumulative damage in fatigue", ASME Journal of Applied Mechanics, Vol. 12, pp. A159-A164

[6.10] Schijve J., (2009) "Fatigue of Structures and Materials Second Edition", Springer

[6.11] Rocha M., (2013) "*S*-*N* curve drawn with experimental results of bending fatigue tests of Grade B500B steel rebar (13 specimens)", Personal communication

This page is intentionally left blank.

Appendix A

Examples of fatigue strengthening design of RC members using UHPFRC and R-UHPFRC

This page is intentionally left blank.

Examples of fatigue strengthening design of RC members using UHPFRC and R-UHPFRC

Two Examples of fatigue strengthening design of RC members using R-UHPFRC are shown where proposed fatigue design rules of RU-RC members are applied. In addition, a design example of UHPFRC as waterproofing member for RC bridge deck slab is shown.

Fatigue design rules of RU-RC members

The fatigue safety verification of RU-RC members consists of two-level check: macro-level check and meso-level check.

At macro-level, moment resistance of RU-RC member needs to be checked according to:

$$n_{fat} = \frac{0.5 \cdot M_{Rd}}{M_{d,fat}} \geq 1.0 \qquad \textbf{Eq. 1}$$

where n_{fat} is fatigue safety index; M_{Rd} examination value of moment resistance of RU-RC member; $M_{d,fat}$ examination value of maximum acting moment due to fatigue loading.

At meso-level, stress range in steel rebars in the R-UHPFRC layer needs to be checked according to:

$$\Delta\sigma_{sd}(Q_{fat}) \leq \Delta\sigma_{sd,D} \qquad \textbf{Eq. 2}$$

where $\Delta\sigma_{sd}$ is examination value of stress range in steel rebars due to fatigue; Q_{fat} characteristic value of fatigue loading; $\Delta\sigma_{sd,D}$ examination value for fatigue endurance limit of straight steel rebars. According to the current design codes, $\Delta\sigma_{sd,D}$ = 115 MPa for straight steel rebar of diameter smaller than 20 mm is often used. Considering that UHPFRC reduces its modulus of deformation due to fatigue and thus stress in steel rebars increases because stress transfers from UHPFRC to steel rebars, stress range in steel rebars in the R-UHPFRC layer needs to be checked for the long-term fatigue safety.

When UHPFRC is not reinforced with steel rebars and UHPFRC layer is applied for waterproofing of RC members, stress in UHPFRC need to be checked according to:

$$\sigma_{U,fat,max}(Q_{fat}) \leq 0.3 \cdot (f_{Ue} + f_{Uu}) \qquad \textbf{Eq. 3}$$

where $\sigma_{U,fat,max}$ is maximum fatigue stress in UHPFRC; Q_{fat} characteristic value of fatigue loading; f_{Ue} elastic limit strength of UHPFRC; f_{Uu} tensile strength of UHPFRC.

Assumptions and conditions

Figure 1 shows constitutive laws of the three components of RU-RC members. UHPFRC is assumed to enter and remain in the strain-hardening domain and the behaviour of UHPFRC in tension is represented by a bi-linear stress-strain curve until the ultimate strength. The behaviour of steel rebar is represented by a bi-linear elastic-plastic stress-strain curve. The behaviour of normal strength concrete in compression is represented by a linear stress-strain curve until the ultimate strength. Tables 1 and 2 list typical material properties of UHPFRC, steel rebar and concrete.

The ultimate resistance of RU-RC member is calculated according to the sectional model in Figure 2. Fatigue stress in steel rebars is calculated according to the elastic sectional model in Figure 3.

The fatigue safety of RC members and RU-RC members are examined with respect to 10 million cycles which are considered to be realistic for heavily trafficked bridges and usually regarded as a lower bound of the very high cycle fatigue domain.

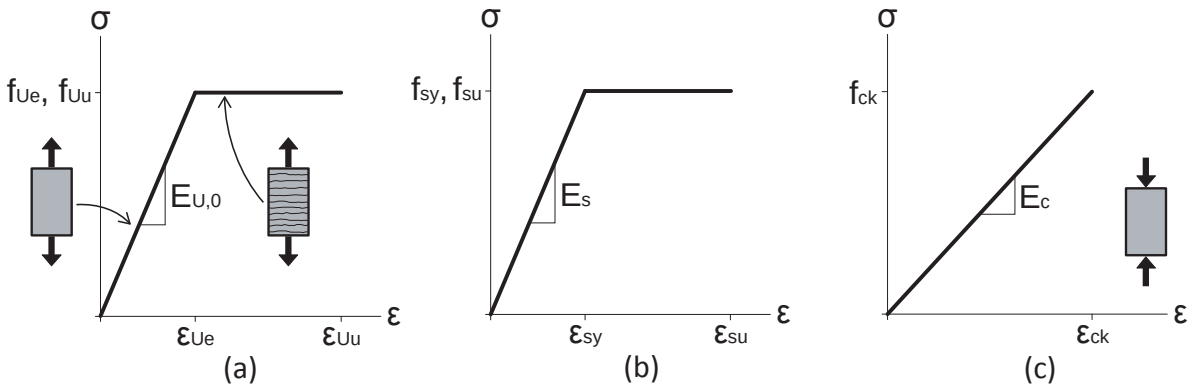

Figure 1 Constitutive laws of the three components of RU-RC members: (a) UHPFRC in tension, (b) steel rebar and (c) concrete in compression

Table 1 Assumed typical material properties of components of R-UHPFRC

UHPFRC	$E_{U,0}$ [GPa]	f_{Ue} [MPa]	ε_{Ue} [‰]	f_{Uu} [MPa]	ε_{Uu} [‰]
	50	10	0.2	10	5
Steel rebar	E_s [GPa]	f_{sy} [MPa]	ε_{sy} [‰]	f_{su} [MPa]	ε_{su} [‰]
	205	500	2.43	500	50

Table 2 Assumed typical material properties of components of RC

Steel rebar	E_s [GPa]	f_{sy} [MPa]	ε_{sy} [‰]	f_{su} [MPa]	ε_{su} [‰]
	205	450	2.19	450	100
Concrete	E_c [GPa]	f_{ck} [MPa]	ε_{ck} [‰]		
	33	30	0.90		

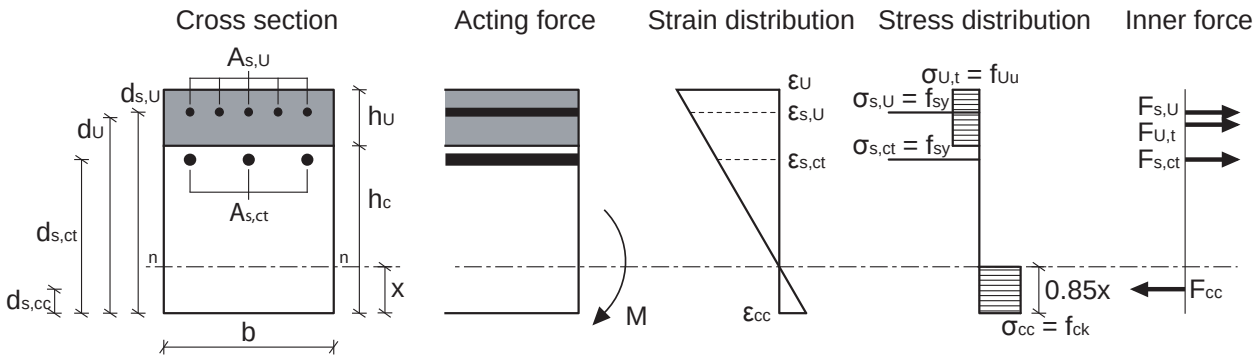

Figure 2 Sectional model for calculation of ultimate resistance

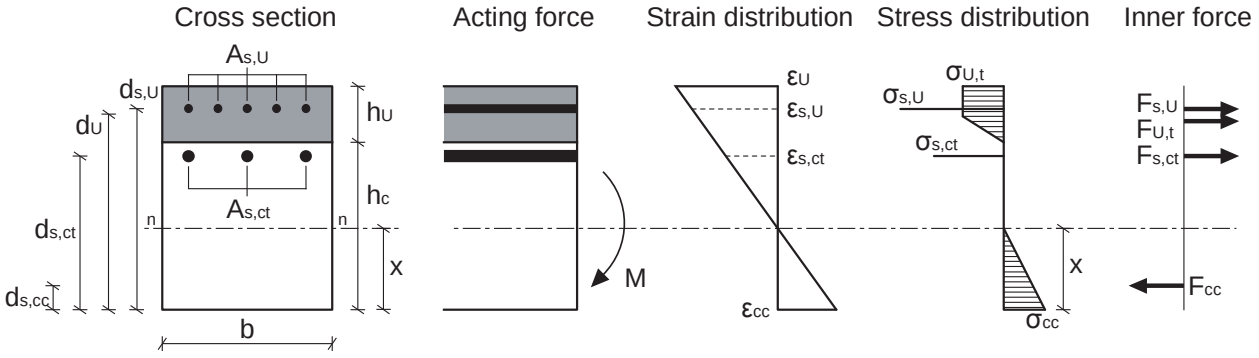

Figure 3 Elastic sectional model for calculation of fatigue stress

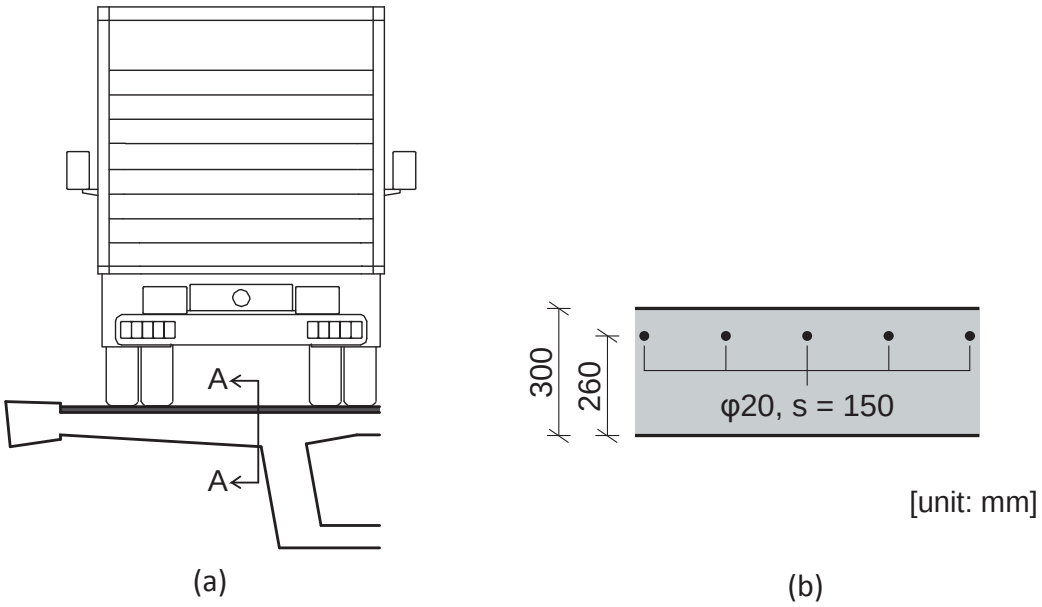

Figure 4 (a) A part of bridge cross section and (b) deck slab reinforcement details at A-A section

Acting bending moment at A-A section due to fatigue

Maximum bending moment: $M_{fat,max}$ = 150 kNm/m

Minimum bending moment: $M_{fat,min}$ = 20 kNm/m

(1) Fatigue safety verification of existing RC deck slab at A-A section

Stress range in top steel rebars as calculated using the model shown in Figure 3 without R-UHPFRC layer:

$$\Delta\sigma_{s,ct}(Q_{fat}) \approx 263 \text{ MPa} \geq \Delta\sigma_{sd,D} = 115 \text{ MPa} \rightarrow \text{OUT}$$

RC deck slab needs to be strengthened for fatigue. 40 mm-thick R-UHPFRC layer with steel rebars of 8 mm diameter is designed to be overlaid on top of the RC deck slab after hydrodemolishing RC top surface of 10 mm-depth. Details of RU-RC member are shown in Figure 5.

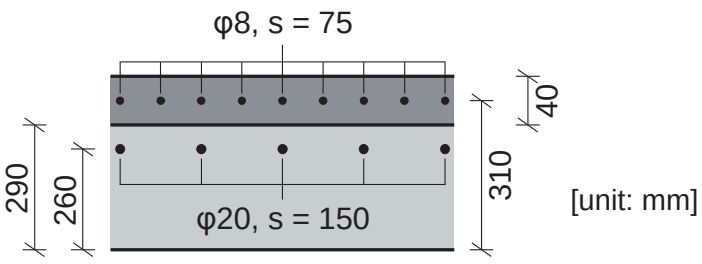

Figure 5 Details of RC deck slab strengthened with R-UHPFRC layer at A-A section (RU-RC member 1-1)

(2) Fatigue safety verification of RU-RC member at A-A section (Figure 5)

[Macro-level check]

Ultimate static resistance of RU-RC member as calculated using the model shown in Figure 2: $\boldsymbol{M_R \approx 368}$ **kNm/m**

$$\boldsymbol{n_{fat} = \frac{0.5 \cdot M_R}{M_{fat,max}} = \frac{184}{150} \geq 1.0 \rightarrow OK}$$

[Meso-level check]

Stress range in steel rebars in the R-UHPFRC as calculated using the model shown in Figure 3:

$$\boldsymbol{\Delta\sigma_{s,U}(Q_{fat}) \approx 75\ MPa < \Delta\sigma_{sd,D} = 115\ MPa \rightarrow OK}$$

However, UHPFRC is strained into the strain-hardening domain by maximum bending moment ($\varepsilon_{U,fat,max} \approx 0.42$ ‰) and thus reduces its stiffness due to fatigue. Consequently, stress in steel rebars increases and stress range in steel rebars in the R-UHPFRC needs to be checked for the long term fatigue safety.

Decrease of UHPFRC stiffness $E_{U,fat}$ due to fatigue is determined by proposed fatigue damaging relationship of $E_{U,fat}$ [Section 5.5 and Section 6.3]. Considering that steel rebar ratio of the R-UHPFRC layer is 1.70 %, the fatigue damaging relationship of $E_{U,fat}$ is modified and its normalised equations are obtained as:

$$E_{U,fat,n} = 0.36 + 0.64 \cdot \sin^2\left(\frac{LogN + 5.7}{11.4}\pi\right) \quad \text{for} \quad N \leq 100{,}000 \qquad \textbf{Eq. 4}$$

$$E_{U,fat,n} = -6.64 \cdot 10^{-2} \cdot LogN + 0.72 \quad \text{for} \quad 100{,}000 < N \qquad \textbf{Eq. 5}$$

For each cycle, $\Delta\sigma_{sd,U}$ is calculated and evolution of $\Delta\sigma_{sd,U}$ is shown in Figure 6. At about 15,000 cycles $\Delta\sigma_{sd,U}$ becomes larger than 115 MPa and thus fatigue safety is not satisfied in the long term. By changing the size of steel rebars in the R-UHPFRC layer from ϕ8 to ϕ10 (Figure 7), fatigue safety of RU-RC member at A-A section is checked again.

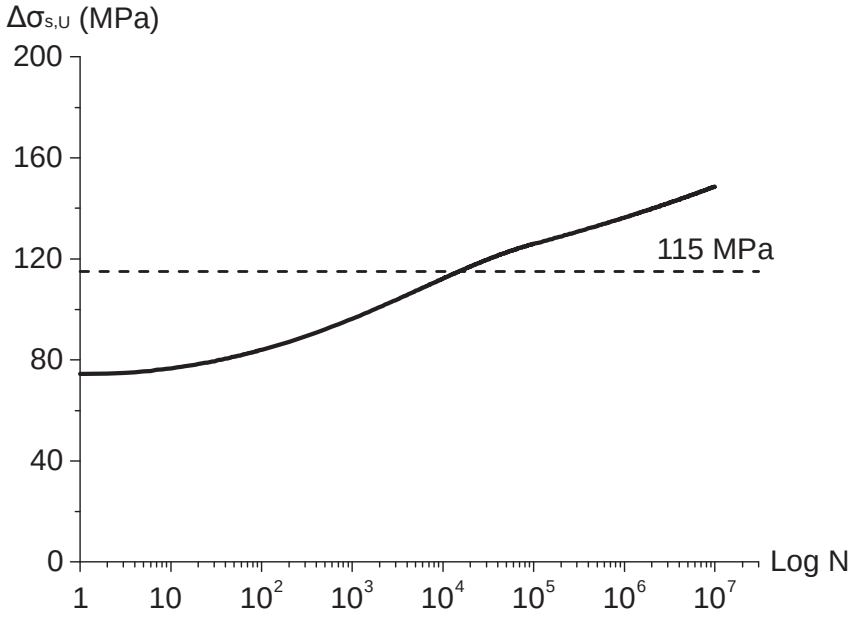

Figure 6 RU-RC member 1-1: evolution of stress range in steel rebars in the R-UHPFRC

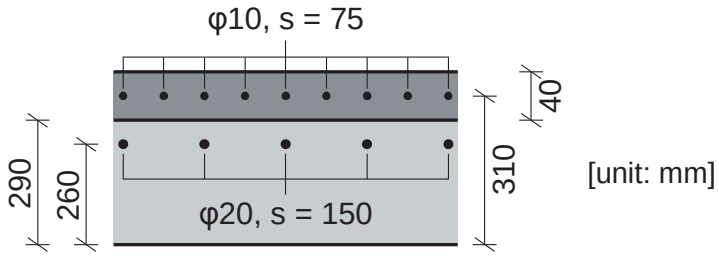

Figure 7 Modified details of RC deck slab strengthened with R-UHPFRC layer at A-A section (RU-RC member 1-2)

(3) Second try: fatigue safety verification of RU-RC member at A-A section (Figure 7)

[Macro-level check]

Ultimate static resistance of RU-RC member as calculated using the model shown in Figure 2: $\boldsymbol{M_R \approx 394\ kNm/m}$

$$\boldsymbol{n_{fat} = \frac{0.5 \cdot M_R}{M_{fat,max}} = \frac{197}{150} \geq 1.0 \rightarrow OK}$$

[Meso-level check]

Stress range in steel rebars in the R-UHPFRC as calculated using the model shown in Figure 3:

$$\boldsymbol{\Delta\sigma_{s,U}(Q_{fat}) \approx 66\ MPa < \Delta\sigma_{sd,D} = 115\ MPa \rightarrow OK}$$

However, UHPFRC is strained into the strain-hardening domain by maximum bending moment ($\varepsilon_{U,fat,max} \approx 0.36$ ‰) and thus reduces its stiffness due to fatigue. Consequently,

stress in steel rebars increases and stress range in steel rebars in the R-UHPFRC needs to be checked for the long term fatigue safety.

Decrease of $E_{U,fat}$ due to fatigue is determined by modified fatigue damaging relationship of $E_{U,fat}$ based on steel rebar ratio of the R-UHPFRC layer (= 2.69 %).

$$E_{U,fat,n} = 0.59 + 0.41 \cdot \sin^2\left(\frac{LogN + 5.7}{11.4}\pi\right) \quad \text{for} \quad N \le 100{,}000 \qquad \textbf{Eq. 6}$$

$$E_{U,fat,n} = -4.25 \cdot 10^{-2} \cdot LogN + 0.82 \quad \text{for} \quad 100{,}000 < N \qquad \textbf{Eq. 7}$$

For each cycle, $\Delta\sigma_{sd,U}$ are calculated and evolution of $\Delta\sigma_{sd,U}$ is shown in Figure 8. $\Delta\sigma_{sd,U}$ remains smaller than 115 MPa during 10 million cycles and thus fatigue safety is satisfied in the long term.

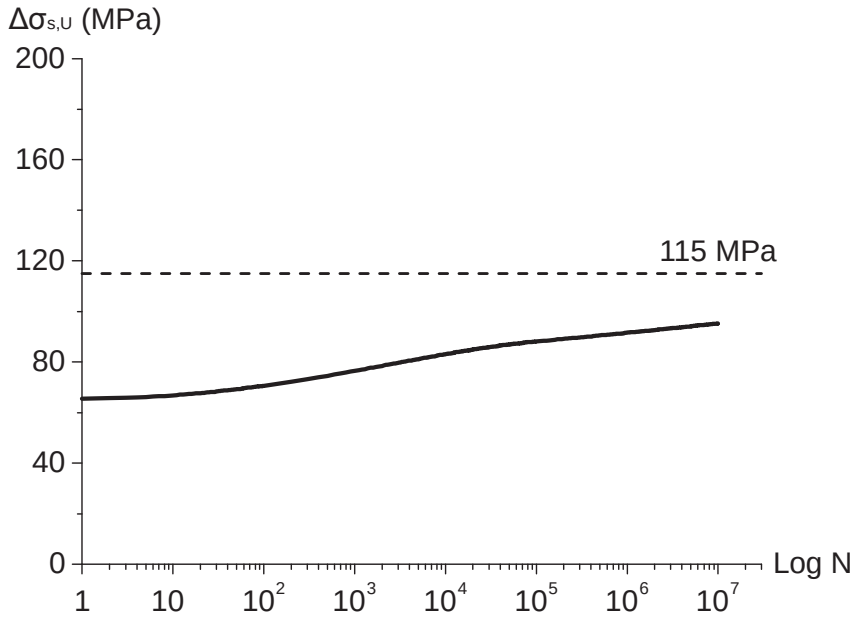

Figure 8 RU-RC member 1-2: evolution of stress range in steel rebars in the R-UHPFRC

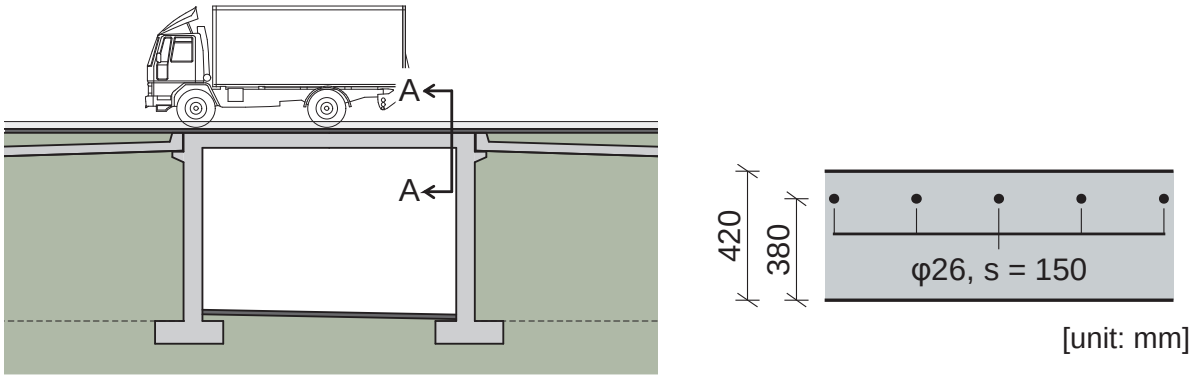

Figure 9 (a) Bridge profile and (b) deck slab reinforcement details at A-A section

Acting bending moment at A-A section due to fatigue

Maximum bending moment: $M_{fat,max}$ = 270 kNm/m

Minimum bending moment: $M_{fat,min}$ = 30 kNm/m

(1) Fatigue safety verification of existing RC deck slab at A-A section

Stress range in top steel rebars as calculated using the model shown in Figure 3 without R-UHPFRC layer:

$$\boldsymbol{\Delta\sigma_{s,ct}(Q_{fat}) \approx 197\ MPa \geq \Delta\sigma_{sd,D} = 95\ MPa \rightarrow OUT}$$

RC deck slab needs to be strengthened for fatigue. 40 mm-thick R-UHPFRC layer with steel rebars of 10 mm diameter is designed to be overlaid on top of the RC deck slab after hydrodemolishing RC top surface of 10 mm-depth. Details of RU-RC member are shown in Figure 10.

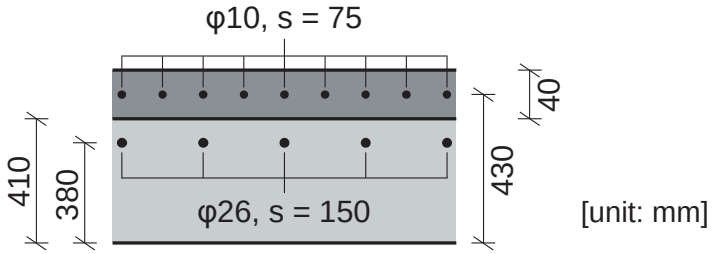

Figure 10 Details of RC deck slab strengthened with R-UHPFRC layer at A-A section (RU-RC member 2-1)

(2) Fatigue safety verification of RU-RC member at A-A section (Figure 10)

[Macro-level check]

Ultimate static resistance of RU-RC member as calculated using the model shown in Figure 2: $\boldsymbol{M_R \approx 754}$ **kNm/m**

$$\boldsymbol{n_{fat} = \frac{0.5 \cdot M_R}{M_{fat,max}} = \frac{377}{270} \geq 1.0 \rightarrow OK}$$

[Meso-level check]

Stress range in steel rebars in the R-UHPFRC as calculated using the model shown in Figure 3**:**

$$\boldsymbol{\Delta\sigma_{s,U}(Q_{fat}) \approx 82 \text{ MPa} < \Delta\sigma_{sd,D} = 115 \text{ MPa} \rightarrow OK}$$

However, UHPFRC is strained into the strain-hardening domain by maximum bending moment ($\varepsilon_{U,fat,max} \approx 0.39$ ‰) and thus reduces its stiffness due to fatigue. Consequently, stress in steel rebars increases.

Decrease of $E_{U,fat}$ due to fatigue is determined by modified fatigue damaging relationship of $E_{U,fat}$ based on steel rebar ratio of the R-UHPFRC layer (= 2.69 %).

$$E_{U,fat,n} = 0.59 + 0.41 \cdot \sin^2\left(\frac{LogN + 5.7}{11.4}\pi\right) \quad \text{for} \quad N \leq 100{,}000 \qquad \textbf{Eq. 8}$$

$$E_{U,fat,n} = -4.25 \cdot 10^{-2} \cdot LogN + 0.82 \quad \text{for} \quad 100{,}000 < N \qquad \textbf{Eq. 9}$$

For each cycle, $\Delta\sigma_{sd,U}$ is calculated and evolution of $\Delta\sigma_{sd,U}$ is shown in Figure 11. $\Delta\sigma_{sd,U}$ remains smaller than 115 MPa during 10 million cycles and thus fatigue safety is satisfied in the long term.

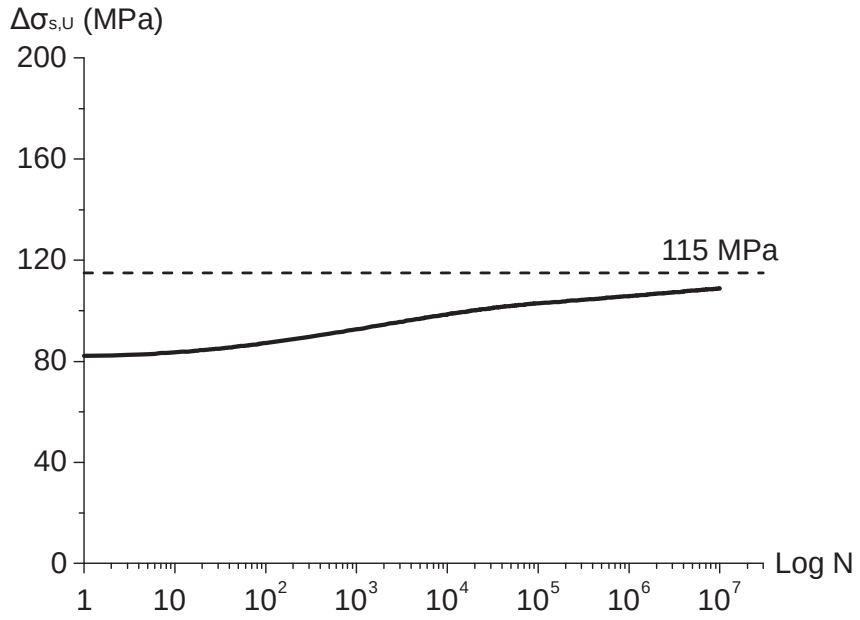

Figure 11 RU-RC member 2-1: evolution of stress range in steel rebars in the R-UHPFRC

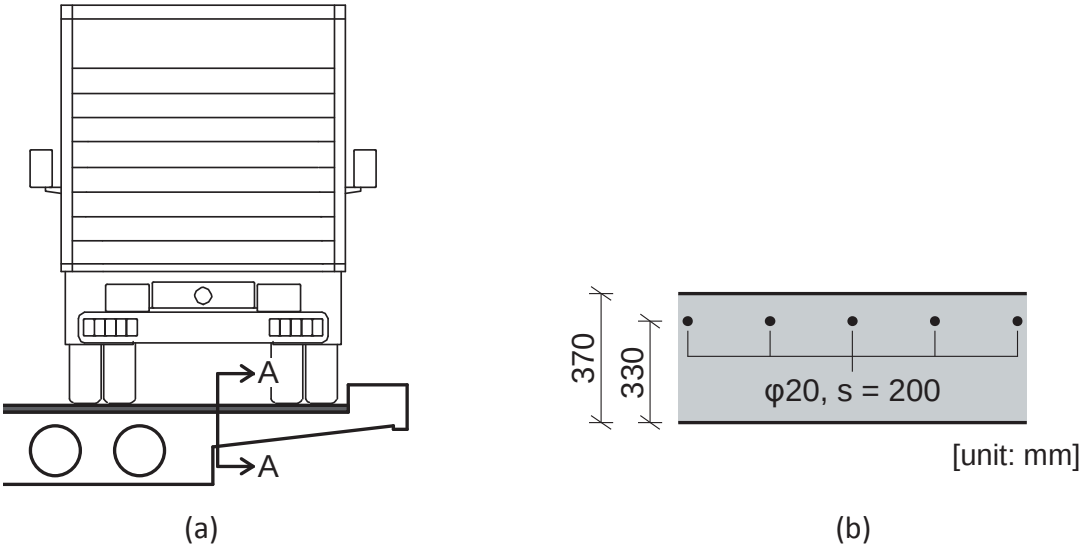

Figure 12 (a) A part of bridge cross section and (b) deck slab reinforcement details at A-A section

Acting bending moment at A-A section due to fatigue

Maximum bending moment: $M_{fat,max}$ = 75 kNm/m

Minimum bending moment: $M_{fat,min}$ = 20 kNm/m

(1) Fatigue safety verification of existing RC deck slab at A-A section

Stress range in top steel rebars as calculated using the model shown in Figure 3 without R-UHPFRC layer:

$$\Delta\sigma_{s,ct}(Q_{fat}) \approx 114 \text{ MPa} < \Delta\sigma_{sd,D} = 115 \text{ MPa} \rightarrow \text{OK}$$

Since the RC deck slab is not waterproofed, 35 mm-thick UHPFRC layer is designed to be overlaid as waterproofing member on top of the RC deck slab after hydrodemolishing RC top surface of 10 mm-depth. Details of UHPFRC-RC member are shown in Figure 13.

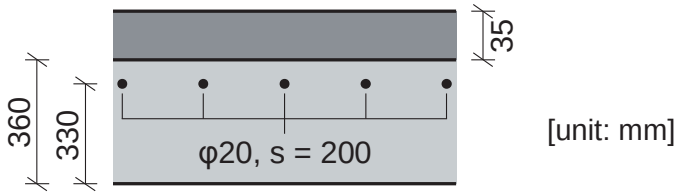

Figure 13 Details of RC deck slab waterproofed with UHPFRC layer at A-A section

(2) Fatigue safety verification of UHPFRC-RC member at A-A section (Figure 13)

Maximum stress in UHPFRC as calculated using the model shown in Figure 3:

$$\sigma_{U,fat,max}(Q_{fat}) \approx 5.9 \text{ MPa} < 0.3 \cdot (f_{Ue} + f_{Uu}) = 6 \text{ MPa} \rightarrow \text{OK}$$

Thus, fatigue safety is satisfied.

This page is intentionally left blank.

Appendix B

Test reports

Report 1 **Tensile fatigue test of Ultra-High Performance Fibre Reinforced Concrete (UHPFRC)**

Report 2 **Tensile fatigue test of Ultra-High Performance Fibre Reinforced Concrete reinforced with steel rebars (R-UHPFRC)**

Report 3 **Bending fatigue test of R-UHPFRC – RC composite beams**

These test reports are available at https://infoscience.epfl.ch/record/190677.

This page is intentionally left blank.

Curriculum vitae

Tohru Makita

Date of birth: 28.06.1974

Nationality: Japanese

E-mail: t.makita.ab@c-nexco.co.jp

EDUCATION

06.2009 – present	Doctoral candidate Laboratory of Maintenance and Safety of Structures (MCS), École Polytechnique Fédérale de Lausanne (EPFL), Lausanne, Switzerland Doctoral thesis: *Fatigue behaviour of UHPFRC and R-UHPFRC – RC composite members*
04.1998 – 03.2000	Master of Engineering in Global Environmental Engineering, Kyoto University, Kyoto, Japan
04.1994 – 03.1998	Bachelor of Engineering in Civil Engineering, Kyoto University, Kyoto, Japan

PROFESSIONAL EXPERIENCE

10.2005 – present	Engineer, Central Nippon Expressway Company Limited, Nagoya, Japan ● *Implementation and development of new technologies for rehabilitation and strengthening of bridges* ● *Management of bridge standards* ● *Management of maintenance of expressway structures*
04.2002 – 09.2005	Engineer, Japan Highway Public Corporation, Tokyo, Japan ● *Management of construction of expressway structures*
04.2000 – 01.2001	Engineer, Sogo Engineering Consultants Company Limited, Osaka, Japan ● *Seismic retrofitting design of a cable-stayed bridge* ● *Finite element analysis of connections of steel girders*

PROFESSIONAL LICENSE

03.2008	Professional Engineer, Japan

SKILLS

Software	MATLAB, CUBUS, ORIGIN, AutoCAD, ATENA,
Language	Japanese (mother tongue), English (intermediate), French (basic knowledge)

PUBLICATIONS

Makita T., Brühwiler E. (2014) "Tensile fatigue behaviour of Ultra-High Performance Fibre Reinforced Concrete combined with steel rebars (R-UHPFRC)", International Journal of Fatigue, Vol. 59, pp. 145-152

Makita T., Brühwiler E., (2014) "Damage models for UHPFRC and R-UHPFRC tensile fatigue behaviour", submitted to Engineering Structures

Makita T., Brühwiler E., (2013) "Modelling of fatigue behaviour of bridge deck slab elements strengthened with reinforced UHPFRC", submitted to 7th International Conference on Bridge Maintenance, Safety and Management (IABMAS 2014)

Makita T., Brühwiler E., (2013) "Fatigue behaviour of composite R-UHPFRC – RC structural members", Proceedings of the RILEM-*fib*-AFGC International Symposium on Ultra-High Performance Fibre-Reinforced Concrete (UHPFRC 2013), Ed. by Toutlemonde F., Resplendino J., Marseille, France, pp. 167-176

Makita T., Brühwiler E., (2013) "Tensile fatigue behaviour of ultra-high performance fibre reinforced concrete (UHPFRC)", Materials and Structures, Published online: 23 April, 2013

Makita T., Brühwiler E., (2012) "Fatigue behaviour of bridge deck slab elements strengthened with reinforced UHPFRC", Proceedings of 6th International Conference on Bridge Maintenance, Safety and Management (IABMAS 2012), Ed. by Biondini F., Frangopol D. M., Stresa, Italy, pp. 1974-1980